



## Attribution-NonCommercial 2.0 KOREA

**You are free to :**

- **Share** — copy and redistribute the material in any medium or format
- **Adapt** — remix, transform, and build upon the material

**Under the following terms :**



**Attribution** — You must give [appropriate credit](#), provide a link to the license, and [indicate if changes were made](#). You may do so in any reasonable manner, but not in any way that suggests the licensor endorses you or your use.



**NonCommercial** — You may not use the material for [commercial purposes](#).

You do not have to comply with the license for elements of the material in the public domain or where your use is permitted by an applicable exception or limitation.

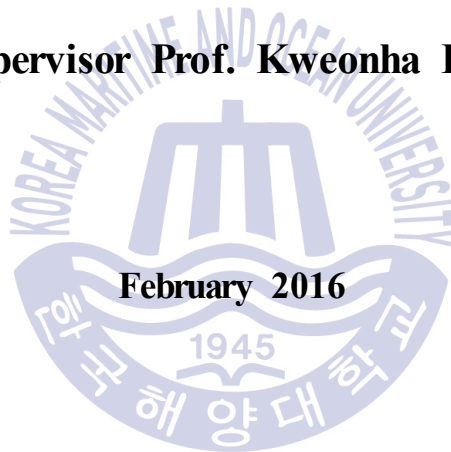
This is a human-readable summary of (and not a substitute for) the [license](#).

[Disclaimer](#) 

# **Master's Thesis**

## **Numerical Analysis of Innovative Hydrogen Mitigation Measure and Passive Autocatalytic Recombiner in Nuclear Power Plant**

**Supervisor Prof. Kweonha Park**



**February 2016**


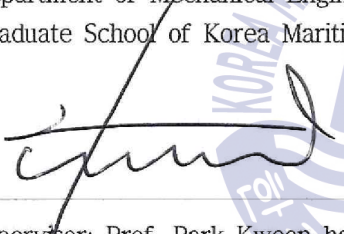
**Department of Mechanical Engineering  
Graduate School of Korea Maritime and  
Ocean University**

**Chong Lee Khor**

We certify that we have read this thesis and that, in our opinions, it is satisfactory in scope and quality as a thesis for the degree of Master of Mechanical Engineering, submitted by Khor Chong Lee.

THESIS COMMITTEE

Chairperson: Prof. Cho Jong-rae, PhD  
Department of Mechanical Engineering,  
Graduate School of Korea Maritime and Ocean University

  
Co-chairperson: Prof. Lee Young-ho, PhD  
Department of Mechanical Engineering,  
Graduate School of Korea Maritime and Ocean University  
Supervisor: Prof. Park Kweon-ha, PhD  
Department of Mechanical Engineering,  
Graduate School of Korea Maritime and Ocean University

9 December 2015

Department of Mechanical Engineering  
Graduate School of Korea Maritime and Ocean University

본論文을허중리의 工學碩士

學位論文으로認准함

위원장: 공학박사 조종래

위원: 공학박사 이영호

위원: 공학박사 박권하



2015년12월9일

한국해양대학교 대학원

기계공학과

## Table of Contents

Table of Contents .....	IV
List of Tables .....	VII
List of Figures .....	VIII
Abstract .....	XII
Nomenclature .....	XV
Greek Symbols .....	XVI
Abbreviations .....	XVI
 Chapter 1 Introduction .....	 1
1.1 History background .....	1
1.2 Overview of international hydrogen risk assessment .....	2
1.3 Study outline .....	3
1.4 Passive autocatalytic recombiner (PAR) .....	4
 Chapter 2 Consideration on hydrogen explosion in APR1400 containment building small breakup loss of coolant accident .....	 7
2.1 General .....	7
2.2 Background introduction .....	8
2.3 Calculations grids and conditions .....	10
2.3.1 Geometry and grids .....	10
2.3.2 Mathematical model and calculation conditions .....	11
2.4 Results and condition .....	15
2.4.1 Gas behavior and hydrogen explosion risk .....	15
2.4.2 Gas concentration and explosion risk .....	20
2.4.3 Hydrogen explosion scenario .....	28

<b>Chapter 3 Proposal and analysis of hydrogen mitigation system guiding hydrogen in containment .....</b>	<b>30</b>
3.1 General .....	30
3.2 Introduction .....	31
3.3 Proposal of a mitigation system .....	33
3.3.1 Simulation conditions .....	33
3.4 Results and discussion .....	35
3.4.1 Gas behavior in the shallow reservoir containment	35
3.4.2 Gas behavior in the deep reservoir containment ...	38
 <b>Chapter 4 CFD analysis of the effect of different PAR locations against hydrogen recombination rate .....</b>	<b>43</b>
4.1 General .....	43
4.2 Introduction .....	43
4.3 Mathematical modeling .....	45
4.4 KNT PAR calculations .....	48
4.4.1 Mesh and conditions .....	48
4.4.2 Results .....	50
4.5 PAR installed locations .....	51
4.5.1 Mesh and conditions .....	51
4.5.2 Results and discussion .....	62
 <b>Chapter 5 Proposal and analysis of flow considered-design new PAR models .....</b>	<b>65</b>
5.1 General .....	65
5.2 Introduction .....	65

5.3 Mathematical model and calculation condition .....	68
5.4 Model description .....	71
5.5 Results and discussion .....	75
5.5.1 Flow induction .....	75
5.5.2 Gas distribution variations scenario .....	76
5.5.3 Hydrogen induced area .....	79
5.5.4 Maximum PAR recombination performance .....	83
 Chapter 6 Conclusion .....	 89
 Acknowledgement .....	 92
 References .....	 93



## List of Tables

<b>Table 2.1</b> Hydrogen explosion scenario chart .....	29
<b>Table 3.1</b> Test condition .....	35
<b>Table 4.1</b> Hydrogen reduction fraction contour of KNT PAR simulation result (cut plane) .....	50
<b>Table 4.2</b> Simulation test input condition .....	53
<b>Table 4.3a</b> Hydrogen reduction changes in the nuclear containment .....	54
<b>Table 4.3b</b> Hydrogen reduction changes in the nuclear containment .....	58
<b>Table 5.1</b> Analysis condition .....	74
<b>Table 5.2</b> Hydrogen recombination pattern in the PARs of different velocity variation .....	76
<b>Table 5.3</b> Steam production pattern in the PARs of different velocity variation .....	77
<b>Table 5.4</b> Oxygen removal pattern in the PARs of different velocity variation .....	77
<b>Table 5.5</b> The streamline pattern of hydrogen velocity in the upward-directed gas flow case .....	80
<b>Table 5.6</b> The streamline pattern of hydrogen velocity in sideward-directed gas flow case .....	81
<b>Table 5.7</b> The streamline pattern of hydrogen velocity in the upward with sideward-directed gas flow case .....	82

## List of Figures

<b>Fig. 1.1</b> Sketch of a generic parallel-plate passive autocatalytic recombiner .....	5
<b>Fig. 1.2</b> How the PAR recombines hydrogen and air .....	6
<b>Fig. 2.1</b> Inner shape of the containment building of the APR1400 nuclear plant .....	11
<b>Fig. 2.2</b> Calculation grids and enlarged grids near failure position .....	11
<b>Fig. 2.3</b> Flow rate of gases in SBLOCA .....	13
<b>Fig. 2.4</b> Pressure and temperature curve .....	14
<b>Fig. 2.5</b> Distribution of hydrogen and steam in the containment building at 4800s .....	15
<b>Fig. 2.6</b> Distribution of hydrogen, steam and air at 7000s .....	16
<b>Fig. 2.7</b> Distribution of hydrogen, steam and air at 14,000s .....	17
<b>Fig. 2.8</b> Distribution of hydrogen, steam and air at 20,000s .....	18
<b>Fig. 2.9</b> Distribution of hydrogen, steam and air at 33,000s .....	19
<b>Fig. 2.10</b> Distribution of hydrogen, steam and air at 54,000s .....	20
<b>Fig. 2.11</b> Monitor points of gas concentration .....	20
<b>Fig. 2.12</b> Gas volume fractions against time from the accident was taken place (Point 1) .....	21
<b>Fig. 2.13</b> Gas volume fractions and explosions possibility at the top of the containment (Point 1) .....	21
<b>Fig. 2.14</b> Gas volume fractions against time from the accident was taken place (Point 2) .....	22
<b>Fig. 2.15</b> Gas volume fractions and explosions possibility at the middle left part of the containment (Point 2) .....	23
<b>Fig. 2.16</b> Gas volume fractions against time from the accident was taken place (Point 3) .....	23

<b>Fig. 2.17</b> Gas volume fractions and explosions possibility at the middle part of the containment (Point 3) .....	23
<b>Fig. 2.18</b> Gas volume fractions against time the accident was taken place (Point 4) .....	24
<b>Fig. 2.19</b> Gas volume fractions and explosions possibility at the middle right part of the containment (Point 4) .....	24
<b>Fig. 2.20</b> Gas volume fractions against time from the accident was taken place (Point 5) .....	25
<b>Fig. 2.21</b> Gas volume fractions and explosions possibility at the bottom left part of the containment (Point 5) .....	25
<b>Fig. 2.22</b> Gas volume fractions against time from the accident was taken place (Point 6) .....	26
<b>Fig. 2.23</b> Gas volume fractions and explosions possibility at the bottom center part of the containment (Point 6) .....	26
<b>Fig. 2.24</b> Gas volume fractions against time from the accident was taken place (Point 7) .....	26
<b>Fig. 2.25</b> Gas volume fractions and explosions possibility at the bottom right of the containment (Point 7) .....	27
<b>Fig. 2.26</b> Gas volume fractions against time from the accident was taken place (Point 8) .....	27
<b>Fig. 2.27</b> Gas volume fractions and explosions possibility at the bottom compartment of the containment (Point 8) .....	28
<b>Fig. 3.1</b> Steam and hydrogen volume fraction distribution in a containment .....	32
<b>Fig. 3.2</b> A concept design of hydrogen mitigation system actively controlled distribution .....	33
<b>Fig. 3.3</b> Inner shapes of Type I shallow air reservoir air containment .....	34

Fig. 3.4 Inner shape of Type II deep air reservoir air containment ..	35
Fig. 3.5 Steam and air released volume .....	36
Fig. 3.6 Hydrogen volume fraction distribution .....	37
Fig. 3.7 Comparisons of hydrogen released mass and remaining mass .....	38
Fig. 3.8 Steam and air volume distribution .....	39
Fig. 3.9 Hydrogen volume fraction distribution .....	40
Fig. 3.10 Hydrogen mass reduction graph .....	41
Fig. 3.11 Total reduction percentage in every scenarios of hydrogen released .....	41
Fig. 4.1 Conceptual diagram of KNT honeycomb model integral test facility (ITF) .....	49
Fig. 4.2 Actual conceptual diagram of KNT integral test facility ....	49
Fig. 4.3 Hydrogen reduction rate comparison .....	51
Fig. 4.4 Different locations where the PAR model was installed ....	51
Fig. 4.5 CFX mesh of KNT PAR .....	52
Fig. 4.6 Meshes of the KNT PAR and the containment .....	52
Fig. 4.7 Results of PAR installed at the center of the containment	62
Fig. 4.8 Results of PAR installed at the side of the containment ...	63
Fig. 4.9 Gas volume fractions against time from the accident was taken place (Point 6) .....	64
Fig. 5.1 Analysis grids of the hypothetical nuclear containment .....	72
Fig. 5.2 Honeycomb-shaped catalyst .....	72
Fig. 5.3 Guiding wall, the highlighted area at the bottom of a PAR structure .....	73
Fig. 5.4 Results of PAR installed at the center of the containment	75
Fig. 5.5 Hydrogen induced area of the upward-directed gas flow case .....	79

<b>Fig. 5.6</b> Hydrogen induced area of the sideward-directed gas flow case .....	80
<b>Fig. 5.7</b> Hydrogen induced area of the upward with sideward-directed gas flow case .....	81
<b>Fig. 5.8</b> The hydrogen recombination rate mass flux in over hydrogen concentration of upward-directed flow case .....	83
<b>Fig. 5.9</b> Maximum hydrogen recombination rate with velocity variation in upward-directed flow case .....	84
<b>Fig. 5.10</b> The hydrogen recombination rate mass flux in over hydrogen concentration of sideward-directed flow case .....	85
<b>Fig. 5.11</b> Maximum hydrogen recombination rate with velocity variation in upward with sideward-directed flow case .....	86
<b>Fig. 5.12</b> The hydrogen recombination rate mass flux in over hydrogen concentration of upward with sideward-directed flow case .....	86
<b>Fig. 5.13</b> Maximum hydrogen recombination rate with velocity variation in upward with sideward-directed flow case .....	87

# Numerical Analysis of Innovative Hydrogen Mitigation Measure and Passive Autocatalytic Recombiner in Nuclear Power Plant

Khor Chong Lee

Department of Mechanical Engineering  
Graduate School of Korea Maritime and Ocean University

## Abstract

The basic goal of severe accident management in nuclear power plants (NPPs) is the protection of the containment integrity and the containment becomes the ultimate barrier against the release of fission products to the environment. There are various potential challenges to the containment integrity during a severe accident in a light water reactor (LWR). For most NPPs, severe accidents lead to hydrogen release rates that exceed the capacity of hydrogen control measures at conventional design basis accident. High local hydrogen concentrations can be reached in a short time, leading to combustible gas mixtures in the containment. Moreover, a long term pressure build-up may occur due to steam generation through decay heat and/or through the generation non-condensable gas from the interaction of the molten core with the containment basement concrete.

The implementation of hydrogen mitigation measures is aimed in general to prevent and limit hydrogen explosion consequences for the

containment, the reactor and auxiliary buildings. Therefore, depending on the NPP type, hydrogen mitigation measures are designed to meet specific safety criteria and requirements. In addition to mitigation measures, gas composition monitoring system is often used to check if the requirements are satisfied and to provide relevant information to NPP operators during accident and severe accident conditions.

Passive autocatalytic recombiners (PARs) have been developed and have become commercially available hardware in the last decade. PARs are simple devices, consisting of a catalyst surfaces arranged in an open-ended enclosure. In the presence of hydrogen (with available oxygen), a catalytic reaction occurs spontaneously at the catalyst surfaces and the heat of reaction produces natural convection flow through the enclosure, exhausting the warm, humid hydrogen-depleted air and drawing fresh gas from below. Thus, PARs do not need external power or operator action. PAR capabilities are ultimately subject to mass transfer limitations and may not keep up with high hydrogen release rates in small volumes, for example, as could exist in the immediate vicinity of the hydrogen release.

In this study, various tests were conducted on different PAR's designs to investigate and improve the hydrogen recombination rate. The innovative modifications on the current PAR model were carried out to foresee the unpredictable conditions and potential risks in the NPPs, and hence be adaptable in any circumstances to mitigate the hydrogen mitigation consequences. Although there is none hydrogen mitigation measures could be the best resolution in every single NPPs, the lessons learnt from the Fukushima accidents that hydrogen safety inspection was carried out on all Korean NPPs by Korean government and PARs will be implemented in all operating and under-construction plants.

**Keywords:** *Passive autocatalytic recombiner (PAR), Hydrogen explosion, Potential risk, Severe accident, Honeycomb-shaped catalyst, New design, Hydrogen explosion scenario, PAR installed location*



## Nomenclature

Variable	Description	SI units
$A_S$	Surface area of catalyst	$[mm^2]$
$C$	Concentration of hydrogen	-
$F$	Force	$[N]$
$LHV_{H_2}$	Lower heating value	-
$m_a$	The mass of air	$[g]$
$m_h$	The mass of hydrogen	$[g]$
$N$	Number of catalyst	-
$P$	Pressure	$[Pa]$
$P_a$	Partial time of air	$[s]$
$P_h$	Partial pressure of hydrogen	$[Pa]$
$P_s$	Partial time of steam	$[s]$
$P_{tot}$	Total pressure of hydrogen	$[Pa]$
$R_a$	Ideal gas constant of air	$[J/kg\ K]$
$R_h$	Ideal gas constant of hydrogen	$[J/kg\ K]$
$R_{PAR}$	Hydrogen concentration	-
$T$	Temperature	$[K]$
$t$	Time	$[s]$
$Uj$	Velocity tensor	$W/m^2\ K$
$V_{tot}$	Total volume of the building	$[m^3]$
$w$	turbulent frequency	-

## Greek symbols

Variable	Description	SI units
$\rho$	Gas density	$[kg/m^3]$
$\mu$	Air viscosity	$[Pa \cdot s]$
$\nu$	Coefficient of dynamic viscosity	$[m^2/s]$
$\tau$	Shear stress	$[N/m^2]$
$\theta_p$	Section pitch angle	$[^\circ]$
$\theta_t$	Section twist angle	$[^\circ]$
$k$	Turbulence kinetic energy	$[N]$
$\phi$	Properties	-
$S$	Source term	-

## Abbreviations

Short form	Description
PAR	Passive autocatalytic recombiner
KNT	Korea Nuclear Technology
KAERI	Korea Atomic Energy Research Institute
OECD	Organization for Economic Co-operation and Development
NEA	Nuclear Energy Agency
SBLOCA	Small-break loss-of-coolant accident
LOCA	Loss-of-coolant accident

# Chapter 1 Introduction

## 1.1. History background

On 28th March 1979, at the Three Mile Island 2 (TMI-2) nuclear power plant near Harrisburgh, Pennsylvania, United States, the second day of the accident, that became one of the unfortunate milestones in the history of civilian use of nuclear power, an intense hydrogen burn occurred in the containment. Hydrogen had been generated during the degradation of the reactor core by zirconium-water interaction and had been accumulating in the containment. Hydrogen was released to the containment from the reactor cooling system through the pressurizer and reactor coolant drain tank at a vent. The hydrogen burn occurred 9 hours and 50 minutes after the initiation of the accident. Analyses performed after the accident asserted that, by the time the burn occurred, the generated hydrogen had become well-mixed throughout most of the containment. Hydrogen combustion was trigger but did not cause any severe damage: the pressure spike, which lasted less than a few seconds, reached an appropriate maximum value of 2.8 bar. The entire burn lasted approximately 12s. In fact, this combustion of approximately 350kg of hydrogen caused the only serious pressure load during the whole accident. Since the TMI-2 containment withstood this load, no consequences for the environment occurred. But the hydrogen burn at the TMI-2 plant revealed a serious gap in the knowledge in the field of nuclear activity,

The Fukushima Daiichi accident in Japan occurred on 11th March 2011 due to the common-cause failure resulting from an earthquake and a

massive tsunami. The natural event that exceeded the design basis conditions resulted in loss of heat removal systems and subsequently led to core melting and a large release of radioactive materials to the environment. Loss of ultimate heat sinks and cooling systems designated for the station blackout (SBO) resulted in successive severe core damage in Daiichi units 1, 2, and 3. Another diverting event was a hydrogen explosion that significantly damaged the reactor building in Units 1 and 3, which eventually led to the leakage of radioactive substances.

## 1.2 Overview of international hydrogen risk assessment

The experiences of the Fukushima Daiichi underlined the importance of providing counter-measures against the risks of fissions products release and hydrogen explosion under severe accidents. Since the Fukushima accident, intensive discussions of the Japanese regulation framework have continued to include the requirements of severe accident countermeasures which should be backfitted to all existing nuclear power plants.

After the large explosions in the Fukushima accident, a precise prediction of gas distribution under various containment thermal hydraulic conditions has become important issue. The explosion behavior can be estimated from precise hydrogen distribution in the containment. However, it is not easy to precisely predict the hydrogen distribution in a containment where many structures and components exist. In addition, hydrogen experts are interested in hydrogen explosion behavior based on the hydrogen distribution because the reactor building was destroyed by hydrogen explosions in the Fukushima plants.

An international activity commenced after the Fukushima accident to

remove the hydrogen threat is the performance tests of PARs, which can stimulate an accident without electricity under severe accidents conditions. Thus, the OECD/NEA Thermal-hydraulic, Hydrogen, Aerosol and Iodine (THAI) Project was performed [1]. The frame of the first phase of the OECD-THAI project was aimed at providing nonexistent or inaccessible experimental data for the validation of developed analysis methods and codes to predict hydrogen distribution, combustion behavior, and PAR behavior under representative reactor conditions. Significant progress has been achieved by demonstrating the transferability of helium to hydrogen distribution behavior and by providing comprehensive data for the validation of computational fluids dynamics (CFD) and lumped parameter simulation codes.

### 1.3 Study outline

In the chapter 2, an explosion scenario simulation which lasted for almost 15 hours was studied to investigate the hydrogen generation mechanism, the hydrogen behavior, and the hydrogen distribution. The data obtained in the chapter 2, will be used in the chapter 3 for proposing a new concept-designed hydrogen mitigation system. It is aimed to improve the efficiency of the counter-measurement against the hydrogen explosion scenario in nuclear containment building. The new proposed system takes account of the hydrogen behavior and hydrogen distribution data which obtained from the previous chapter to suggest a more effective counter-measurement system. Besides, the role of the PAR's location is studied in the chapter 4, to investigate the hydrogen recombiners efficiency according to their installed location in nuclear power plants. The PARs are installed at different locations in a containment building and compared their respective hydrogen removal

efficiency. In chapter 5, a little modifications are made to the original Korea Nuclear Technology (KNT) honeycomb PAR body with the intention to improve the hydrogen recombination process. Compared with the original design of PAR, KNT-made PAR altered the PAR catalyst became honeycomb shape. The hydrogen recombination rate increases due to the enlarged surface area of the honeycomb shape catalyst. In this study, a pyramidal-shaped guidance wall is added to the body of PAR to increase the air flow channel into the PAR for recombination process. The study provides the numerical analysis of hydrogen risk counter-measurements and an innovative insight for coping the unpredictable hydrogen risk along with PAR efficiency for removing the hydrogen and mixing the containment atmosphere.

#### 1.4 Passive autocatalytic recombiner (PAR)

Catalytic  $H_2 / O_2$  reaction either onto surfaces or within porous media is the essential of a large variety of applications in industry. In particular, it has been proposed as a strategy for preventing the formation of potentially detonable or highly flammable atmospheres in nuclear containments. Several designs of PARs have been commercialized by companies and implemented within actual facilities for hydrogen control in several countries.

The main feature of PAR is their passive behavior, i.e. their ability to effectively recombine hydrogen driven by natural convection flow (Fig. 1.1, Fig 1.2) across the device powered by the heat generated in the self-sustained catalytic reaction at the surface (heterogeneous reaction). On the other hand, risk of reaction initiation in the gaseous phase (homogeneous reaction) must be considered as a shortcoming of this kind of devices under high hydrogen concentrations. For preventing this

undesired effect, innovative PAR designs have been proposed for controlling high plate temperatures under hydrogen-rich environments.

The different PAR design conceived by several manufacturers feature the catalytic material, either distributed as a thin coating onto metallic planar surfaces (vertical parallel plates or surfaces), or within a ceramic porous matrix of pellets in cartridges.

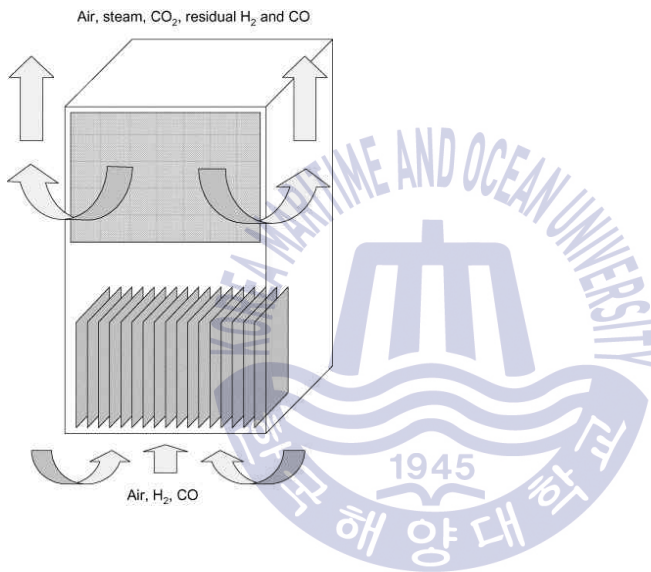


Fig. 1.1 Sketch of a generic parallel-plate passive autocatalytic recombiner

## Passive Autocatalytic Recombiner

### A Hydrogen Management System

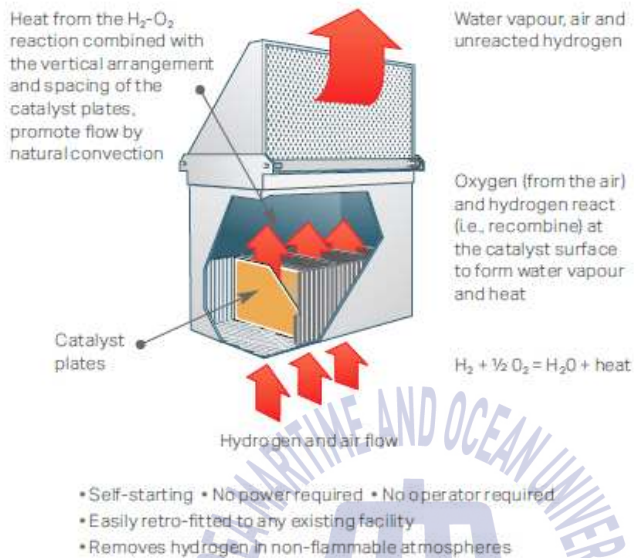


Fig. 1.2 How the PAR recombines hydrogen and air [2]

## Chapter 2 Consideration on hydrogen explosion in APR1400 containment building during small breakup loss of coolant accident

### 2.1 General

This chapter describes the analytical result of the potential risk of hydrogen gas up to 15 hours after the failure takes place. The major cause of the disaster occurred in Fukushima Daiichi nuclear reactor was the detonation of accumulated hydrogen in the reactor containment by highly increased reactor core temperatures after the failure of the emergency cooling system. The hydrogen risk should be considered in severe accident strategies in current and future NPPs. A hydrogen explosion scenario is proposed. Hydrogen is accumulated at the top of the dome during hydrogen release period, but there is no risk of explosion because most of the upper part of the dome is occupied by steam. As a result, the steam is greatly released, and the steam pushes down hydrogen to the compartment's lower part of the building with high air density. At this period, there is a possibility of small explosion, and the steam condensation is a dormant action in the building. The light hydrogen rises up slowly with air. Then most of the hydrogen gas is gathered on top of the building, with large amount of air nearby. If there is an ignition, there is a high possibility that massive hydrogen explosion will take place.

## 2.2 Introduction

On 11 March 2011, a massive earthquake of Richter scale 9.0 followed within an hour by a tsunami with waves of 10 to 14m struck the Fukushima Daiichi (FD) nuclear complex operated by Tokyo Electric Power Company (TEPCO).

Due to the delay of recovery and delivery of cooling system to the reactor cores, some segments of the fuel rods apparently were exposed and overheated which resulted in the exothermic reaction involving uranium oxide fuel rods and the zirconium fuel cladding. The generated hydrogen gas that was vented to the suppression pool along with the steam and other radioactive nuclides released from the damaged fuel rods [3]. The hydrogen gas and other volatile radioactive nuclides were collected in the secondary containment structure and eventually reacted with oxygen in the containment air [4]. This resulted in hydrogen explosion that destroyed the roof of the secondary containment structure [5].

As shown in Fukushima accident, all the designed emergency cooling measures would fail under extreme or hypothetical conditions, the chemical reaction of steam and strongly overheated zircaloy could produce significant amounts of hydrogen [6]. This hydrogen would then be released into the containment through the breakage [7]. Without a counter measurement, flammable mixtures may then be formed and cause combustion that could threaten the integrity of the containment [8,9]. The Fukushima accident has warned us the control and mitigation measurement of the hydrogen risk is still a safety issue for nuclear power plant [10,11,12].

Passive autocatalytic recombiners (PARs) are widely equipped in

numerous containments of light water reactors (LWR). PAR is so-called passive because it requires no external power input to run function [13,14]. The materials most commonly used in the PAR as the catalysts are platinum or palladium. It has been proven ability to reduce the deflagration or detonation risk. The recombination reaction occurs spontaneously at the surfaces, and the water vapor as a product of reaction through the recombiner will act as a natural convective flow currents promote mixing of combustible gases in the containment [15,16].

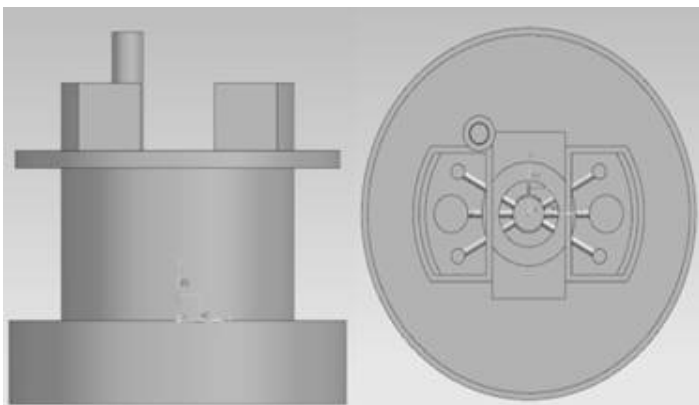
Despite the installation of PARs, it has been generally recognized that the temporary existence of flammable gas clouds cannot be fully excluded during certain postulated accident scenarios. Therefore, reliable computer modeling is needed to assess the associated residual risk of possible hydrogen deflagrations and to optimally design the hydrogen mitigation systems in order to reduce this risk as far as possible [17,18]. CFD is used to determine the evolution the hydrogen distribution within the containment for a relatively large number of postulated accident scenarios [19,20,21] For the most critical scenarios, more refined hydrogen distribution analyses are performed using CFD based containment model.

The hydrogen behavior during hydrogen release was computed by using CFD code [22]. The current knowledge is not enough to understand the hydrogen behavior during the hydrogen explosion, which is needed to be analyzed carefully to set the mitigation measurement. In this study, the potential risk of hydrogen gas is analyzed up to 15 hours after the failure happened during a small-breakup-loss-of-coolant-accident, and a hydrogen explosion scenario is considered.

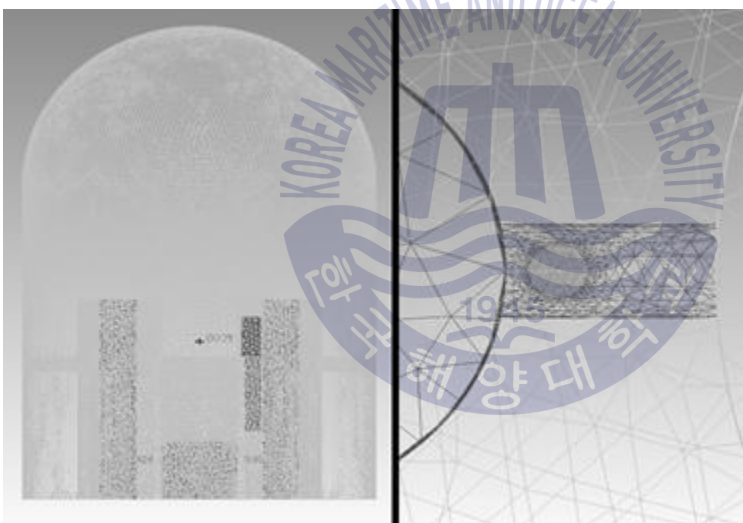
## 2.3 Calculation grids and conditions

### 2.3.1 Geometry and grids

Fig. 2.1 and 2.2 show the inner shape and the calculations grids of the containment building of the APR1400 nuclear plant respectively. The APR1400 is an evolutionary pressurized water reactor with its origins in the CE System 80+ design. The 1,400 MW APR1400 nuclear reactor design is currently under operation at Shin Kori 3&4 and Shin Hanul in Korea. The facilities to mitigate severe accidents are designed to meet the procedural requirements and criteria of the U.S. NRC regulations. The diameter and height are 22.86m and 79.4m, respectively. The lower part of the containment is composed of some compartments and pipe lines. The in-containment refueling water storage tank (IRWST) is placed on the bottom as annular shape, which depth is 3.5m. The reactor vessel is located in the middle and two steam generators and cooler pumps are placed to be symmetrical. Compartment panels are located among the parts, and the parts are connected with pressurized tubes. The failure locations are assumed on the pressurized tube surface. The total number of grids is 2,700,000 and the grids are generated using NX 7.5 and ICEM-CFD codes. The grids are densely generated near the failure range to reduce error from high velocity and high pressure gradient.



**Fig. 2.1** Inner shape of the containment building of the APR1400 nuclear plant



**Fig. 2.2** Calculation grids and enlarged grids near failure position

### 2.3.2 Mathematical model and calculation conditions

The calculation code used in this study is ANSYS CFX. Transient term is discretized with second order backward Euler scheme. It is second-order accurate in time, and given by

$$\frac{\partial}{\partial t} \int_v \rho \phi dV = V \frac{1}{\Delta t} \left( \frac{3}{2} (\rho \phi) - 2 (\rho \phi)^0 + \frac{1}{2} (\rho \phi)^{00} \right) \quad (2.1)$$

where  $( )^0$  and  $( )^{00}$  are the old and one more step old time level solution values.

The  $k$ - $\omega$  based SST model is used on turbulent flow, which accounts for the transport of the turbulent shear stress and gives highly accurate predictions of the onset and the amount of flow separation under adverse pressure gradients. It solves two transport equations, one for the turbulent kinetic energy,  $K$ , and one for the turbulent frequency,  $\omega$ . The equations are given as

$$\frac{\partial(\rho k)}{\partial t} + \frac{\partial(\rho U_j k)}{\partial x_j} = \frac{\partial}{\partial x_j} \left[ \left( \mu + \frac{\mu_t}{\sigma_k} \right) \frac{\partial k}{\partial x_j} \right] + P_k - \beta' \rho k \omega + P_{kb} \quad (2.2)$$

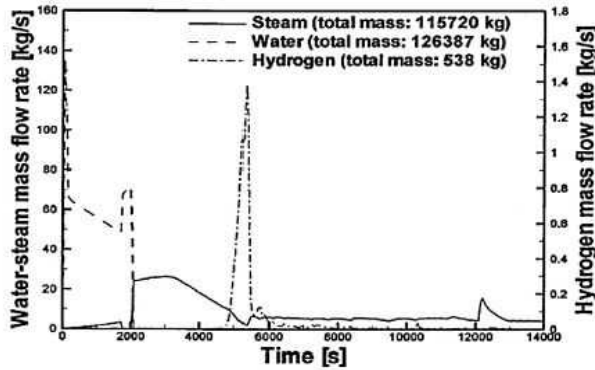
$$\frac{\partial(\rho \omega)}{\partial t} + \frac{\partial(\rho U_j \omega)}{\partial x_j} = \frac{\partial}{\partial x_j} \left[ \left( \mu + \frac{\mu_t}{\sigma_\omega} \right) \frac{\partial \omega}{\partial x_j} \right] + \alpha \frac{w}{k} P_k - \beta' \rho w^2 + P_{wb} \quad (2.3)$$

For buoyancy calculations, a source term is added to the momentum equation as follows:

$$S_{buoy} = (\rho - \rho_{ref})g \quad (2.4)$$

The calculation conditions are given as the accident scenario of SBLOCA-70 [23]. The accident begins with the failure of the pipe in a steam generator compartment and then the reactor core and the fuel rods are melted down. Hydrogen generated with melting rods released from the pipe failure. The amounts of the steam and hydrogen released during the accident are shown in Fig. 2.3, which is the result simulated by MAAP code. Water and steam released until 2000s and only steam is released to 4800s, and then both steam and hydrogen are released. A lot of hydrogen is released from 5000 s to 5500 s, and then the amount of hydrogen and the steam release rates are reduced rapidly, but some amount of steam is released until 14,000s. Total masses of released

steam and hydrogen are 115,720kg and 538kg, respectively.



(2.7)

Fig. 2.3 Flow rate of gases in SBLOCA

The steam, hydrogen release, temperature and pressure after 14,000s are not given in the KAERI report [24]. However, this study needs more conditions after 14000s. It is assumed that the steam and hydrogen are not released anymore after 14,000s, the pressure and temperature are interpolated the curves until 54,000s.

The initial conditions are given as the values before the accident begins. The initial pressure and temperature in the containment are 1.0 bar and 310K, respectively. The initial volume fractions of air, steam, and hydrogen are 1.0, 0.0 and 0.0, respectively. It is assumed that the leakage failure occur at the top of the pipe in a steam generator compartment.

Temperature curve is extended until 54,000s by second order Newton interpolation method given as:

$$P(x) = f(x_0) + f[x_0, x_1] (x - x_0) + f[x_0, x_1, x_2] (x - x_0) (x - x_1) \quad (2.5)$$

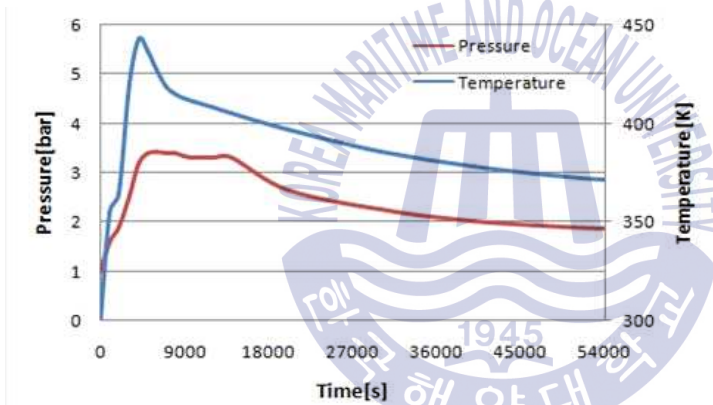
where  $f[x_0, x_1]$ ,  $f[x_0, x_1, x_2]$  are 1st and 2nd divided difference respectively.

$$f[x_0, x_1] = \frac{f(x_0) - f(x_1)}{x_0 - x_1}, f[x_1, x_2] = \frac{f(x_1) - f(x_2)}{x_1 - x_2} \quad (2.6)$$

$$f[x_0, x_1, x_2] = \frac{f(x_1, x_2) - f(x_0, x_1)}{x_2 - x_0}$$

Then the pressure curve is extended until 54,000s. Assuming there is no additional inlet gases, air and hydrogen gas pressures are able to calculate by ideal gas equation. The steam will condenses on the wall surface of the nuclear building, therefore in this study the steam pressure is assumed as proportional to the saturated pressure at the given temperature. The curves are given in Fig. 2.4.

**Fig. 2.4** Pressure and temperature curve



Steam condensation mass during  $t$  ( $= t_1 \sim t_0$ ) is calculated as

$$\Delta m_s = m_s t_0 - m_s t_1 + m_s \dot{m} \quad (2.8)$$

$$\text{where } m_s t_0 = \frac{P_s V_{t0t}}{R_s T_{t0}}, m_s t_1 = \frac{P_s V_{t0t}}{R_s T_{t1}} \quad (2.9)$$

$$P_s = P_{t0t} - P_a - P_h \quad (2.10)$$

$$P_a = \frac{m_a R_a T}{V_{t0t}}, P_h = \frac{m_h R_h T}{V_{t0t}} \quad (2.11)$$

where are the total masses of steam in the containment building at  $t_0$  and  $t_1$ ,  $P_s$ ,  $P_a$ ,  $P_h$  are partial pressures of steam, air and hydrogen,

respectively.  $P_{\text{tot}}$ ,  $V_{\text{tot}}$  are the total pressure and volume of the building.  $m_a$ ,  $m_h$  are the masses of air and hydrogen,  $R_a$ ,  $R_h$  are the ideal gas constant of air and hydrogen, and  $T_{t_0}$  is the temperature at  $t_0$ .

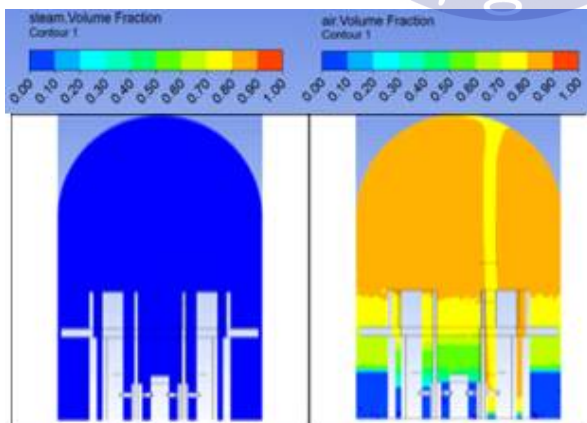
## 2.4 Results and condition

The gas distribution variations of hydrogen, steam, and air from 7000 s to 54000 s are given in the section below. The variations to 7000s are given by the previous report NED 278 (2014) 229-238 [25].

### 2.4.1 Gas behavior and hydrogen explosion risk

*a) Stage 1: Induction of steam (0 - 4800s) [no risk of hydrogen explosion]*

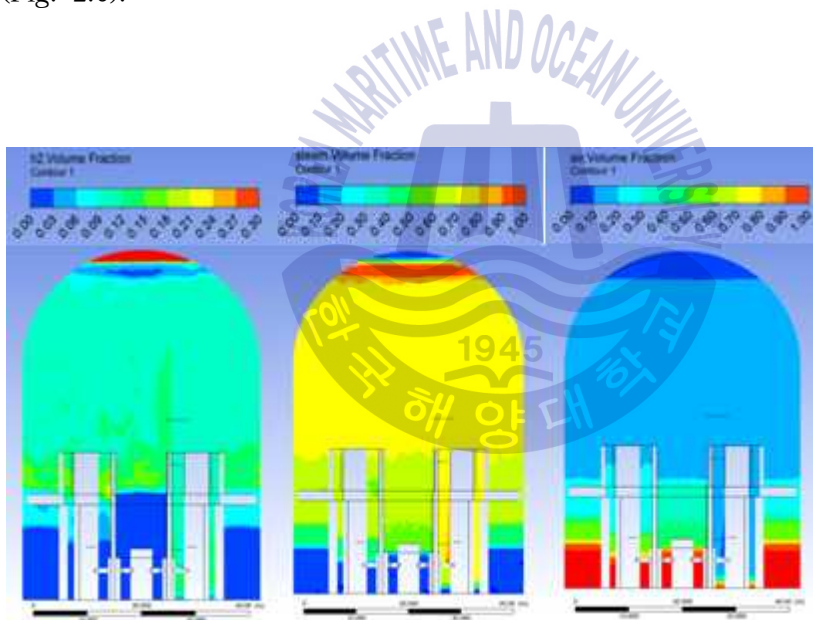
This stage is early period soon after accident. During this period, only steam is released from the failure place. Hot steam ejected from the place directly goes up to the building and fills up the building. At the time when the hydrogen release begins, the released stem is already distributed all over the containment. The volume fraction of the steam is over 80% in the upper part of the containment as shown in Fig. 2.5. Therefore, there is no risk of hydrogen explosion at this stage.



**Fig. 2.5** Distribution of hydrogen and steam in the containment building at 4800s

*b) Stage 2: Induction of steam and hydrogen (5000 - 7000s) [almost no risk of hydrogen explosion]*

The released hydrogen directly goes up with flow already developed with steam, and flows down at the ceiling wall surface. The amount of hydrogen release is reduced rapidly from 6000s. The flow velocity is reduced further at 7000s, and the flow motion mainly governed by buoyancy and diffusivity. Most of the hydrogen moves to the top of the containment but there is already occupied with over 80% of steam. Therefore the possibility of hydrogen explosion is very low at this stage (Fig. 2.6).



**Fig. 2.6** Distribution of hydrogen, steam and air at 7000s

*c) Stage 3: Steam induction with tiny amount of hydrogen induction (7000 - 14,000s) [localized risk of hydrogen explosion]*

In this stage, some steam is continuously released, while the amount of releasing hydrogen becomes very small. The hydrogen which filled the top of containment at 7000s, was replaced by the hot steam at 8000s.

Then the steam pushes down the hydrogen which was distributed at the upper part of containment. The hydrogen layer moves to the bottom part of the containment, and some amount of hydrogen are trapped among the compartments in the lower part of the containment as shown in Fig. 2.7. In the lower part, there is a lot of air beneath the hydrogen layer, therefore, a minor scale of hydrogen explosion may take place at the bottom part of containment.

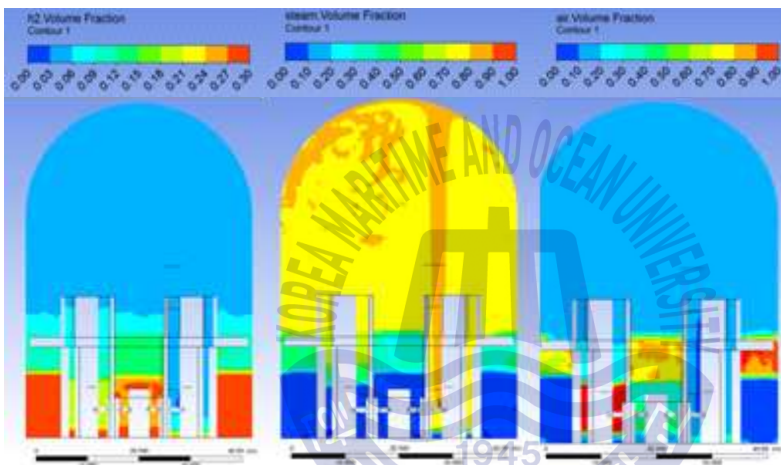
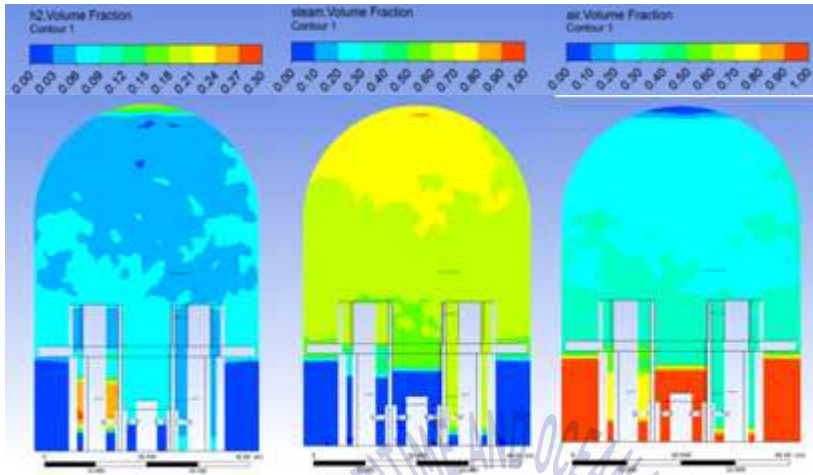


Fig. 2.7 Distribution of hydrogen, steam and air at 14,000s

*d) Stage 4: High temperature metal stable period (14,000 – 33,000s)  
[localized risk reducing of hydrogen explosion]*

There is no inlet gas in the stage. Early of this stage until 20,000s, the hydrogen rises up from the bottom, and the space between compartments, while the steam which was on the top of containment disperse. At this period the upper part of the containment is occupied with over 70% of steam, and a small amount of hydrogen is suspended at the bottom among the compartments as shown in Fig. 2.8. There is

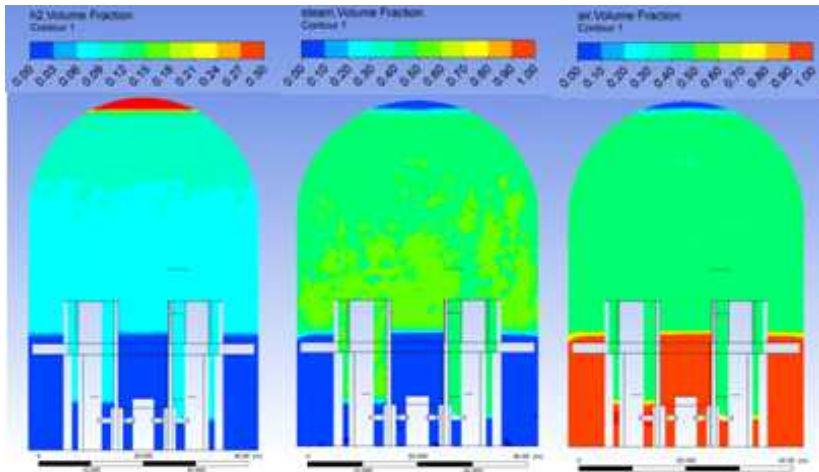
still a risk of localized hydrogen explosion, but the risk is reduced (Fig. 2.9).



**Fig. 2.8** Distribution of hydrogen, steam and air at 20,000s

In the late of this stage from 20,000s, a layer of hydrogen cloud is formed on the top of the containment building with hydrogen rising. Hydrogen distributions overall in the middle of the containment, steam concentration is reduced, and air concentration is increased slowly. But still over 60% of steam occupied the middle area which acted as a barrier between hydrogen and air.

The hydrogen explosion risk is reduced in this stage because the hydrogen concentrated between the compartments rises up and distribute widely over the containments.



**Fig. 2.9** Distribution of hydrogen, steam and air at 33,000s

*e) Stage 5: Hydrogen contact with air (after 33000s) [High risk of hydrogen explosion]*

The air which rises up with hydrogen distributes in the middle of containment, and the concentration is increased up to 90 vol% locally. Hydrogen gas layer is continuously increased on the top of the containment, and the large amount of steam underwent condensation process and the steam was pushed down by hydrogen and rising air.

A large amount of hydrogen makes a thick layer at the top and large amount of air beneath the hydrogen layer in this stage (Fig. 2.10). Therefore, a massive scale of hydrogen explosion might be took place as the hydrogen could contact with large amount of air.

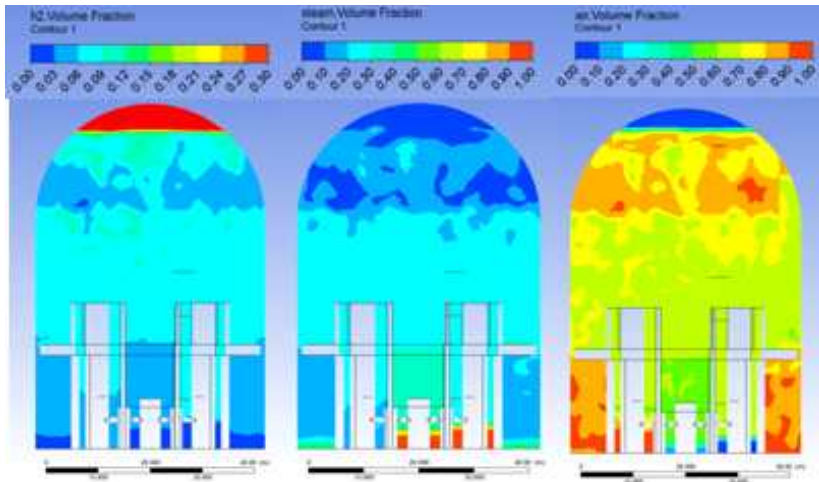


Fig. 2.10 Distribution of hydrogen, steam and air at 54,000s

#### 2.4.2 Gas concentration and explosion risk

Fig. 2.12 shows gas volume fractions and their variation with time from the accident at the monitoring points given in Fig. 2.11. The flammability limits based on the volume percent of hydrogen are 4.0 to 75.0. The limits of detonability of hydrogen in air are 18.3 to 59% by volume.

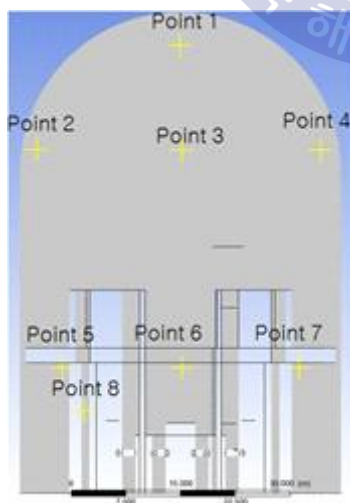


Fig. 2.11 Monitor points of gas concentration

Point 1 is located at the top of the containment, the gas composition was 75 vol% of steam, 15 vol% of hydrogen and 15 vol% of air at 6000 s. Soon after the location is filled with over 90 vol% of steam followed by rapid reduction of hydrogen release. The hydrogen remains less than 5% until 20,000s, and then increased slowly. Air concentration increases continuously, while steam decreases. The gas concentration values indicate nothing explosion until 29,000s, then the conditions got into burn limit regime and enter detonation regime at 48,000s, as shown in Fig 2.13, which means that hydrogen explosion (brown region) might be take place at the top of containment.

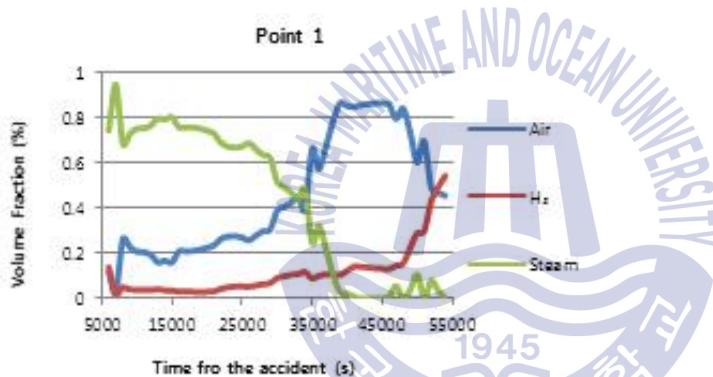


Fig. 2.12 Gas volume fractions against time from the accident at place (Point 1)

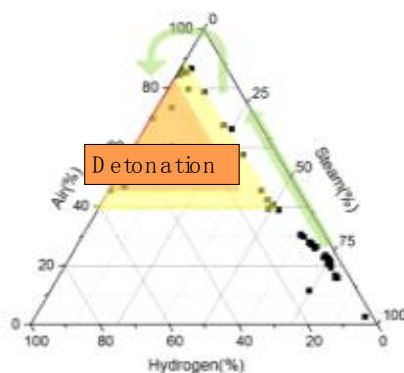
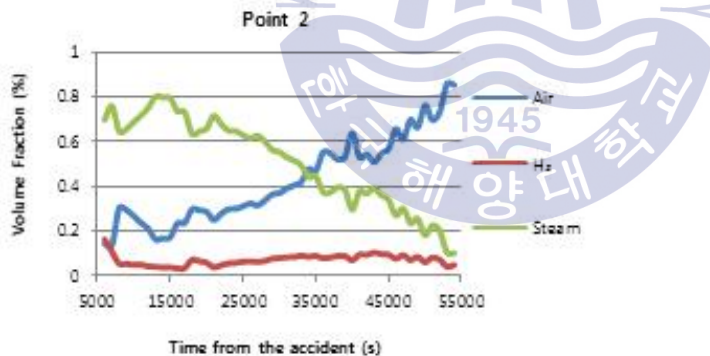


Fig. 2.13 Gas volume fractions and explosions possibility at the top of the containment (Point 1)

Point 2, point 3 and point 4 are located at the middle part of the containment. Point 2 and point 4 are located at the left side and right side of the containment. The gas composition of these 2 points was 68 vol% of steam, 18 vol% of hydrogen and 14 vol% of steam. Point 3 is located at the center of middle part, it has a slightly different gas composition, 78 vol% of steam, 10 vol% of hydrogen and 12 vol% of air. Despite of the locations, the gas composition change is almost same as the accident time continued. The concentration of steam is decreasing while the air is continuously increasing. The hydrogen is increased slowly until it finally exceeds the flammability limit at 32,000 s. This condition remains until 54,000 s with no great elevation of hydrogen concentration. Therefore, it seems that there is almost no risk of hydrogen explosion would take place at the middle part of containment.



**Fig. 2.14** Gas volume fraction against time from the accident at place (Point 2)

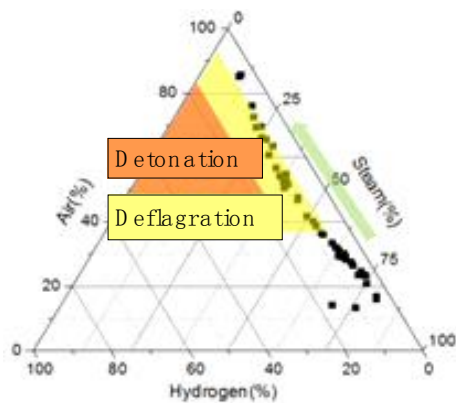


Fig. 2.15 Gas volume fractions and explosions possibility at the middle left part of the containment (Point 2)

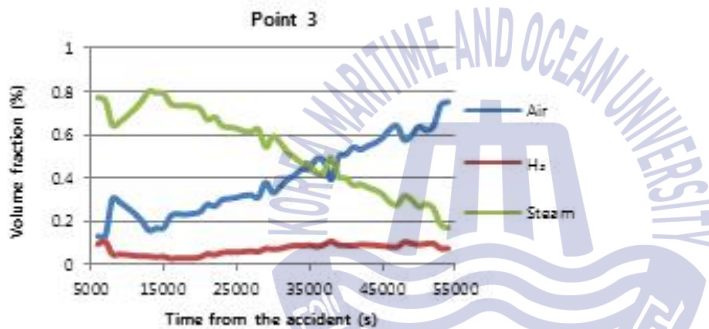


Fig. 2.16 Gas volume fractions against time from the accident was taken place (Point 3)

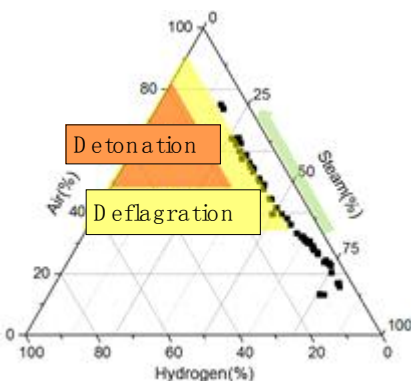
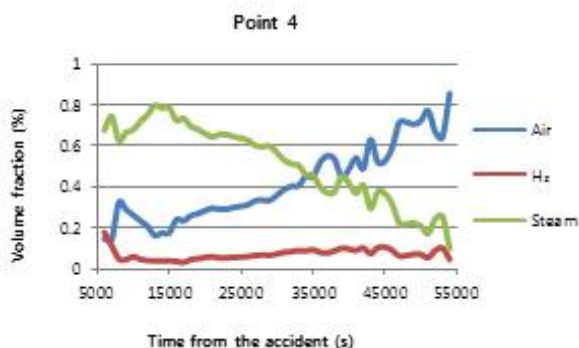
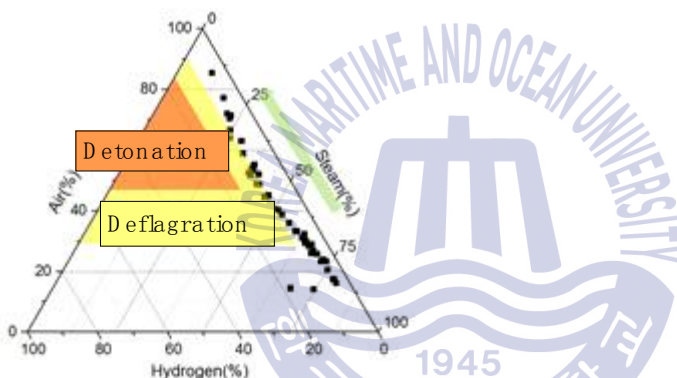


Fig. 2.17 Gas volume fractions and explosions possibility at the middle part of the containment (Point 3)



**Fig. 2.18** Gas volume fractions against time from the accident was taken place (Point 4)



**Fig. 2.19** Gas volume fractions and explosions possibility at the middle right part of the containment (Point 4)

Point 5, point 6 and point 7 are located at the bottom part of the containment. The gas composition is 75 vol% of steam, and 15 vol% of air only. Hydrogen begin appear at the bottom part of containment from 6000s onwards, and rapidly increase to the burning limit and soon reach the detonation limit 10,000 s. At point 7, the hydrogen volume fraction reaches the 30.2 vol% around 14,000 s. From 8000 s until 1,8000 s, the bottom part of containment are associated with multiple chances of hydrogen burning and explosion risk (3 times of hydrogen burn and 2

times of hydrogen explosion), as the concentration of hydrogen fluctuate a few times over the burning limit and the detonation limit.

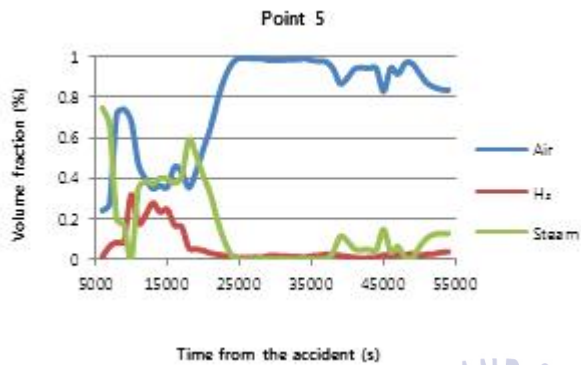


Fig. 2.20 Gas volume fractions against time from the accident was taken place (Point 5)

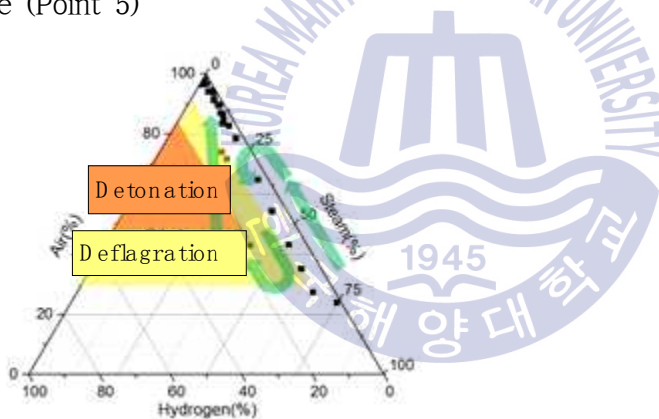


Fig. 2.21 Gas volume fractions and explosions possibility at the bottom left part of the containment (Point 5)

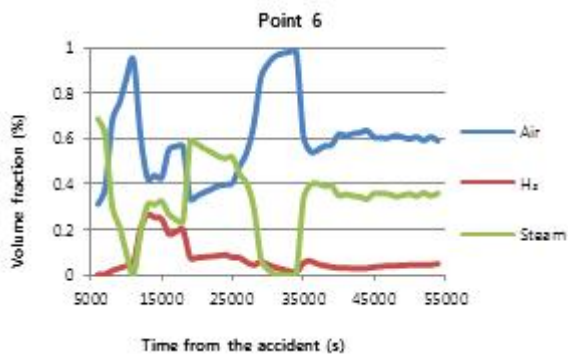


Fig. 2.22 Gas volume fractions against time from the accident was taken place (Point 6)

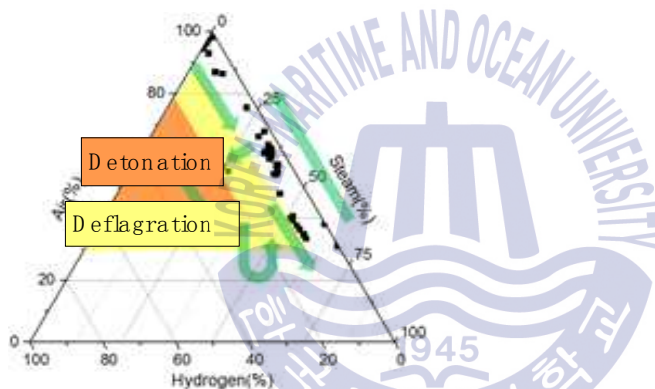


Fig. 2.23 Gas volume fractions and explosions possibility at the bottom center part of the containment (Point 6)

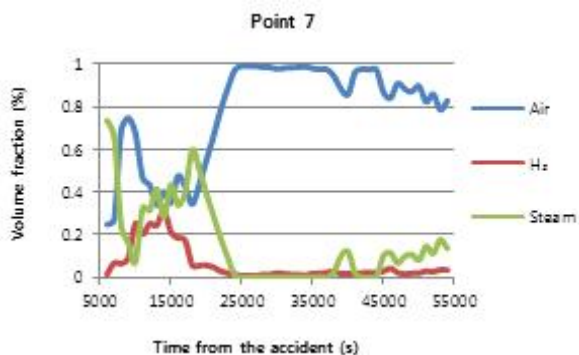
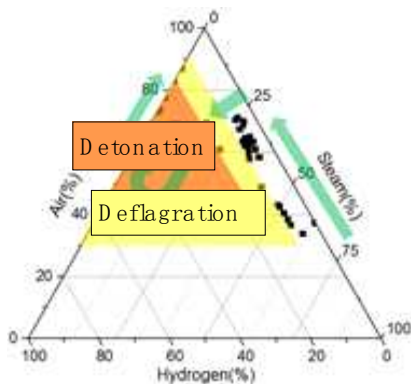
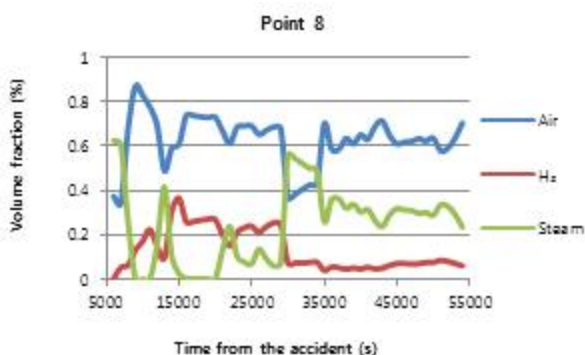


Fig. 2.24 Gas volume fractions against time from the accident was taken place (Point 7)



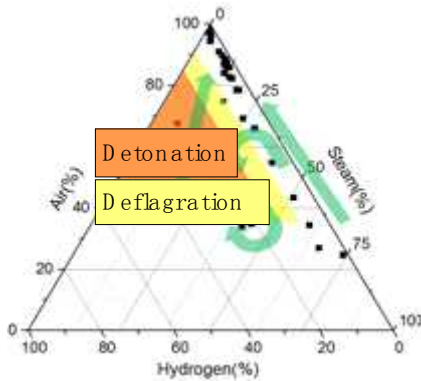
**Fig. 2.25** Gas volume fractions and explosions possibility at the bottom right of the containment (Point 7)

Point 8 is located at the bottom compartment of the containment. At 6000 s, the gas composition is 63 vol% of steam, 37 vol% of air and 0 vol% of hydrogen. The hydrogen volume begin to increase at point 8 area from 6,000 s until 30,000 s, it has over the burning limit. Meanwhile the air volume fraction at the point 8 is always higher than 35 vol% and the steam volume fraction was rather low to act as an insulator. It provides a favorable condition for burning and explosion. From 6000 s until 30,000 s, there are possible 3 times of hydrogen burning and 3 times of hydrogen detonation would take place.



**Fig. 2.26** Gas volume fractions against time from the accident was taken

place (Point 8)



**Fig. 2.27** Gas volume fractions and explosions possibility at the bottom compartment part of the containment (Point 8)

### 2.4.3 Hydrogen combustion scenario

- Stage 1: no hydrogen released until 4800s, there is no risk of hydrogen explosion
- Stage 2: a sharp increase of hydrogen volume in the containment, but hydrogen is induced in the steam cloud, hydrogen has no contact with air. Therefore, there is almost no risk of hydrogen explosion in this stage
- Stage 3: a minor scale of localized hydrogen explosion may take place at the compartment part of the containment, due to some amount of hydrogen with large amount of air are accumulated there.
- Stage 4: reduced risk of localized hydrogen explosion as some amount of hydrogen begins to disperse away from the compartment but a small amount still suspended around the compartment.
- Stage 5: very high chances of hydrogen explosion may take place at the top of containment, where a rich hydrogen layer formed could

contact with large amount of air which rises from the bottom of containment (Table 1)

**Table 2.1** Hydrogen explosion scenario chart

Stage	1	2	3	4	5
Simplified gas distribution chart					
Description	No risk of hydrogen explosion (only steam is released in this stage)	Almost no risk of hydrogen explosion (hydrogen released in steam cloud, no contact with air)	Possibly risk of localized hydrogen explosion (a minor scale of hydrogen explosion may take place at the bottom part of containment)	Reduced risk of localized explosion (a small amount of hydrogen suspended around the compartment, could have contact with air)	High risk of hydrogen at the top of the containment, where hydrogen layer formed could contact with large amount of air would lead to a massive scale of hydrogen

## Chapter 3 Proposal and analysis of hydrogen mitigation system guiding hydrogen in containment

### 3.1 General

This study is about hydrogen mitigation system in a containment building like offshore or nuclear plant. A hydrogen explosion is possibly happened after condensation of steam, if hydrogen released with steam in a containment buildings. Passive autocatalytic recombiner is the one of the measures, but the performance of this equipment is not sure, because the distribution of hydrogen is very irregular and is not predicted correctly. This study proposes a new approach to improve the hydrogen removing performance with hydrogen-guiding property. The steam is simulated and analysed. The results show that the shallow air containment reduced over 55% of the released hydrogen and the deep air containment type reduces over 80% of released hydrogen.

### 3.2 Introduction

Many works have been done to reduce hydrogen risk in a containment building, for example, pre-inerting, post-accident inerting, post-accident dilution, passive auto-catalytic recombiner (PAR), igniter, catalytic recombiner and igniter (dual concept), post accident dilution (PAD) and catalytic recombination, containment atmosphere dilution by inert gas injection and catalytic recombination. engineered mixing and deliberate ignition [26].

The selection of measurement for hydrogen mitigation is highly plant specific. Certain containment designs preclude the implementation of other measures [27]. Furthermore, each type of the various measures has the strength and weakness [28]. There is not only single strategy or technique that is universally appropriate for all designs and accident scenarios [29], or even for all phases of an accident in a particular design [30].

PARs are widely equipped in numerous containments of European light water reactors (LWR) [31]. PAR is so-called because require no external power input to run function. They are self-starting and self-feeding [32]. The material most commonly used in PAR as the catalysts are platinum or palladium, due to its ability to absorb hydrogen and oxygen [33]. It has been proven ability to reduce the deflagration or detonation risk.

Hydrogen is a burnable gas, which means that is reacts chemically with water to form steam:  $2\text{H}_2 + \text{O}_2 \rightarrow 2\text{H}_2\text{O}$

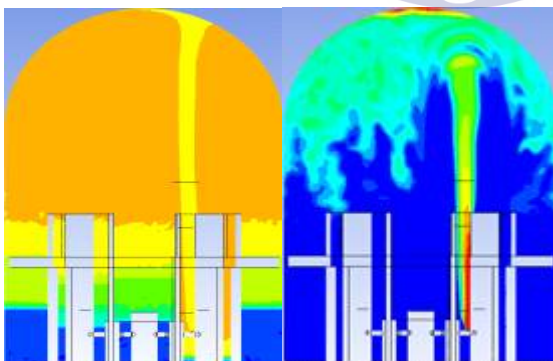
This chemical reaction releases energy in the form of heat. The lower heat of combustion amounts of 120kJ per gram of hydrogen. In an accident situation in a nuclear power plant, combustion will usually occur in a premixed “cloud”. consisting of hydrogen, air, usually steam, and even other gases [34]. Although hydrogen is a burnable gas, it does not ensure that it will burn immediately when mixed with oxygen. For a combustion to take place, the physical phenomenon has to be triggered by some initiating events: ignition and a favorable condition. The physical condition that defines the conditions is a gas cloud, necessary for the sustainability of hydrogen combustion, is the composition [35]. The ranges of species concentrations within which the cloud is burnable are called “flammability limits” There is a “lower flammability (a necessary minimum concentration of burnable gas), and a “higher flammability

limits“ (a maximum concentration of burnable gas, as the mixture should also contain a sufficient amount of oxidant).

Potential risk could be reduced based on the “lower flammability limits“ theory. Therefore, the PAR was designed to convert the hydrogen gas in the containments, in order to keep the hydrogen concentration under “lower flammability limits“ [36]. The PAR works spontaneously as soon as the hydrogen concentration begins to increase in the atmosphere [37]. The recombination reaction occurs spontaneously at the surfaces, and the water vapor as a product of reaction through the recombiner as natural convective flow currents promote mixing of combustible gases in the containment [38].

However, PAR must be placed on existing hydrogen and reaction air. If not, PAR is not working. Previous work submitted in Journal of Nuclear Engineering and Design showed that hydrogen distribution is irregular and dependent on failure locations, and air is not sufficient for recombination process as shown in Fig. 3.1 [39].

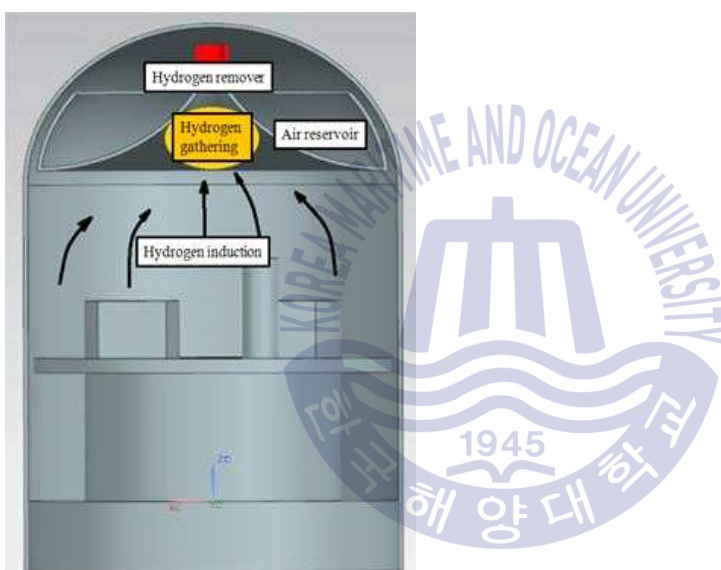
This study proposes a new system design to remove hydrogen effectively, and analyses of its performance.



**Fig. 3.1** Steam and hydrogen volume fraction distribution in a containment

### 3.3 Proposal of a mitigation system

A new concept design of hydrogen mitigation system actively controlled hydrogen distribution as shown in Fig. 3.2. The hydrogen induction may be occurred at any places where accidents happened. The hydrogen need to be gathered and collected at a place, and react with the surrounding air in the air reservoir to produce steam. Therefore, the hydrogen can be removed more effectively.



**Fig. 3.2** A concept design of hydrogen mitigation system actively controlled hydrogen distribution

#### 3.3.1 Simulation conditions

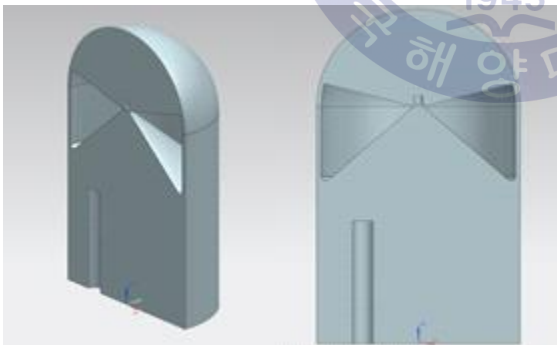
Fig. 3.3 and Fig. 3.4 show the inner shapes of the containment building. The containment building is a cylindrical shape with dome top, and the structure in the lower compartment of the building is removed. The conceptual idea of an air reservoir space is added and hydrogen remover are added at the top of the containment. The air reservoirs are

given as two different types of shallow air reservoir (Type I) and the deep air reservoir (Type II) which depths are 12m and 18m respectively.

The diameter and the height of the building are 22m and 80m respectively. The total number of grids is 2,700,000 and the grids are generated using NX7.5 and ICEM-CFD nodes. The grids are densely generated near the hydrogen removal to reduce error from high velocity and high pressure gradient.



**Fig. 3.3** Inner shapes of Type I shallow air containment type



**Fig. 3.4** Inner shapes of Type II deep air reservoir air containment

The calculation conditions are given in Table 3.1. There are four different situation of hydrogen released amount of 120kg, 200kg, 300kg and 440kg in order to compare the performance of new concept design

hydrogen mitigation system.

**Table 3.1** Test condition

Initial conditions	Temperature		298K
	Pressure		1atm
	Gas velocity		0 m/s
	Gases		Air 100%
Inlet conditions	Temperature		800K
	Steam flow-in	Duration	0s – 8000s
		Total mass	16000kg
	Hydrogen flow-in	Duration	6000s – 8000s
		Total mass	120 – 440kg
Calculation models	Turbulence		Shear stress transport model
	Buoyancy		Buoyant model
	Fluid specific model		Density difference model
	Fluid pair model		Mixture model

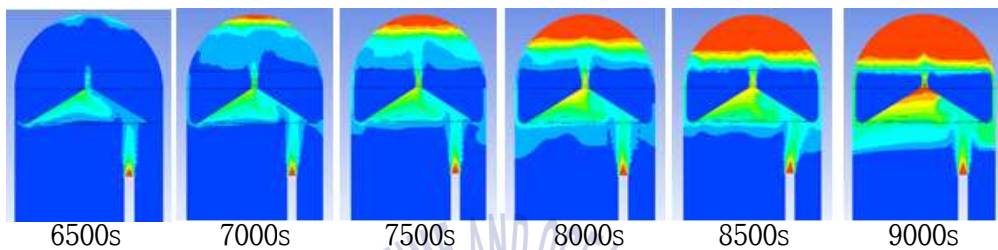
### 3.4 Results and discussion

#### 3.4.1 Gases behaviors in the shallow containment (Type D)

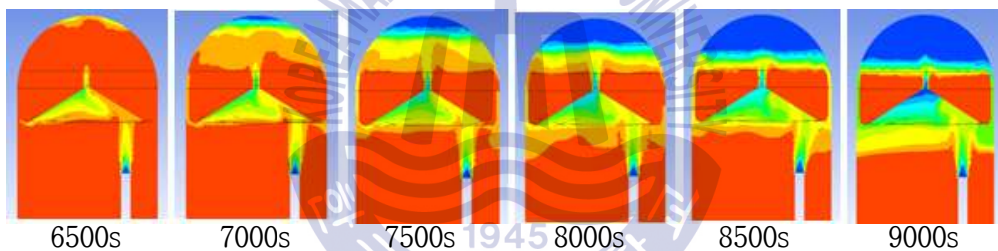
Fig. 3.5 shows the steam and air behaviors during steam release from the steam release beginning (0s) until hydrogen release beginning (6000s). It is assumed that the leakage failure occurs at the lower area of the containment. Most of the hot steam released from the leakage opening was gathered by guidance wall and went through the center hole and the steam was accumulated from the top of the containment

building. Steam began to be accumulated at the top of the containment building from 2000s, which is shown as red color in the figure. Until the 6000s, the steam was accumulated from the hydrogen removal part, and was also accumulated under the guidance wall, while air was remained in the air reservoir.

(a) Steam



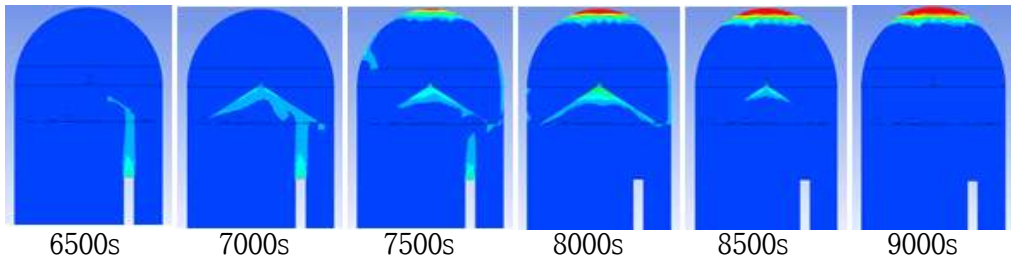
(b) Air



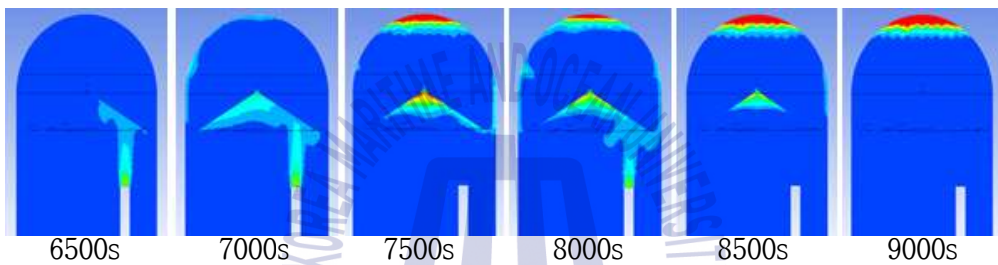
**Fig. 3.5** Steam and air volume

Fig. 3.6 shows hydrogen behaviors during hydrogen release in the case of the total released mass of 120 - 440kg. Hydrogen began to release at 6000s and gradually increased its volume fraction. Some part of hydrogen went up to the hydrogen gathering area through the guiding wall and then to the hydrogen removal part, which hydrogen was removed. The other part of hydrogen went directly up to the top of containment through the gap by the building wall, which hydrogen remained at the top after hydrogen release. The amount of remained hydrogen was increased with the increase of hydrogen release.

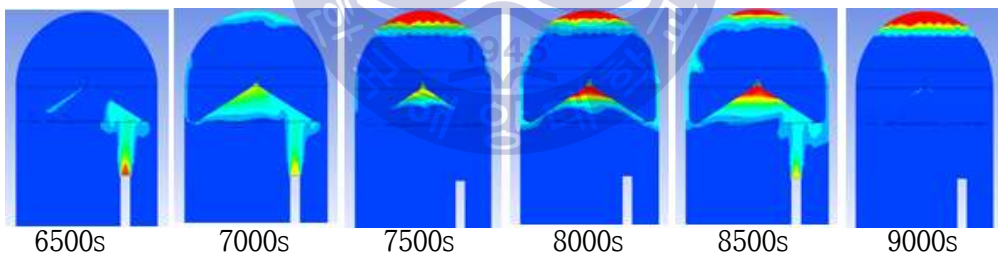
(a) In the case of 120kg release



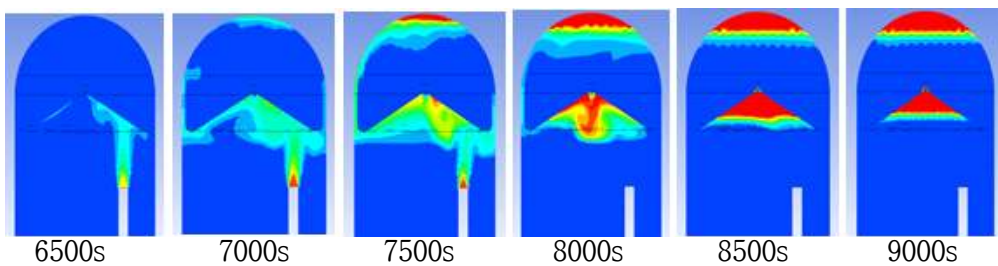
(b) In the case of 200kg release



(c) In the case of 300kg release



(d) In the case of 440kg release



**Fig. 3.6** Hydrogen volume fraction distribution

Fig. 3.7 shows the curves of released hydrogen mass and remaining hydrogen mass in the cases of 120 - 440kg release. Hydrogen release was started at 6000s, and hydrogen was reduced from about 700s when the hydrogen reached on the remover, and then hydrogen was reduced with the time increase. 55-56% of released hydrogen was removed in the cases of 120 - 300kg hydrogen release, but the reduction rate was rapidly reduced to 25% in the case of 440kg hydrogen release.

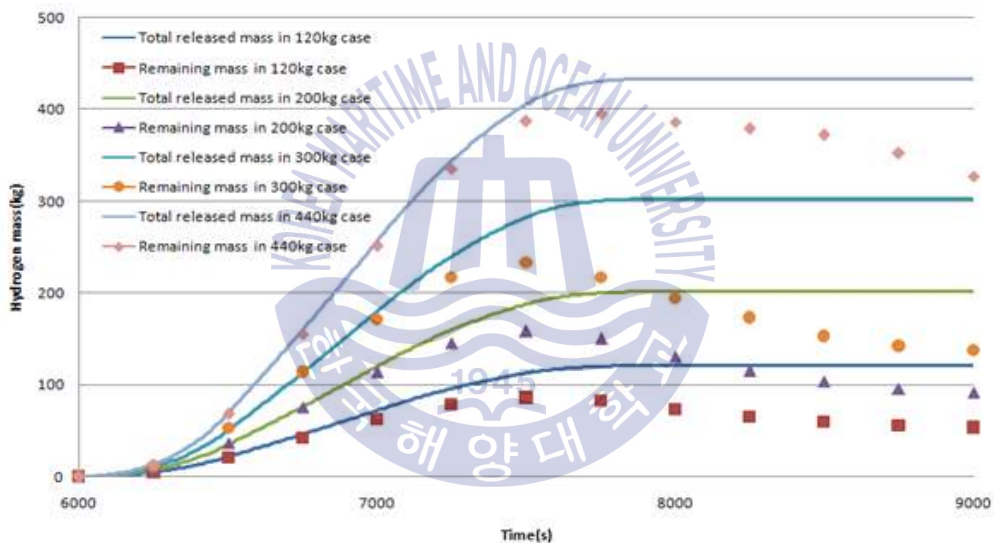


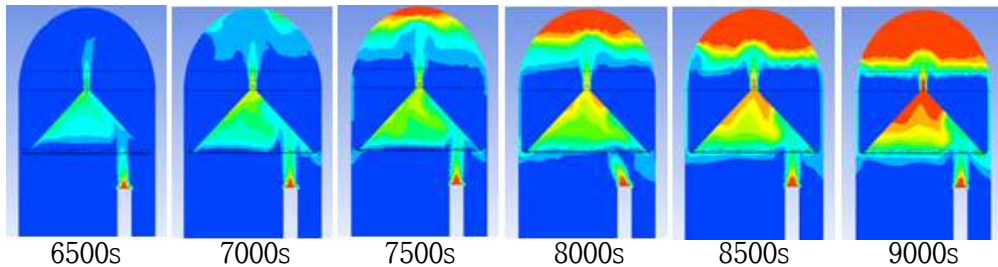
Fig. 3.7 Comparisons of hydrogen released mass and remaining mass

### 3.4.2 Gases behavior in the deep reservoir containment (Type II)

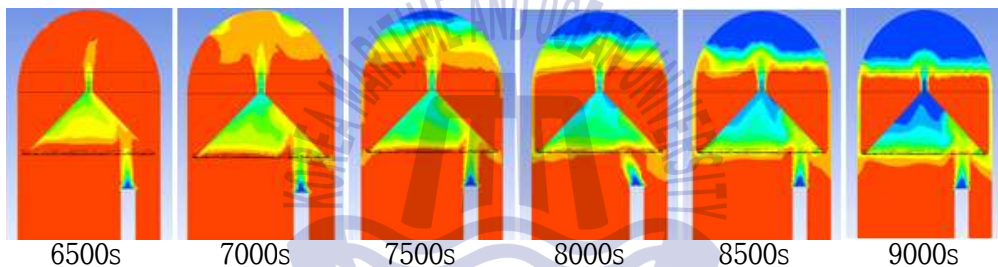
Fig. 3.8 shows the steam, and air behaviors during steam release from the steam release beginning (0s) until hydrogen release beginning (6000s) in the deep hydrogen guiding type (Type II). The steam release condition from inlet is the same as that in the case of shallow guiding type (Type I). The steam behaviors of Type I. Most of the hot steam was gathered by guidance wall and went through the center hole and the

steam was accumulated from the top of the containment building, and air was remained in the air reservoir.

(a) Air



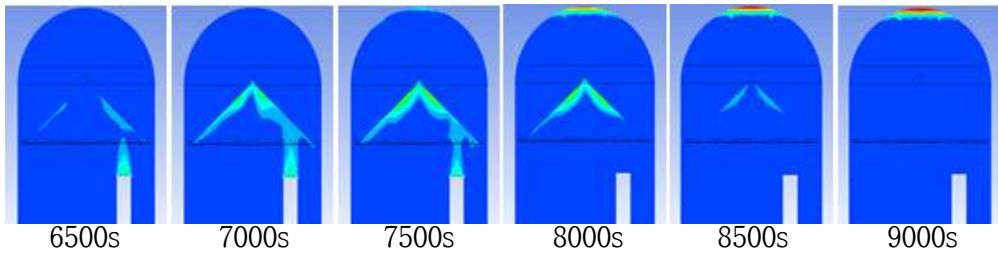
(b) Steam



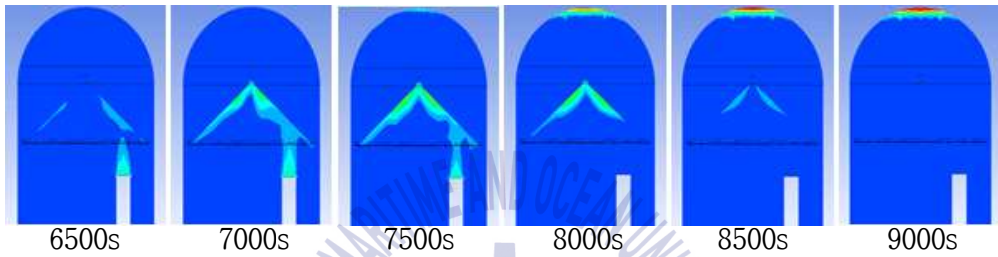
**Fig. 3.8** Steam and air volume distribution

Fig. 3.9 shows hydrogen behaviour during hydrogen release in the case of the total released mass of 120 - 440kg. Comparing to Type I, more hydrogen went up to the hydrogen gathering wall and then to the hydrogen removed by hydrogen remover. The other part of hydrogen which went directly up to the top of the containment through the gap between air reservoir and building wall was also reduced rapidly.

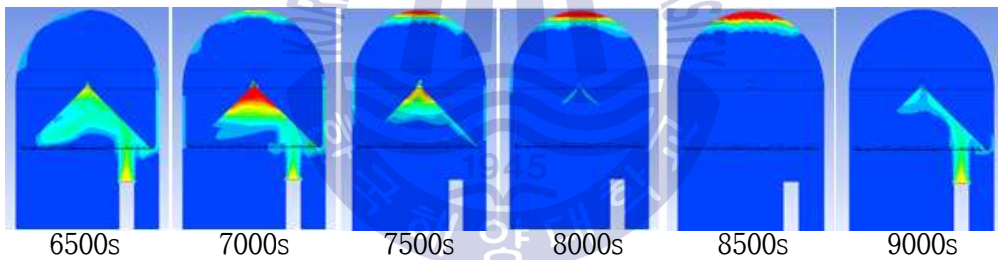
(a) In the case of 120kg hydrogen release



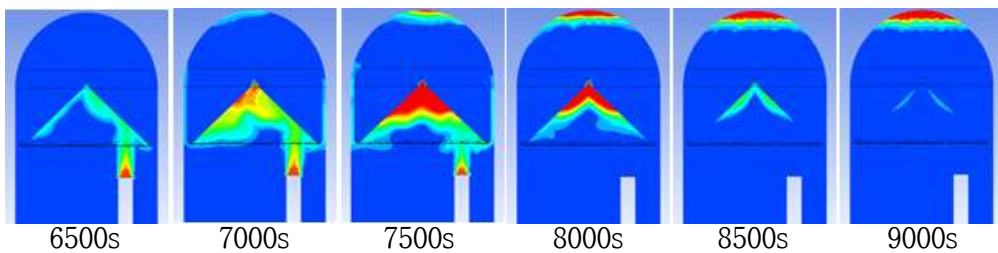
(b) In the case of 200kg hydrogen release



(c) In the case of 300kg hydrogen release



(d) In the case of 440kg hydrogen release



**Fig. 3.9** Hydrogen volume fraction distribution

Fig. 3.10 shows the curves of released hydrogen mass and remaining hydrogen mass in the cases of 120 - 440kg release. Remaining hydrogen

curves are reduced with the time increase, which is similar to Type I, but the reduction rate were much rather than those in Type I.

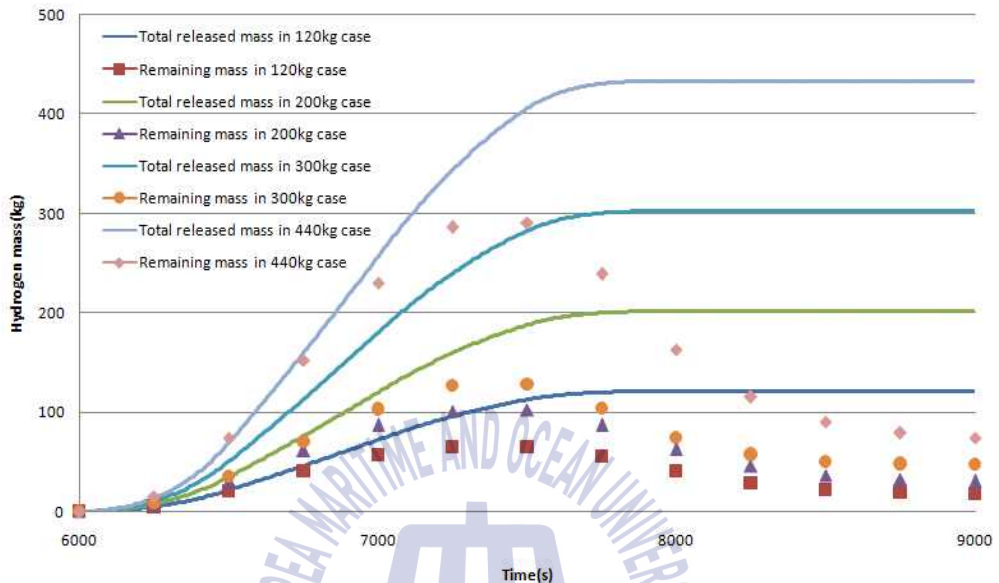


Fig. 3.10 Hydrogen mass reduction graph

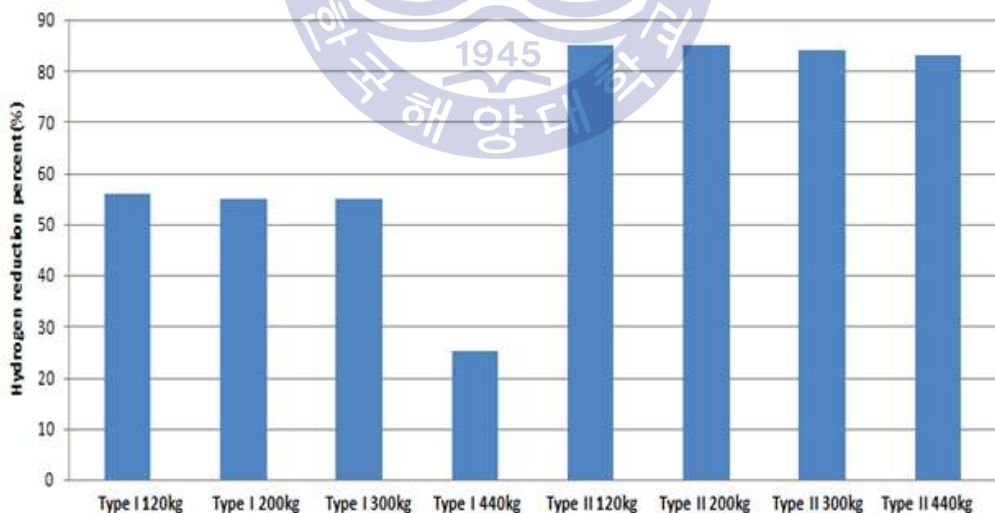


Fig. 3.11 Total reduction percentage in every scenarios of hydrogen released

Fig. 3.11 shows the final percent of hydrogen reductions in the two cases of Type I and Type II with various conditions of hydrogen release amount. In the cases of Type I which have shallow reservoir space, about 55% of total released hydrogen was reduced in the conditions of 120kg to 300kg release, but only 25% was reduced in the condition of 440kg release, because of much hydrogen went through the gap between guidance and wall which led to lower recombination rate at the end. While in the case of Type II which have deep reservoir space, over 80% of total released hydrogen was reduced in all the conditions of 120kg to 440kg release, which means the deep reservoir space is a more favorable condition for the hydrogen recombination process.



## Chapter 4 CFD analysis of the effect of different PAR locations against hydrogen recombination rate

### 4.1 General

Many studies have been conducted on PAR performance, but there are not many on the locations. During a severe accident in nuclear reactor containment, a large amount of hydrogen amount can be produced and soon released into the containment then lead to hydrogen deflagration or detonation. Passive autocatalytic recombiner (PAR) is one of the hydrogen mitigation methods which widely implements in current and advanced light water reactors. Therefore in this study, PAR is installed at different locations in order to investigate the difference of hydrogen reduction rate. The comparison results have shown hydrogen reduction rate of PAR which is proportional to the distance with the hydrogen induction location.

### 4.2 Introduction

The potential danger of hydrogen was first identified after the Three Mile Island accident in 1989, where a large quantity of hydrogen was released into the containment and started combustion. Since then, numerous studies have been taken to mitigate and reduce the potential risk of hydrogen. Recently, the hydrogen explosions during the Fukushima Daiichi accident in March 2011 have showed somehow, that the control and mitigation of the hydrogen risk is still a key safety issue for nuclear power plant [40].

During a loss of coolant accident (LOCA), hydrogen may accumulate within the containment of a nuclear power plant. The hydrogen could result from (i) metal-water reaction involving the zirconium fuel cladding and the reactor coolant; (ii) radiolytic decomposition of water, which will produce oxygen also; and (iii) corrosion of construction materials [41]. Hydrogen is then induced to the reactor coolant system and gradually the entire containment. Assuming the internal conditions of the containment, such as the quality of steam and air present, a flammable gas mixture might combust to generate chemical and thermal load with a potential threat to containment integrity [42,43,44].

Catalytic reaction is widely used due to its lower threshold temperature for the spontaneous catalytic reaction compared to the non-catalyzed reaction. Passive autocatalytic recombiners (PAR) are currently implemented in many modern pressurized water reactors (PWRs) as particular engineered safety feature for mitigating risk in the event of a core melt-down accident accompanied by significant releases of hydrogen gas into the reactor containment [45,46]. The catalyst materials are made of platinum and/or palladium as the catalyst to recombine hydrogen and oxygen gases into water vapor upon contact with the surface of catalyst. Hence, the heat produced during the recombination process creates strong buoyancy effects which raise the influx of surrounding gases to the PAR inlet [47].

Generally, catalysts have been developed in the shape of plate or pellet. For example, the PAR manufacturers like AREVA and AECL utilized plate type catalyst while NUKEM invented a specialized cartridge containing pellet type catalysts. KNT has developed a distinctive PAR model with enhanced hydrogen removal capabilities. The new catalyst

model adopted a larger surface area and the characteristic to enhance the buoyancy-induced convective flow.

Korea Nuclear Technology (KNT) Inc. has developed a PAR model with enhanced hydrogen removal capabilities. The new model adopted the shape of honeycomb, to create a greater catalyst surface area and the enhancement of buoyancy-induced convective flow [48]. The KNT PAR is a stainless housing equipped with catalysts inside the lower part of the box. The design of nuclear containment may caused some hydrogen amount trapper in the containment and unable to be reduced by the mitigation equipment. Therefore, the location where the PAR was installed will indirectly affect the PAR performance. Hence, the residual amount of hydrogen in nuclear power plant will be remained and become a potential risk for the future hydrogen explosion. This study proposed the PAR is installed at different location in the nuclear containment to investigate and compare the difference of hydrogen reduction.

#### 4.3 Mathematical modeling

This study involves the use of CFD which is a computer-based tool that is widely used for analysis and design process. By utilizing the advances in computing power and graphics, creation and analysis of a certain model is much less labor intensive and cheaper than experimental methods.

ANSYS CFX solves the unsteady Navier-Stokes equation in their conservation form. the instantaneous equation of mass (continuity) in the stationary frame is expressed as the following equation:

$$\frac{\partial \rho}{\partial t} + \nabla \cdot (\rho U) = 0 \quad (4.1)$$

And the instantaneous equation for momentum is expressed as shown in the following equation:

$$\frac{\partial \rho}{\partial t} + \nabla \cdot (\rho U \otimes U) = -\nabla \rho + \nabla \cdot \tau + S_M \quad (4.2)$$

These instantaneous equations are averaged for turbulent flows leading to additional terms that need to be solved. While the Navier-Stokes equations describe both laminar and turbulent flows without addition terms, realistic flows involve length scales much smaller than the smallest finite volume mesh. A Direct Numerical Simulation of these flows would require significantly more computing power than what is available now or in the future.

Therefore, much research has been done to predict the effects of turbulence by using turbulence models. These models account for the effects of turbulence without the use of a very fine mesh or direct numerical simulation.

These turbulence models modify the transport equations by adding averaged and fluctuating components. The transport equations are changed to the following two equations.

$$\frac{\partial \rho}{\partial t} + \nabla \cdot (\rho U) = 0 \quad (4.3)$$

$$\frac{\partial \rho U}{\partial t} + \nabla \cdot (\rho U \otimes U) = -\nabla \rho + \nabla \cdot (\tau - \overline{\rho u \otimes u} + S_M) \quad (4.4)$$

The mass equation is not changed but the momentum equation contains extra terms which are Reynolds stresses,  $\overline{\rho u \otimes u}$  and the Reynolds flux,  $\overline{\rho u \otimes}$ . These Reynolds stresses used to be modeled by additional equations to obtain closure. Obtaining closure implies equations to obtain closure. Obtaining closure implies that there are a sufficient number of equations to solve for all the unknowns including the Reynolds stresses and Reynolds fluxes.

Various turbulence models provide various ways to obtain closure. In this investigation, the model utilized was Shear Stress Transport (SST) model. The advantage of using this model is that combines the advantage of other turbulence models (the  $k-\epsilon$ , Wilcox  $k-\omega$  and BSL  $k-\omega$ ).

The characteristic of the Wilcox model is the strong sensitivity to free-stream conditions. Therefore, a blending of the  $k-\omega$  model near the surface and the  $k-\epsilon$  in the outer region was made by Menter which resulted in the formulation of the BSL  $k-\omega$  turbulence model. It consist of a transformation of the  $k-\epsilon$  to a  $k-\omega$  formulation and subsequently adding the resulting equations. The Wilcox model is multiplied by a blending function  $F1$  and transformed  $k-\epsilon$  by another  $1-F1$ .  $F1$  is a function of wall distance (being the value of one near the surface and zero outside the boundary layer). Outside the boundary layer and on the edge of the boundary layer, the standard  $k-\epsilon$  model is used.

However, while the BCL  $k-\omega$  model combines the advantages of both the  $k-\epsilon$  and Wilcox  $k-\omega$  turbulence models, it fails to properly predict the onset and amount of flow separation from smooth surfaces. The  $k-\epsilon$  and Wilcox  $k-\omega$  turbulence models do not account for the transport of the turbulent shear stress resulting in an over-predicting of eddy viscosity. A limiter on the formulation can be used to obtain the proper results. These limiters are given the next equation:

$$V_t = \frac{a_1 k}{\max(\alpha_1 \omega_1 S F_2)} \quad (4.5)$$

$$\text{Where } V_t = \frac{v_t}{\rho} \quad (4.6)$$

$F2$  is a blending function which restricts the limiter to the wall boundary and  $S$  is the invariant measure of the strain rate.

The blending functions are given by the following two equations:

$$F_1 = \tanh(\arg_1^4) \quad (4.7)$$

$$\arg_1 = \min\left(\max\left(\frac{\sqrt{x}}{\beta_r \omega y_r}, \frac{500v}{y^2 \omega}\right), \frac{4\rho k}{CD_{kw} \sigma_{\omega^2} y^2}\right) \quad (4.8)$$

$y$  is the distance to the nearest wall and  $v$  is the kinematic viscosity.

In addition:

$$CD_{kw} = \max\left(2\rho \frac{1}{\sigma_{\omega^2} \omega} \nabla k \nabla \omega, 1.0 \cdot 10^{-10}\right) \quad (4.9)$$

$$F_2 = \tanh(\arg_2^2) \quad (4.10)$$

$$\arg_2 = \max\left(\frac{\sqrt[3]{k}}{\beta' \omega y'}, \frac{500v}{y^2 \omega}\right) \quad (4.11)$$

## 4.4 KNT PAR calculations

### 4.4.1 Mesh and conditions

A ratio 1:1 mesh was designed referred to the KNT PAR's size, which referred to the research paper. To validate the actual-size designed mesh PAR with the real KNT PAR, a test was brought out and compared with the KNT provided data. A simulation created according to the actually size of KNT integral test facility (ITF). The input conditions of the test were more or less similar to the information obtained from KNT Inc. Therefore we could decided the working properties of the mesh. Fig. 4 shows the conceptual diagram of the ITF. The ITF comprises a carbon steel pressure vessel with an internal volume of 10.8 m<sup>3</sup>. It was constructed to perform performance tests in varying conditions of pressure, temperature, humidity, hydrogen concentration and borated water spray. It has a cylindrical shape with ~2.0 m in diameter by ~4.0 m in height. On the top of the pressure vessel, a

safety valve and a relief valve are installed for the purpose of pressurization protection and vent. On the side are installed a manhole and penetration ports for the instrumentation and the injection of air and hydrogen. They are all composed of stainless steel piping and are sealed with leak tightness in high pressure.

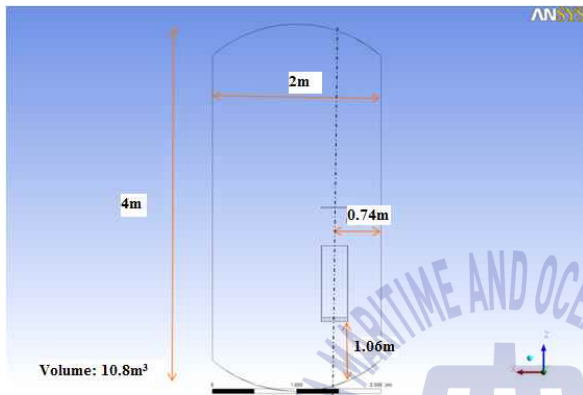


Fig. 4.1 Conceptual diagram of KNT honeycomb model integral test facility (ITF)

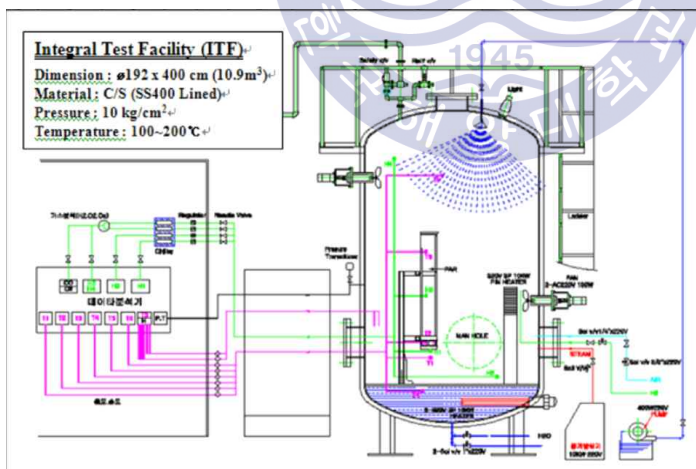
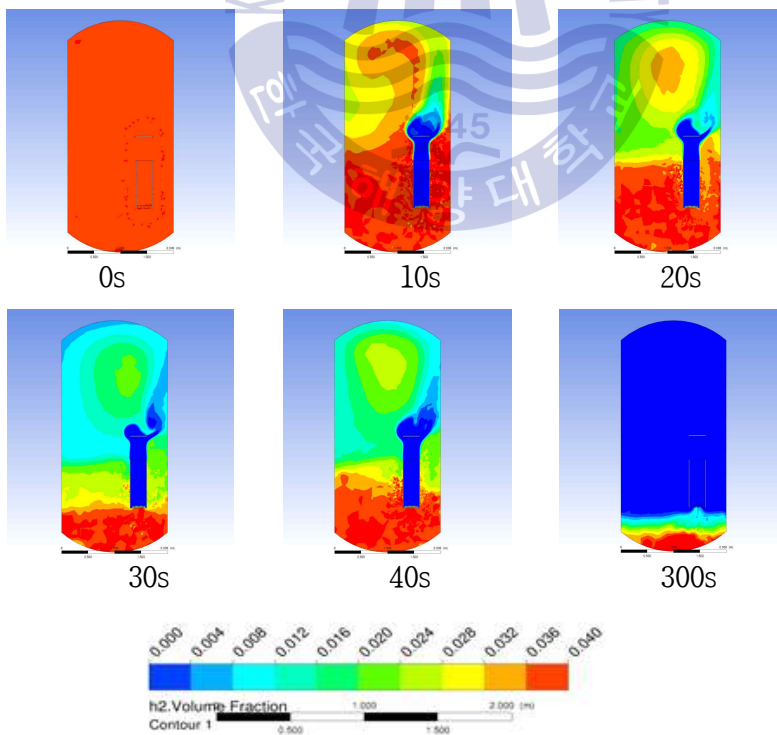


Fig. 4.2 Actual conceptual diagram of KNT integral test facility

#### 4.4.2 Results

The following figures are the results of KNT PAR simulation. The movement of the gases in the containment was moving in a swirling direction and most of the hot steam was accumulated at the top of the containment. The recombination process was continuously going on throughout the experiment but there was a small amount of hydrogen accumulated at the bottom part of containment. The hydrogen in the containment was successfully reduced from 4%, the lower flammability limit and the rest was assumed as oxygen. The experimental mesh was found have a slightly higher recombination rate compared to the KNT PAR, but still reached a same target at the end of the simulation.

**Table 4.1** Hydrogen reduction fraction contour of KNT PAR simulations result (cut plane)



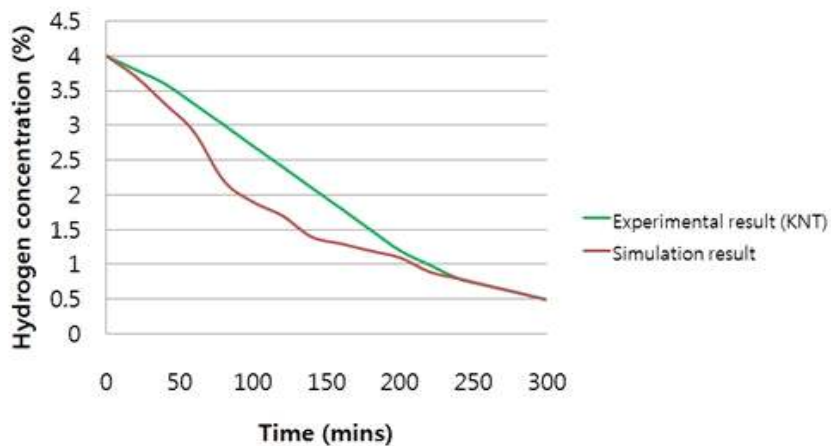


Fig. 4.3 Hydrogen reduction rate comparison

## 4.5 PAR Installed Locations

### 4.5.1 Conditions and mesh

The nuclear containment adopted in this study was merely a square cubic, with the size 5 meter long X 5 meter wide X 5 meter height. The KNT PAR was then placed at the center of the containment, 2 meter from the bottom as the default location. There were only two types of gas in the containment. Hydrogen volume fraction was set as 4% as its lower flammability limit and the rest was assumed as oxygen.

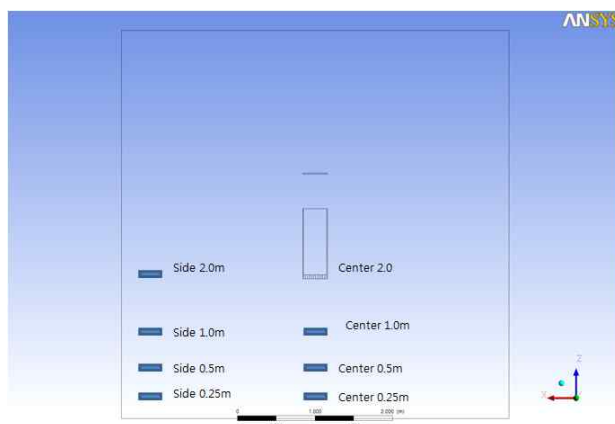


Fig. 4.4 Different locations where the PAR model was installed

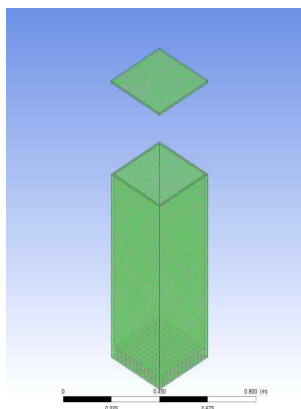


Fig. 4.5 CFX mesh of KNT PAR

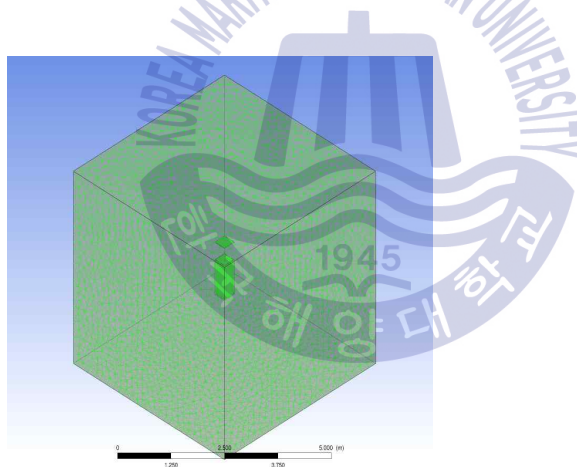


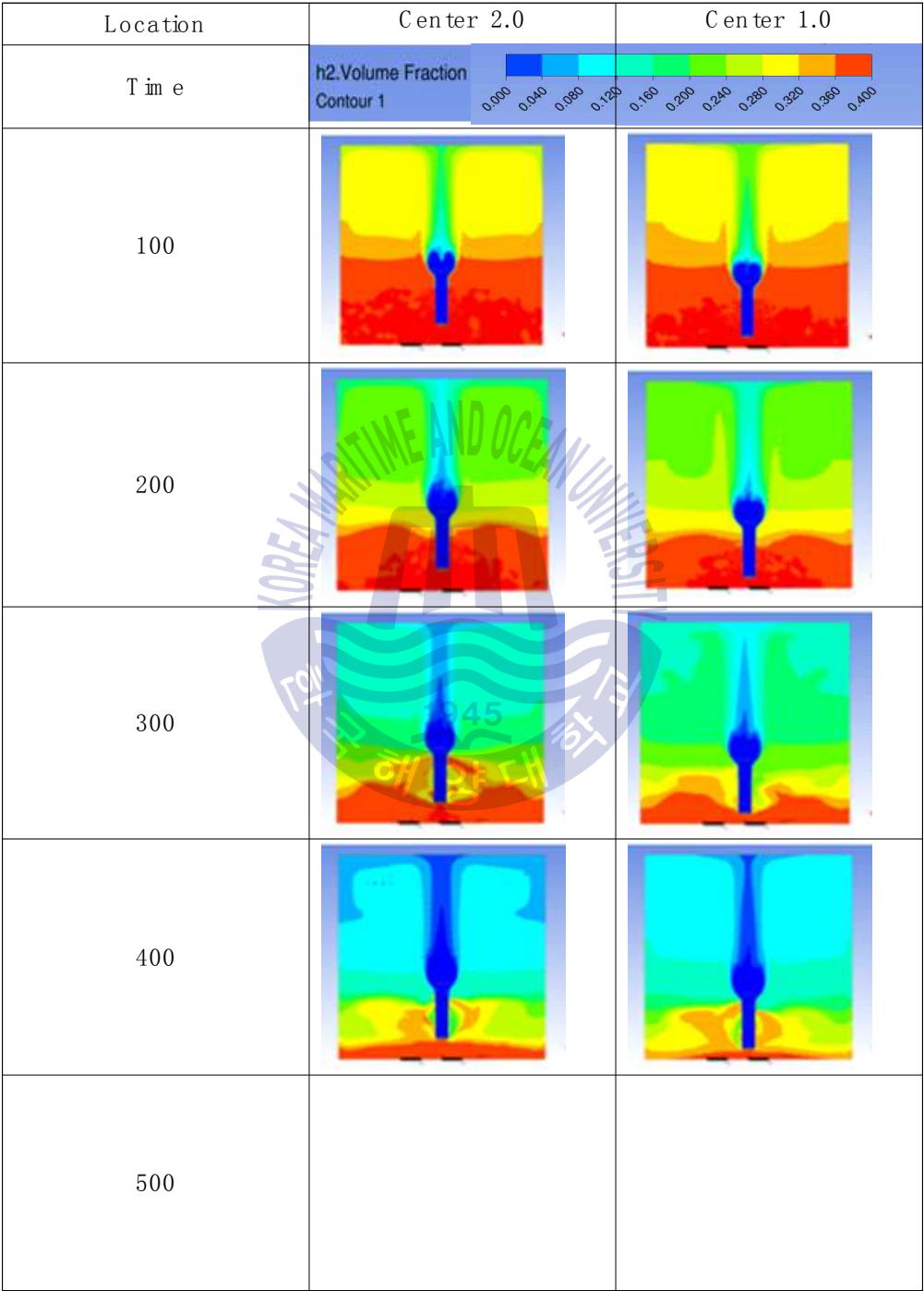
Fig. 4.6 Meshes of the KNT PAR and the containment

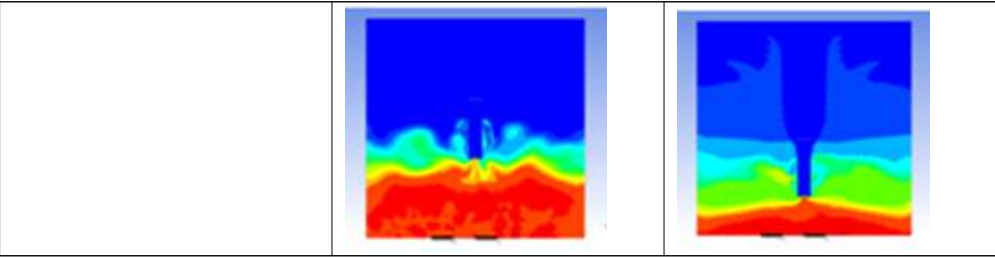
**Table 4.2** Simulation test input condition

Initial conditions	1 bar
Initial temperature	300 K
Initial air volume fraction	0.96
Initial H <sub>2</sub> volume fraction	0.04
PAR location	Center 2.0m, 1.0m, 0.5m, 0.25m
	Side 2.0m, 1.0m, 0.5m, 0.25m

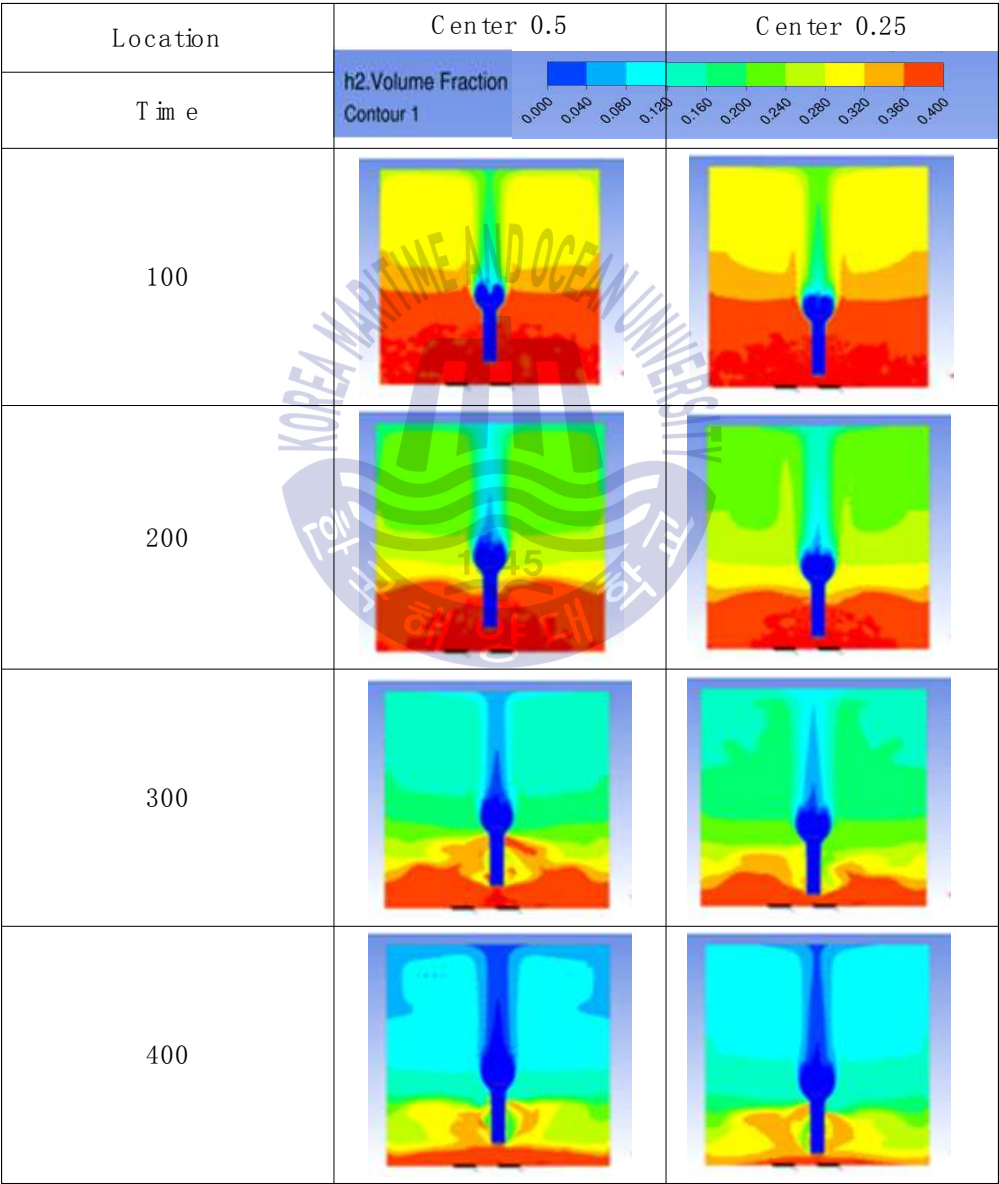
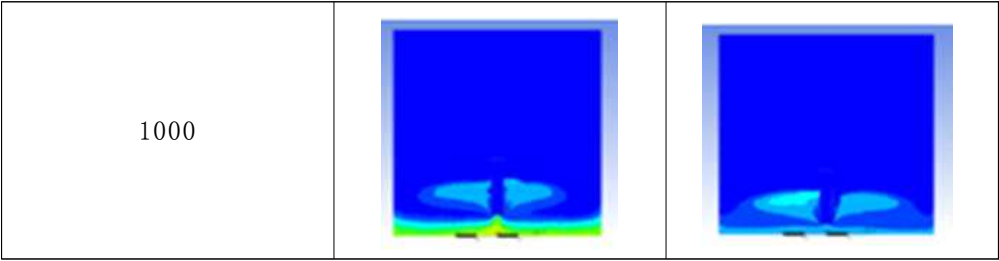
Adiabatic condition is chose as the test condition, which ignore the heat transfer to the compartment walls and also condensation which would result in the mixing of atmosphere.

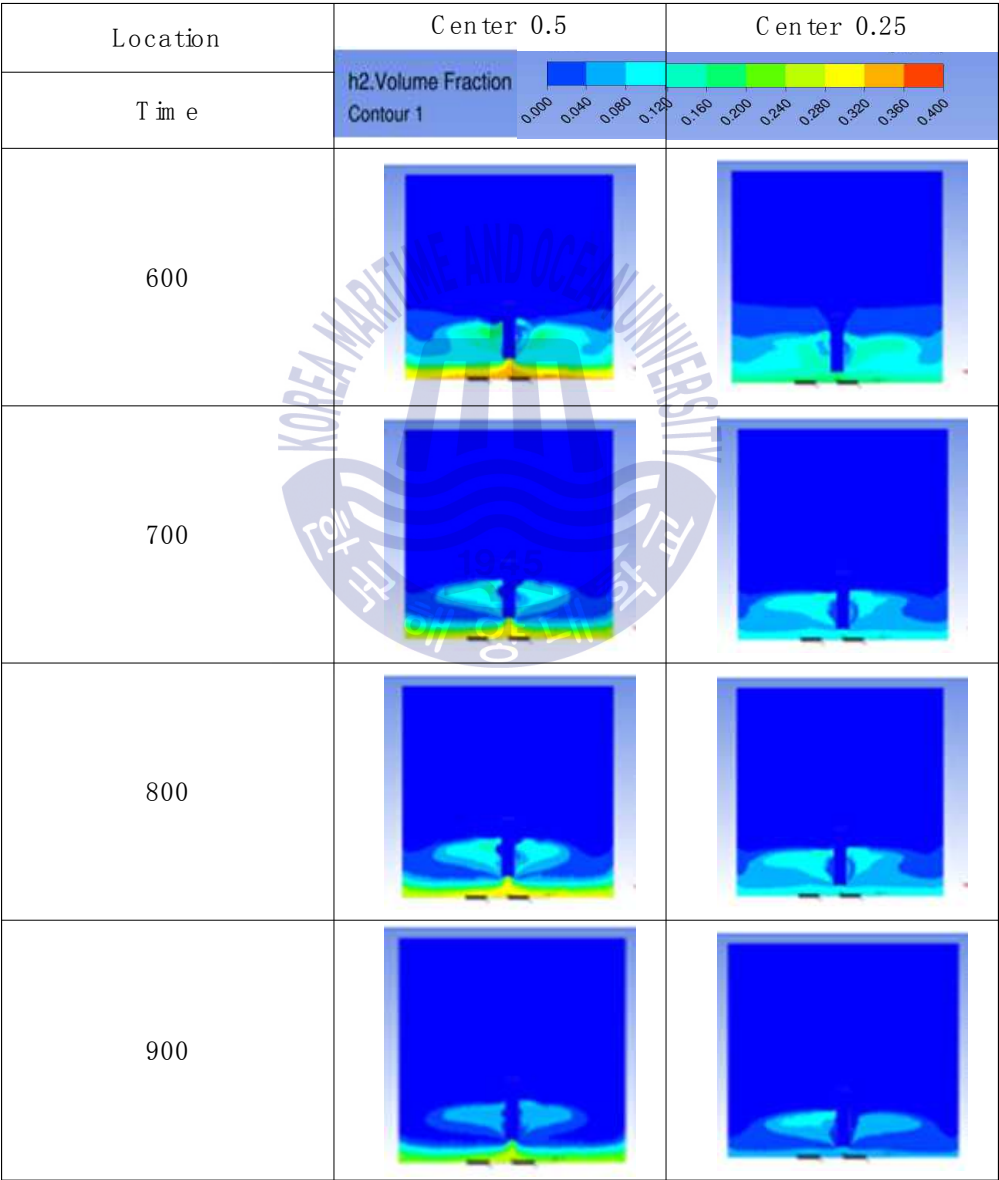
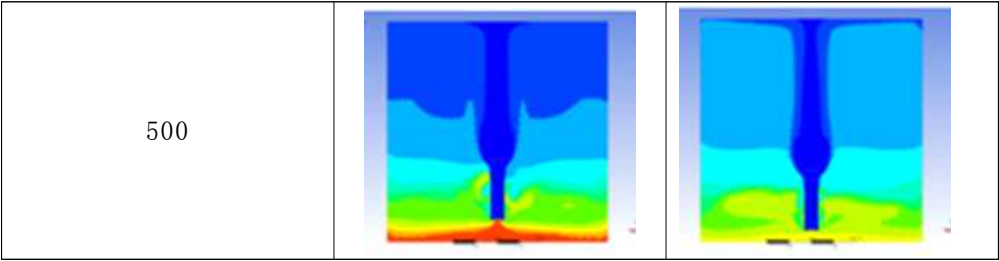
**Table 4.3a** Hydrogen reduction changes in the nuclear containments

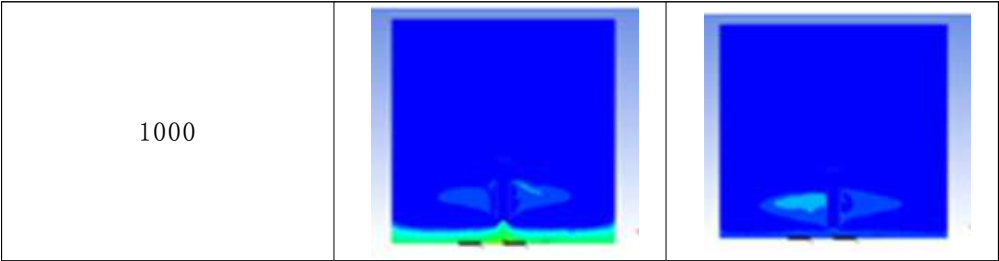




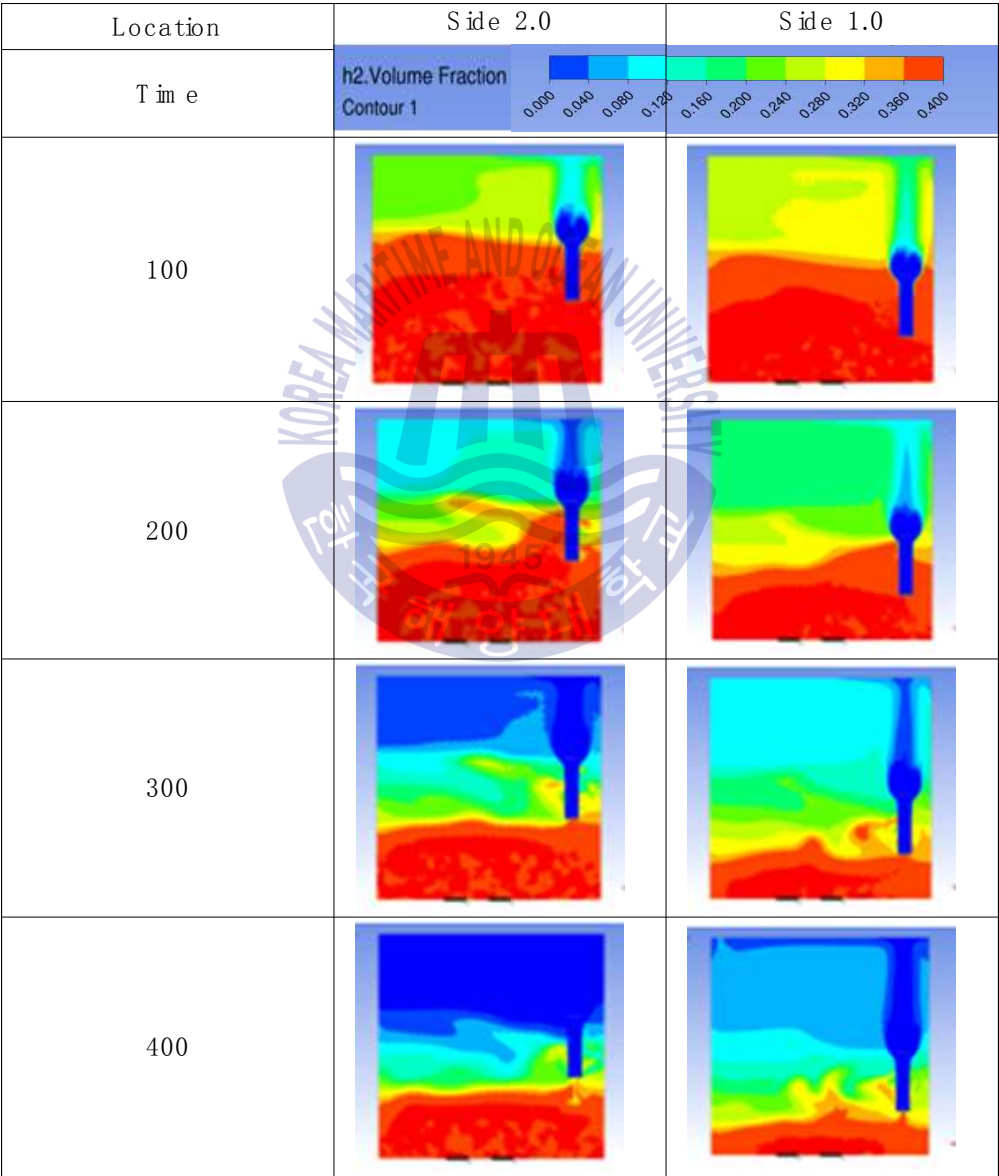
Location	Center 2.0	Center 1.0
Time	<div>h2.Volume Fraction Contour 1</div> <div> </div>	
600		
700		
800		
900		

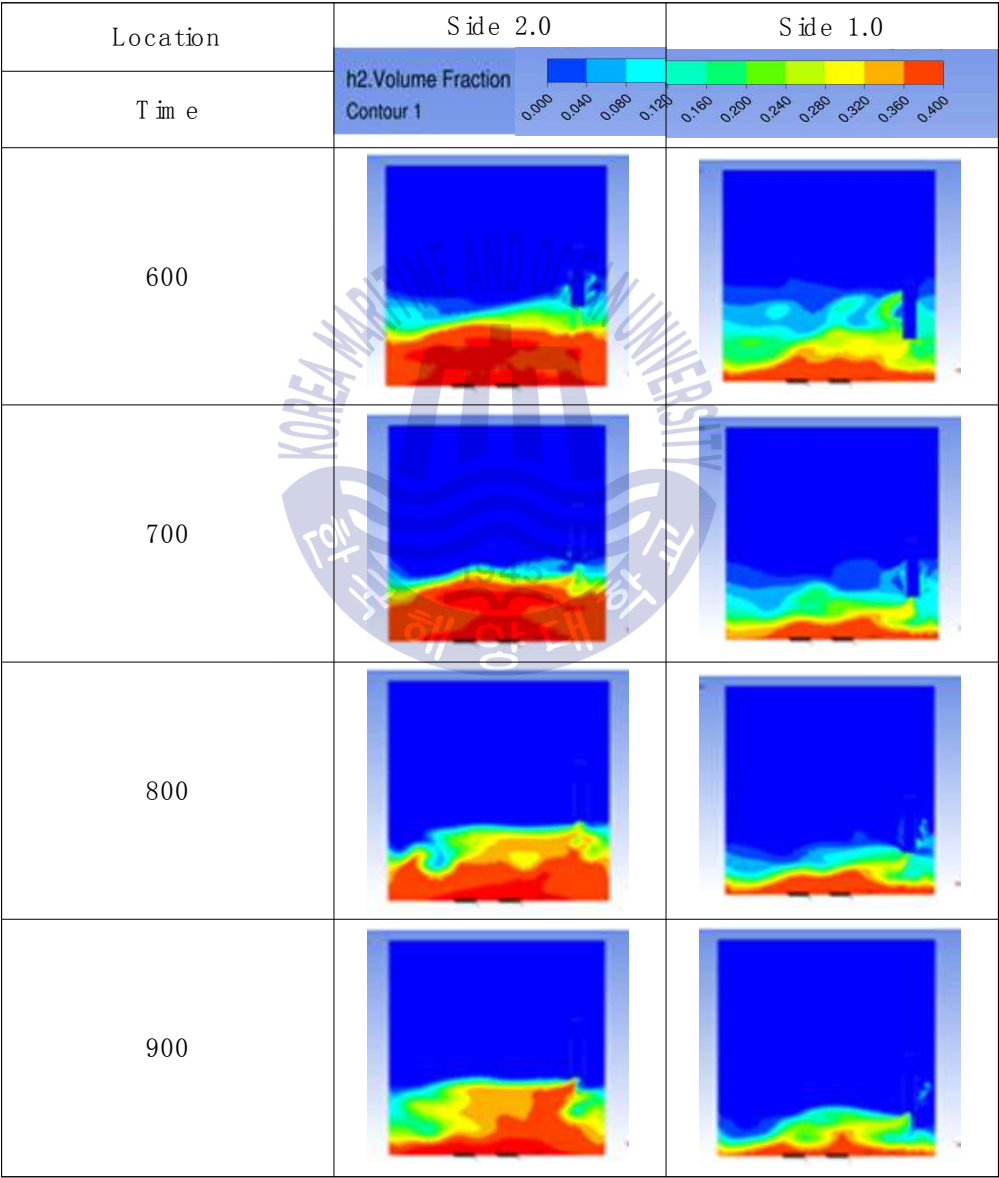
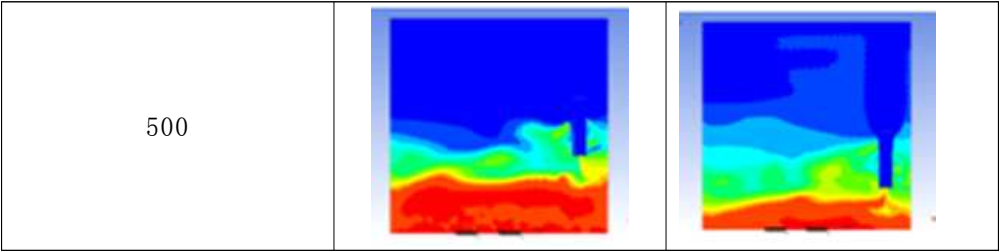


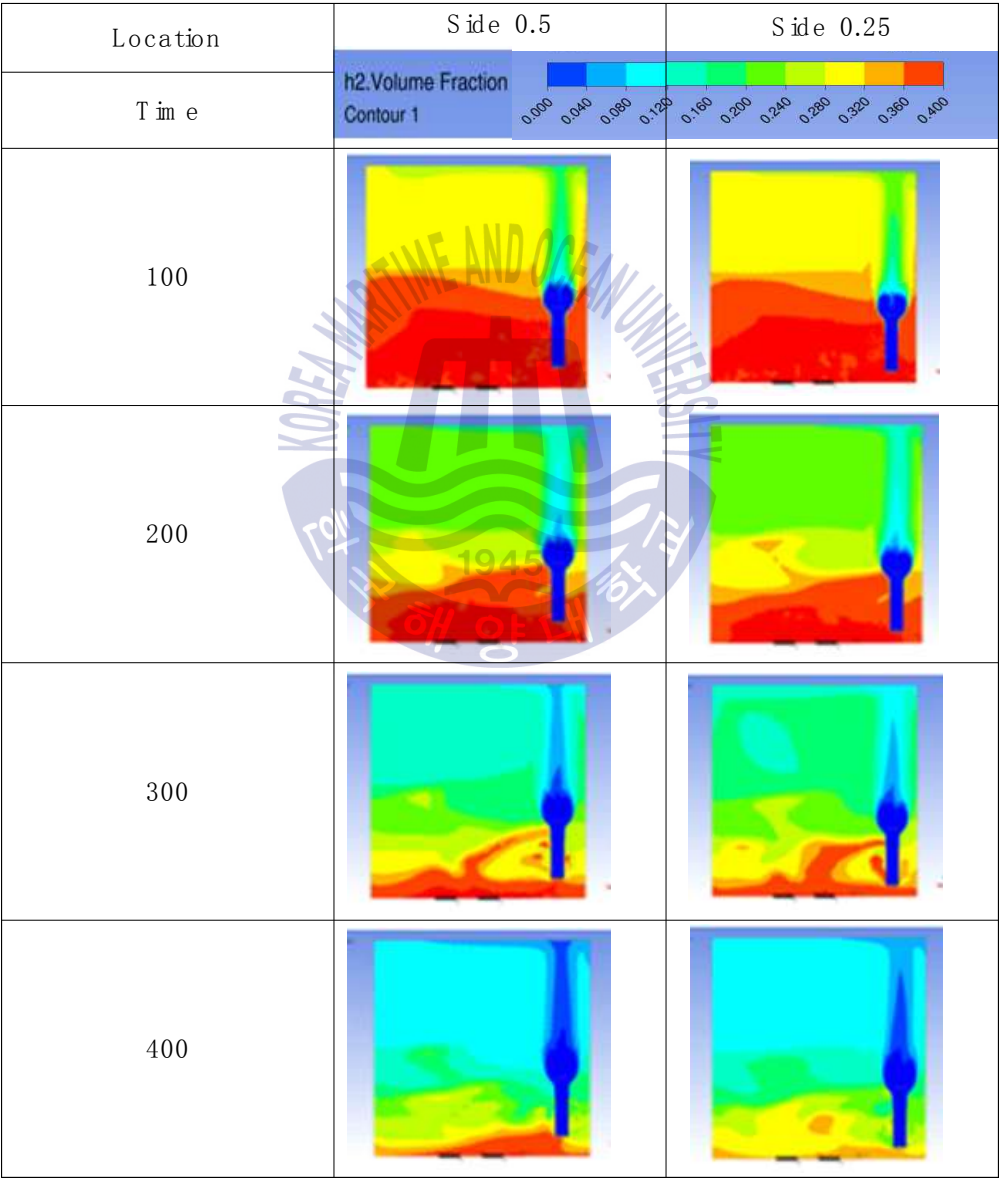
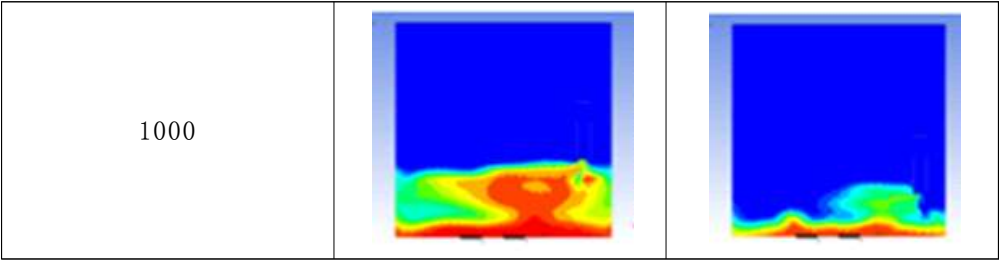


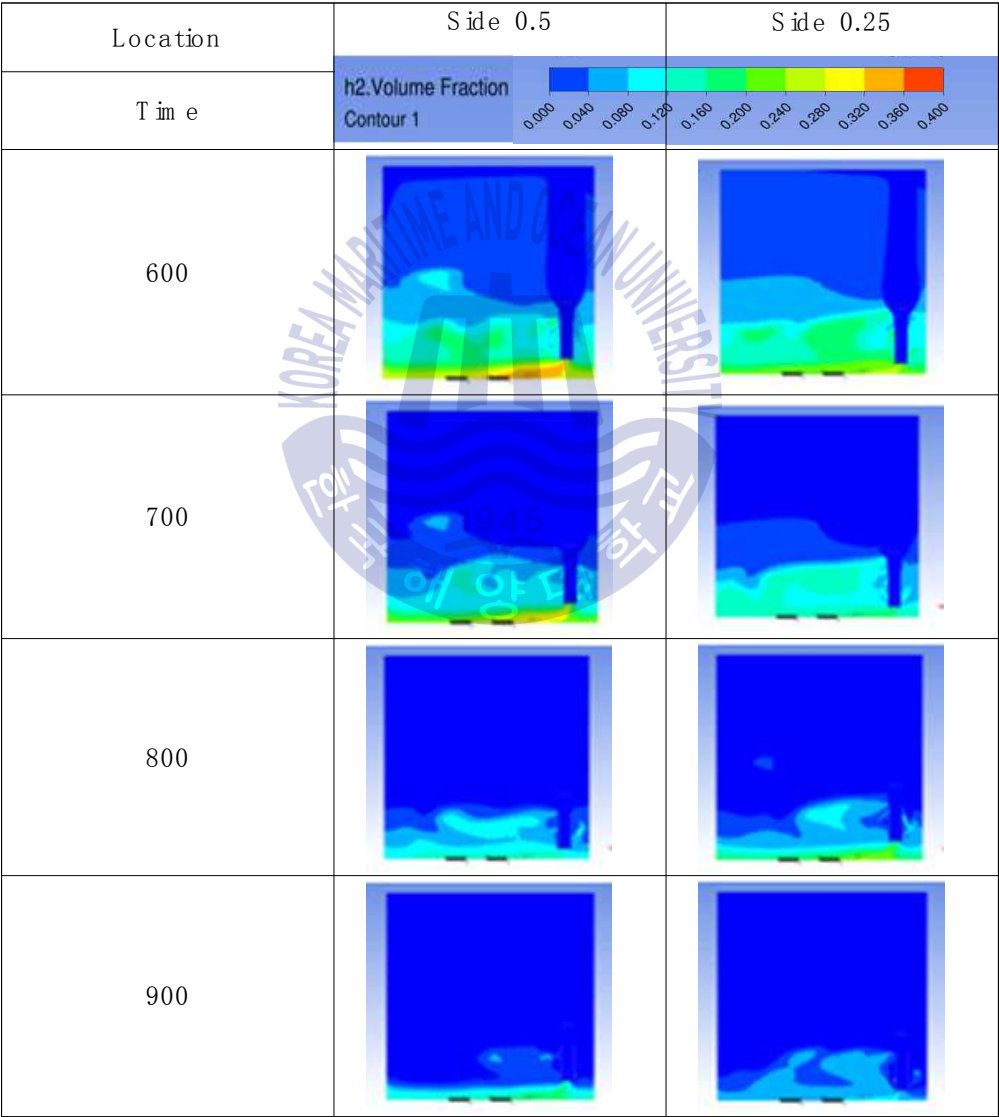
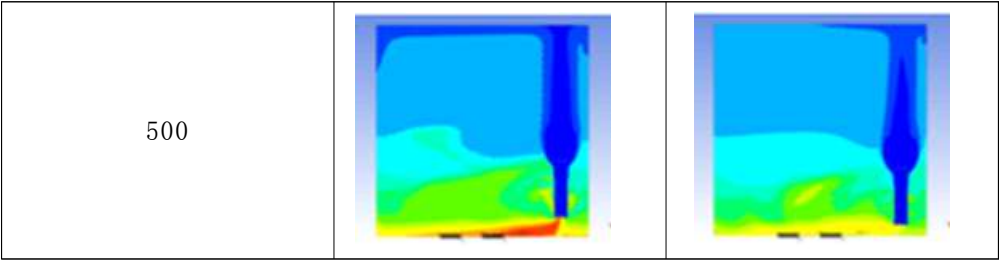


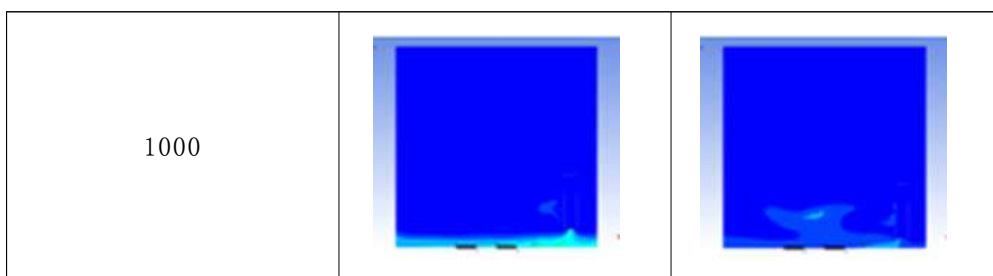
**Table 4.3b** Hydrogen reduction changes in the nuclear containments











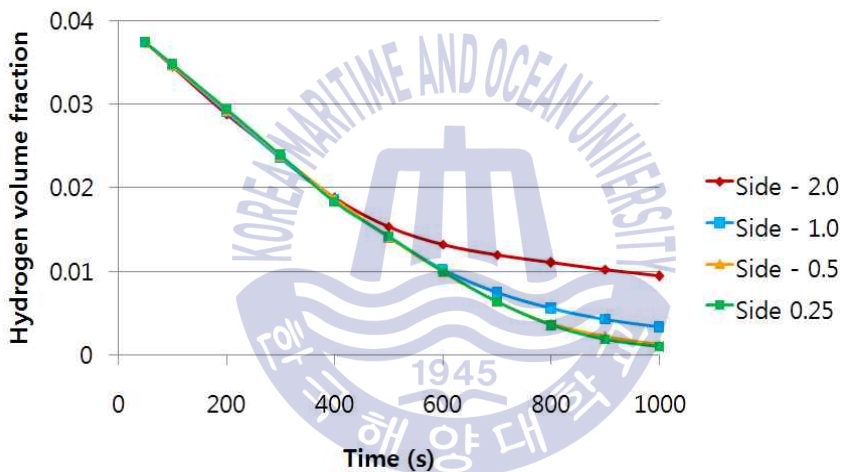
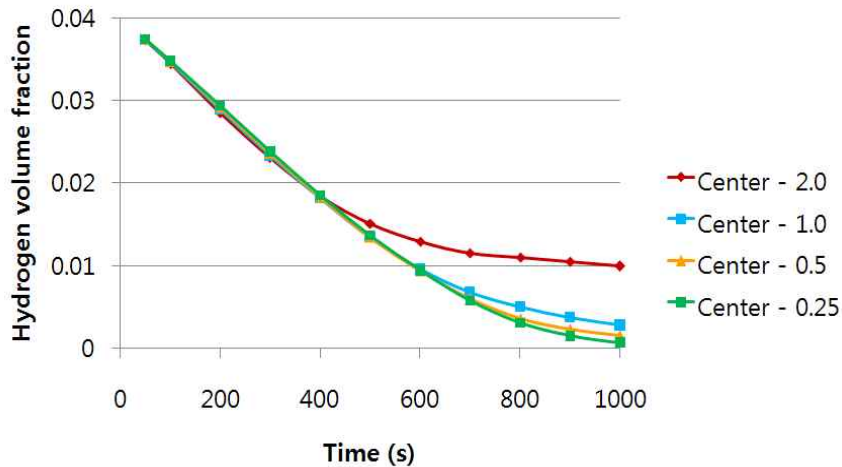
#### 4.5.2 Results and discussion

The two tables above are the hydrogen reduction changes in the nuclear containment from 0 second until 1000 second. The PARs were installed at two different locations and different heights from the hydrogen gas induction source.

The diagrams above showed the hydrogen reduction after 1000 second. The red color represented the original concentration of hydrogen gas, which is the lower flammability 4%, and the blue color represented the hydrogen gas concentration after reduction, which is 0.5%. As the observation from the hydrogen concentration changes in PAR, the concentration of hydrogen gas was underwent reduction and have been removed. However, there was still some residual hydrogen gas in the containment, which was represented by the red color. We could see in the container which the PAR was installed at 2.0 meter from the inlet, have the most residual amount of hydrogen gas. The container which the PAR was installed at the bottommost case, have the least residual amount of hydrogen gas.

**Fig. 4.7** Results of PAR installed at the center of the containment

**Fig. 4.8** Results of PAR installed at the side of the containments



The average of the hydrogen gas amount in the nuclear containment has reduced 75% of the original concentration. But in the nuclear containment cut plane, there were still a large amount of hydrogen gas remained at the bottom.

From the results, we can conclude that the locations where the PAR installed, do have a correlation to the hydrogen reduction rate. If the PAR was installed at a further place from the hydrogen induction source, there were more residual amount of hydrogen gas at the end. In the other way, if the PAR was installed at a place which closer to the hydrogen induction source, there were less residual amount of hydrogen

gas at the end of the test. Due to the buoyancy-induced force, the hydrogen gas which under the inlet of the PAR were difficult to reduce from the containment.

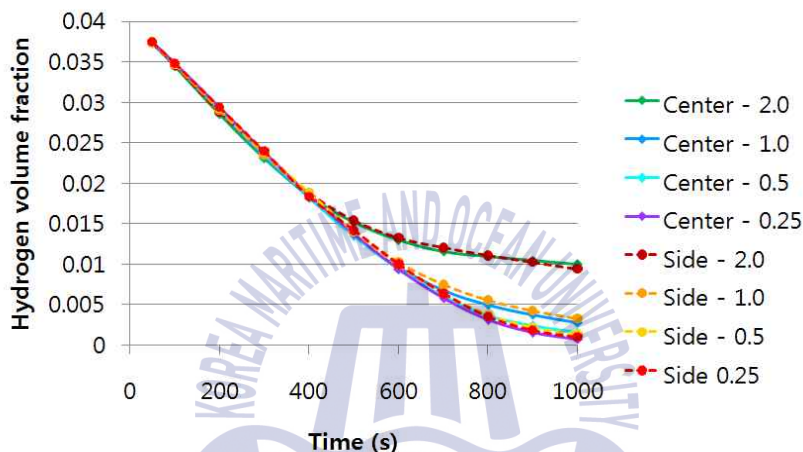


Fig. 4.9 Comparison of hydrogen reduction curves

Nevertheless, the residual amount of hydrogen gas in the containment can't never be ignored. The high concentration hydrogen gas is above of the lower flammability limit, 4%. If this residual amount of hydrogen gas keep remained and never removed from the containment, it will become a risk factor of the future hydrogen explosion. While in the real accident cases which take place in a nuclear power plant, the consequence could be worse. Due to the complicated and irregular shape of the internal structures, there might be more residual amount leftover in the containment and couldn't be removed.

However, the comparison between the PARs which installed at the center and the side at a same height, the differences were not significant.

## Chapter 5: Proposal and analysis of flow considered-design new PAR models

### 5.1 General

Passive autocatalytic recombiner (PAR) is very useful hydrogen mitigation measurement, it is widely implemented in the current and advanced light water reactors (ALWRs). The design of the PARs should be optimized for the specific use under sever accident scenarios. Several techniques and innovations have fused into the PAR, as an effort to increase its efficiency of hydrogen mitigation. This study proposes different concepts of PAR, which applied some changes to the KNT Inc made honeycomb catalyst PAR. Hydrogen volume fraction was given 4 vol. % which tested by KNT to see the performance of PAR in different conditions, and hydrogen concentration from 0 to 20 vol. % to see maximum hydrogen reduction rate. The new concept of PAR was proved to have a greater hydrogen removal performance compared to the 65original honeycomb catalyst PAR.

## 5.2 Introduction

Passive autocatalytic recombiners (PARs) are installed inside the containment of nuclear power plants in many countries in order to remove hydrogen released during a loss-of-coolant accident (LOCA) and to avoid possible threats like hydrogen explosion. Besides the removal of hydrogen, PARs contribute to the containment thermal hydraulics by inducing heat and flow patterns promoting atmosphere mixing. PAR operation has a significant impact on flow and transport processes inside the containment [49,50]. The composition of the containment's atmosphere changed due to the catalytic reaction. The recombination process provides heat and induces buoyancy driven flow [51].

The German Reactor Safety Commission (RSK) has stated that the catalytic recombination is a definite directed measure to cope with the hydrogen in the containment during beyond design-basis accident. As a result of the German Risk Study, Phase B and the occurrence of the TMI-2 severe accident, research was done on hydrogen generation, distribution and combustion, also on how to mitigate potential consequences of hydrogen combustion [52,53,54,55,56]. The distribution of hydrogen, gas mixing, stratification and natural circulation, are the decisive factors for determining the number and position of the required recombiners. The field codes, based on three dimensional models and CFD technique were applied in the specialized nuclear accident scenarios. The application of the CFD tools could obtain more detailed knowledge for proper prediction of the system behavior [57].

Different types of catalytic recombiner have been supplied by PAR manufacturers such as AREVA, NUKEM (formerly NIS), and AECL have

utilized plate type catalysts while NUKEM invented a specialized cartridge containing pellet type catalysts. Korea Nuclear Technology (KNT) Inc also developed a distinctive PAR model with enhanced hydrogen removal capability. To meet the goal, the catalysts adopted a greater surface area without increase the PAR size [58].

The efficiency of mitigation strategies during severe accident scenarios is the key of this study, how to improve the current mitigation measurement's efficiency so as to better cope with the future accident event or even off-normal event and as well reduce its consequences as much as possible.

The analysis of the efficiency and sufficient capacity of PAR needs a reliable prediction of the buoyancy-driven flows and mixing phenomena. Therefore, reliable computer modeling is needed to assess the gas distribution inside the containment and monitor the recombination outcome. CFD is used to determine the hydrogen distribution within the containment for a relatively large number of postulated accident scenarios [59,60,61,62,63].

The effectiveness of a PAR system as a mitigation measure in operating nuclear power plant in order to mitigate the consequences of severe accident has been proven. A PAR system consists of many single PARs which distributed inside the containment to cope a wide range of hydrogen release scenarios. The arrangement of the individual PARs inside the containment is determined by the projected hydrogen release rate, location and distribution, the containment geometry and operational constraints on maintenance areas, accessibility, etc. In order to remove the hydrogen more effectively, the hydrogen distribution and concentration variation must be predicted carefully overall the containment building. Afterward, the positions for installing PAR can be

decided [64,65,66]. Many studies have been performed on hydrogen behavior to find out where and when hydrogen is gathering. However, the distribution of hydrogen inside the containment is unpredictable. Research work analyzing hydrogen distribution and its concentration variation, is insufficient particularly, involving failure of position variation [67,68]. The objective of this work will be more focused on the hydrogen recombination rate as function of PAR inlet design. This study proposes different concepts of PAR, which modify some changes to the PAR structure and investigate which one of them can achieve the maximum hydrogen recombination rate.

### 5.3 Mathematical model & calculation condition

This study involves the use of Computational Fluid Dynamics (CFD) which is a computer-based tool that is widely used for analysis and design purposes. By utilizing the advances in computing power and graphics, creation and analysis of a certain model is less labor intensive and cheaper than experimental methods.

The calculation code used in this study is ANSYS CFX 14. ANSYS CFX solves the unsteady Navier-Stokes equation in their conservation form. The instantaneous equation of mass (continuity) in the stationary frame is expressed as the following equation:

$$\frac{\partial \rho}{\partial t} + \nabla \cdot (\rho U) = 0$$

The simplest conservation of energy equation is as below:

$$\frac{\partial \rho c_p T}{\partial t} + \nabla \cdot (\rho c_p T U) = \nabla \cdot (k \nabla T) + H$$

and the instantaneous equation for momentum is expressed as shown in the following equation:

$$\frac{\delta \rho}{\delta t} + \nabla \cdot (\rho U \otimes U) = -\nabla p + \nabla \cdot \tau + S_M$$

These instantaneous equations are averaged for turbulent flows leading to additional terms that need to be solved. While the Navier-Stokes equations describe both laminar and turbulent flows without addition terms, realistic flows involve length scales much smaller than the smallest finite volume mesh. A Direct Numerical Simulation of these flows would require significantly more computing power than what is available now or in the future. (5.4)

Therefore, much research has been done to predict effects of turbulence by using turbulence models. These models account for the effects of turbulence without the use of a very fine mesh or direct numerical simulation.

These turbulence models modify the transport equations by adding averaged and fluctuating components. The transport equations are changed to the following two equations.

$$\begin{aligned} \frac{\partial \rho}{\partial t} + \nabla \cdot (\rho U) &= 0 \\ \frac{\delta \rho}{\delta t} + \nabla \cdot (\rho U \otimes U) &= -\nabla p + \nabla \cdot (\tau - \rho \overline{U \otimes U}) + S_M \end{aligned} \quad (5.3)$$

The mass equation is not changed but the momentum equation contains extra terms which are Reynolds stresses,  $\rho \overline{U \otimes U}$  and the Reynolds flux,  $\rho \overline{U \otimes U}$ . These Reynolds stresses used to be modeled by additional equations to obtain closure. Obtaining closure implies that there are a sufficient number of equations to solve for all the unknowns including the Reynolds stresses and Reynolds fluxes.

Various turbulence models provide various ways to obtain closure. In this investigation, the model utilized is the Shear Stress Transport (SST) model. The advantage of using this model is of which it combines the advantages of other turbulence models (the  $k-\varepsilon$ , Wilcox  $k-\omega$  and BSL  $k-\omega$ ).

The characteristic of the Wilcox model is the strong sensitivity to free-stream conditions. Therefore, a blending of the  $k-\omega$  model near the surface and the  $k-\varepsilon$  in the outer region was made by Menter which resulted in the formulation of the BSL  $k-\omega$  turbulence model. It consists of a transformation of the  $k-\varepsilon$  to a  $k-\omega$  formulation and subsequently adding the resulting equations. The Wilcox model is multiplied by a blending function  $F_1$  and transformed  $k-\varepsilon$  by another  $1-F_1$ .  $F_1$  is a function of wall distance (being the value of one near the surface and zero outside the boundary layer). Outside the boundary layer and on the edge of the boundary layer, the standard  $k-\varepsilon$  model is used.

However, while the BSL  $k-\omega$  model combines the advantages of both the  $k-\varepsilon$  and Wilcox  $k-\omega$  turbulence models, it fails to fully predict the onset and amount of flow separation from smooth surfaces. The  $k-\varepsilon$  and Wilcox  $k-\omega$  turbulence models do not account for the transport of the turbulent shear stress resulting in an over-predicting of eddy viscosity. A limiter on the formulation can be used to obtain the proper results. These limiters are given the next equation:

$$F_1 = \tanh(\arg^4)$$

$$\arg = \min\left(\max\left(\frac{\sqrt{x}}{\beta^* \omega y}, \frac{500\nu}{y^2 \omega}\right), \frac{4\rho k}{C D_{k\omega \sigma_{\omega 2}} y^2}\right)$$

$y$  is the distance to the nearest wall and  $\nu$  is the kinematic viscosity. In

addition:

$$CD_{kw} = \max(2\rho \frac{1}{\sigma_w 2\omega} \nabla k \nabla \omega, 1.0 * 10^{-10}) \quad (5.11)$$

$$F_2 = \tanh(\arg_2^2)$$

$$\arg_2 = \max(\frac{\sqrt[2]{k}}{\beta' \omega y'}, \frac{500v}{y^2 \omega}) \quad (5.12)$$

The standard form of the hydrogen recombination code correlation for the honeycomb PAR was determined as

$$R_{PAR} = 4.0 \cdot N \cdot \frac{C}{T} \cdot [1 + 1.845 \ln(P)]$$

Then, the heat release rate is given as

$$H_r = \frac{R_{PAR} \cdot LHV_{H_2}}{A_s}$$

LHV<sub>H<sub>2</sub></sub> is lower heating value of hydrogen, the amount of heat released by combusting a specified quantity (initially at 25 °C) and returning the temperature of the combustion products to 150 °C, which assumes the latent heat of vaporization of water in the reaction products is not recovered.

## 5.4 Model description

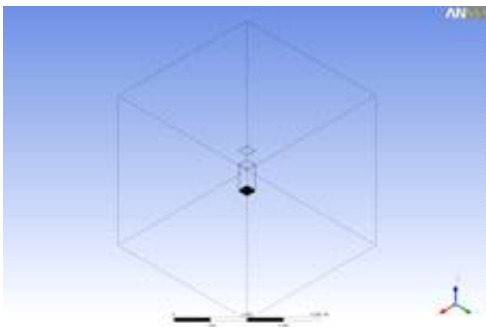
(5.8)

The PAR used in this study is the KNT. Inc designed honeycomb PAR. It is a PAR system with high porous catalyst material in the shape of honeycomb. The honeycomb PAR catalyst has a design characteristic of improved hydrogen removal efficiency by increasing the surface area and enhancing the flow rate through the catalyst at the same time.

From the original honeycomb PAR, we further made some innovative

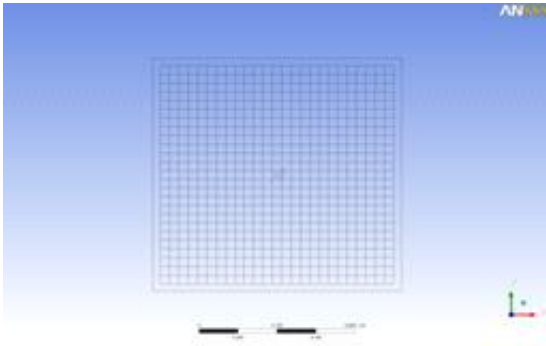
modifications to the model by adding the guidance wall at the bottom of the catalyst, which is located at the base. The intention of such modification is to enhance the gas flow which would be brought into the catalyst and undergo the following recombination process. The guidance wall has a pyramidal shape with an opening at the top and base, which allow the gas to pass through the catalyst. The guidance wall was designed to act serve as a reflector, reflect the gas induced from any directions and channel them with narrowing head then induce them to the catalyst.

There are 3 different models named type 1 PAR, type 2 PAR and type 3 PAR respectively. The difference among these 3 types of PAR is the distance of the guidance wall from the base of PAR, which is 150cm, 75cm and 0cm (attached to the base of PAR body). Fig. 1 shows the analysis grids of the model (5m height x 5m length x 5m wide) and a PAR which placed right at the center. The total numbers of grids is 1,133,816 and the grids are generated by using NX7.5 and ICEM-CFD codes. The simulated PAR was conducted in various conditions of catalyst wall release, gas velocity and gas flow direction.

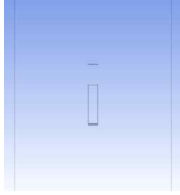
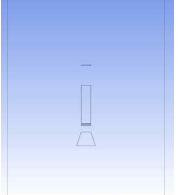
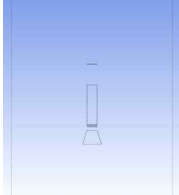
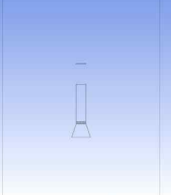


**Fig. 5.1** Analysis grids of the hypothetical nuclear containment

**Fig. 5.2** The honeycomb-shaped catalyst



**Fig. 5.3** Guiding wall, the highlighted area at the bottom of a PAR structure

Type	Original type	Type 1	Type 2	Type 3
Shapes				
Distance of the guidance wall to the PAR body	-	150 mm	75 mm	0 mm
Hydrogen concentration [vol. %] & heat release, ( $\text{Wm}^{-2}$ )	1 (4247), 2 (8575), 3 (12822), 4 (17070), 5 (21397), 7.5 (32056), 10 (42715), 15 (64112), 20 (85750)			
Upward gas flow ( $\text{ms}^{-1}$ )	0, 1, 2, 3			
Sideward gas flow ( $\text{ms}^{-1}$ )	0, 1, 2, 3			
Upward with sideward gas flow ( $\text{ms}^{-1}$ )	0, 1, 2, 3			
Turbulence model	Shear stress transport model (SST model)			
Temperature condition	298K			
Pressure condition	1 bar			

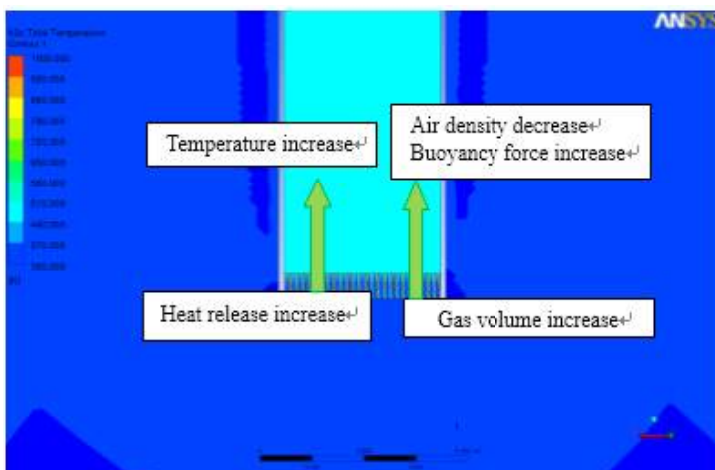
**Table 5.1** Analysis condition

## **5.5 Results and discussion**

### **5.5.1 Flow induction**

The PAR was assumed to be adiabatic except the catalyst part. The heat flux in were introduced to the catalyst wall for the function of hydrogen concentration. The heat flux in provided the initial heat for the recombination process. As the heat flux value got higher, the temperature near the wall also increased. This could lead to the expansion of gaseous when the recombination process took place at the catalyst wall. There is a buoyancy force at the honeycomb hole as where the recombination process takes place. When the hydrogen reacted with the air at the catalyst then the temperature increased, the gas volume increased, the air density decreased and the buoyancy force increased as shown in Fig. 5.4.

**Fig. 5.4** Mechanism of the formation of gas buoyancy force and the interaction with heat release

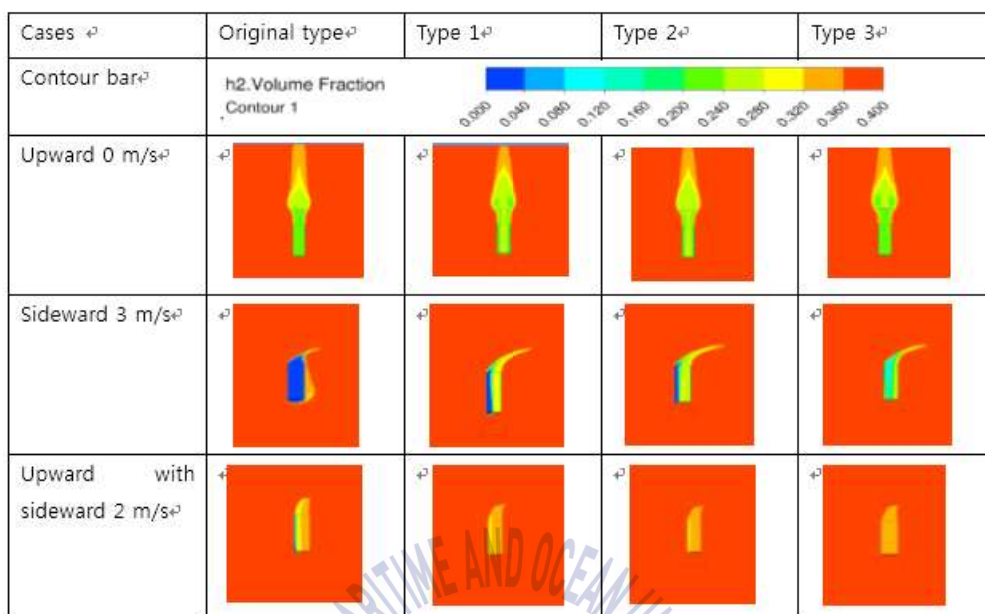


### 5.5.2 Gas distribution variations scenario

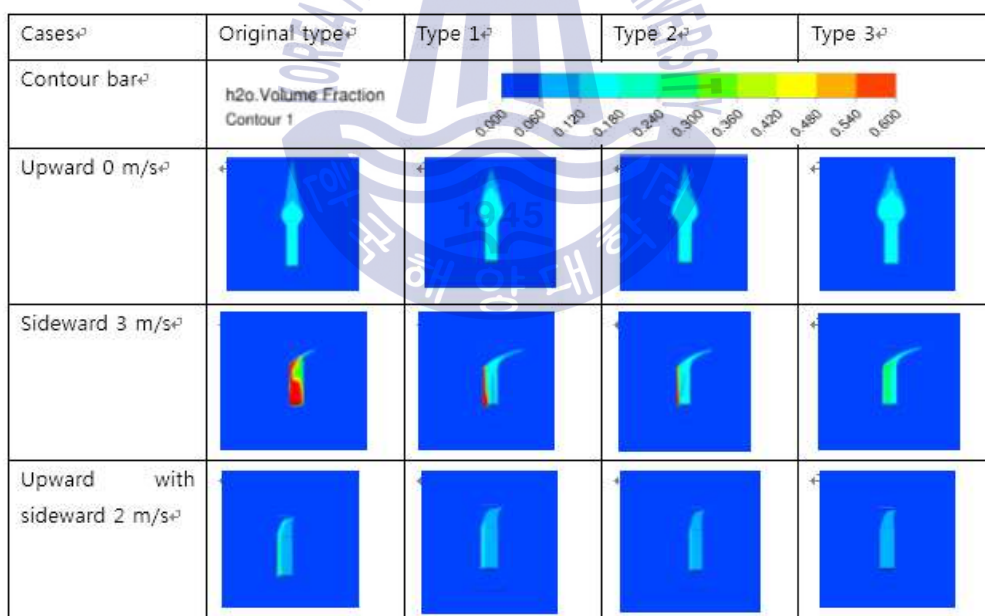
The gas distribution in the case of 4 vol.% of hydrogen is showed in the Table 2 - 4, as the hydrogen and the oxygen being reduced while steam was increasing as the final product of recombination process.

**Table 5.2** Hydrogen recombination pattern in the PARs of different velocity variation

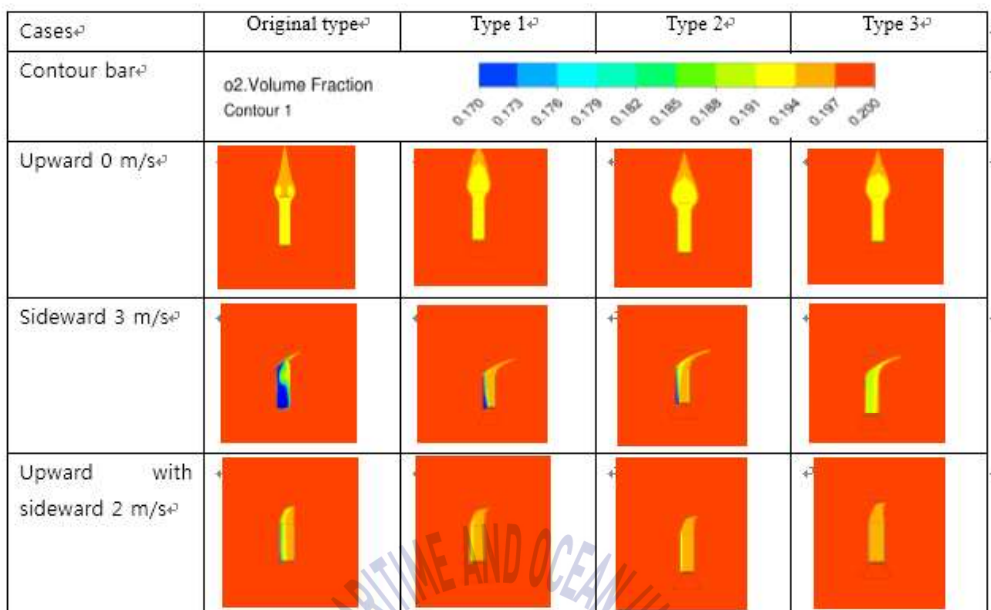
**Table 5.3** Steam production pattern in the PARs of different velocity



variation



**Table 5.4** Oxygen removal pattern in the PARs of different velocity variation



$2 \text{ H}_2 + \text{O}_2 \rightarrow 2 \text{ H}_2\text{O}$ , this exothermic chemical reaction releases energy in the form of heat.

Hydrogen concentration is reduced when the hydrogen gas intact with the honeycomb catalyst. The red color region in the figure represents the original concentration of hydrogen before being removed. The buoyancy force of the recombination process drives the end product, steam out from the outlet of PAR. Hydrogen is unable to be removed well at a high velocity air flow scenario because of higher flow in. In the sideward airflow 3m/s scenario (Table 5.2), the cut plane of recombination process took place in the PAR showed some blue color region, which mean that was all amount of hydrogen flow-in was reduced. It was due to the original honeycomb PAR' s shape, a weak point that limits the flow-in of hydrogen under the hydrogen recombination performance. By installing the new modified PARs, the limitations somehow could be overcome. The guidance wall at the bottom could reflect the incoming gas and channeled them into the PAR

for more efficient recombination. The new type PARs have less blue color region compared to the original type PAR. The lesser gas led into the PAR, the lower the hydrogen recombination rate.

Air and steam concentration are given in Table 5.3 and Table 5.4. Air is reduced together with hydrogen and steam is increased as the final product. Only ‘upward 0 m/s’ , ‘sideward 3 m/s’ and ‘upward with sideward 2 m/s’ cases are chosen among the other test conditions to represent the result because these few selected cases give the more significant findings than the other cases, while the other findings are almost similar.

### 5.5.3 Hydrogen induced area

Hydrogen induced area is the hypothetical area which the inflow gas will be projected and guided by the guidance wall into the catalyst for recombination process. Table 5.5, 5.6, and 5.7 respectively showed the streamline pattern of hydrogen flow in upward, sideward, and upward with sideward case, respectively, in the conditions of 4 vol.% of hydrogen. The  $H_2$  induced area is corresponding to the amount of hydrogen induced to the PAR. In the new concept-designed PAR, the guidance wall promoted the  $H_2$  induced area, which had enabled more amount of gas into the PAR. Consequently, this had also indirectly increased the hydrogen recombination. The base of guidance wall has the same size and same surface area. In the actual scenario, the distance of the guidance from the base of PAR plays a role in affecting the hydrogen recombination rate. The red color line at the bottom of streamline circles represents the induced hydrogen surface area, indicating how much of hydrogen gas could be brought into the PAR

catalyst.

Fig. 5.5 showed the upward case, the guidance wall increases the induced area surface to the PAR, allow more hydrogen to go through. Generally, all the new modified-types of PAR have better hydrogen recombination performance than the original type PAR.

In the sideward case (Fig. 5.6), type 1 work best, compared to the other 2 types of PAR. The wide gap between the guidance wall and the PAR bottom allowed some air came from sideward to be guided into the PAR bottom, led to more hydrogen received by the original catalyst. The original type PAR which lack of guidance wall couldn't intake much gas like the modified type PAR.

In the upward with sideward case (Fig. 5.7), type I and type II work well, but type I is a slightly better., compared to the other 2 types of PAR. The guidance wall and the gap aided the PAR to receive more hydrogen for recombination.

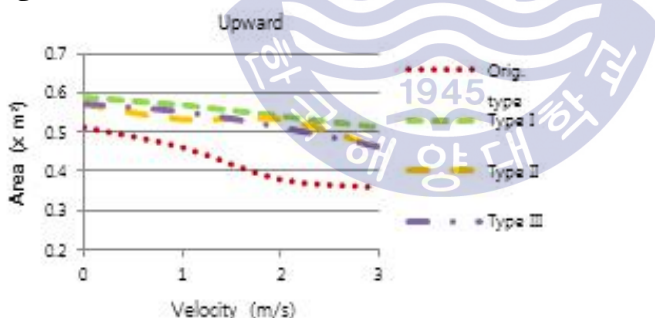
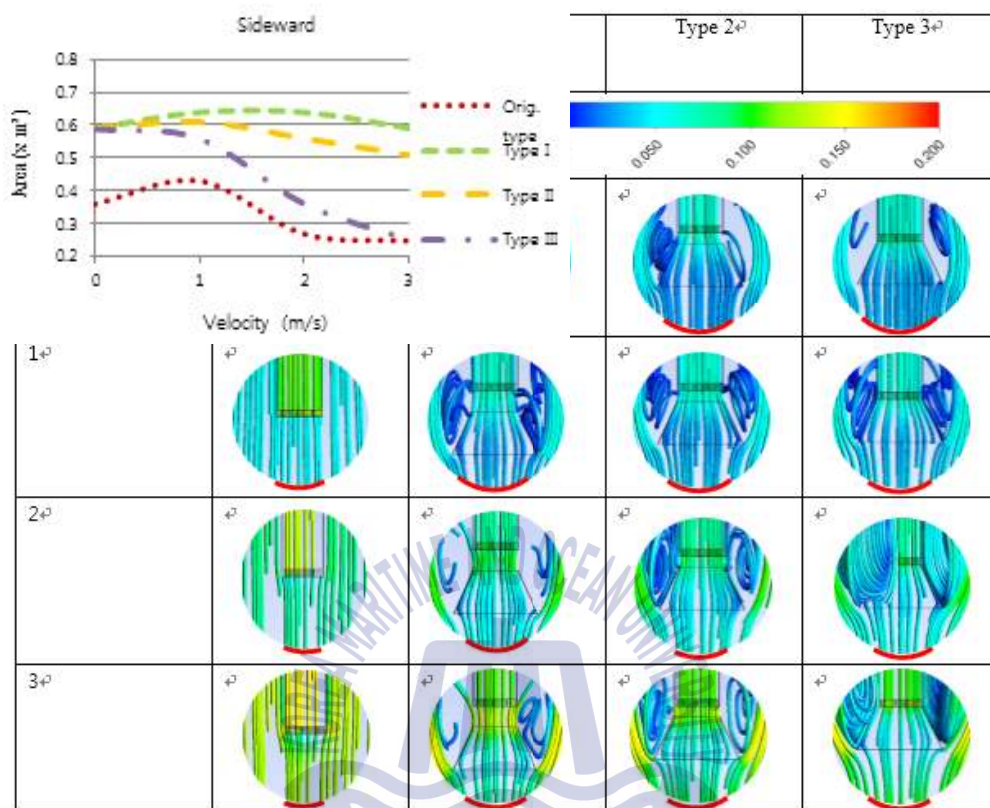


Fig. 5.5 Hydrogen induced area of the upward-directed gas flow case

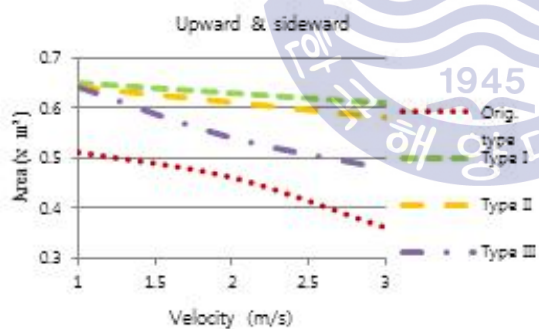
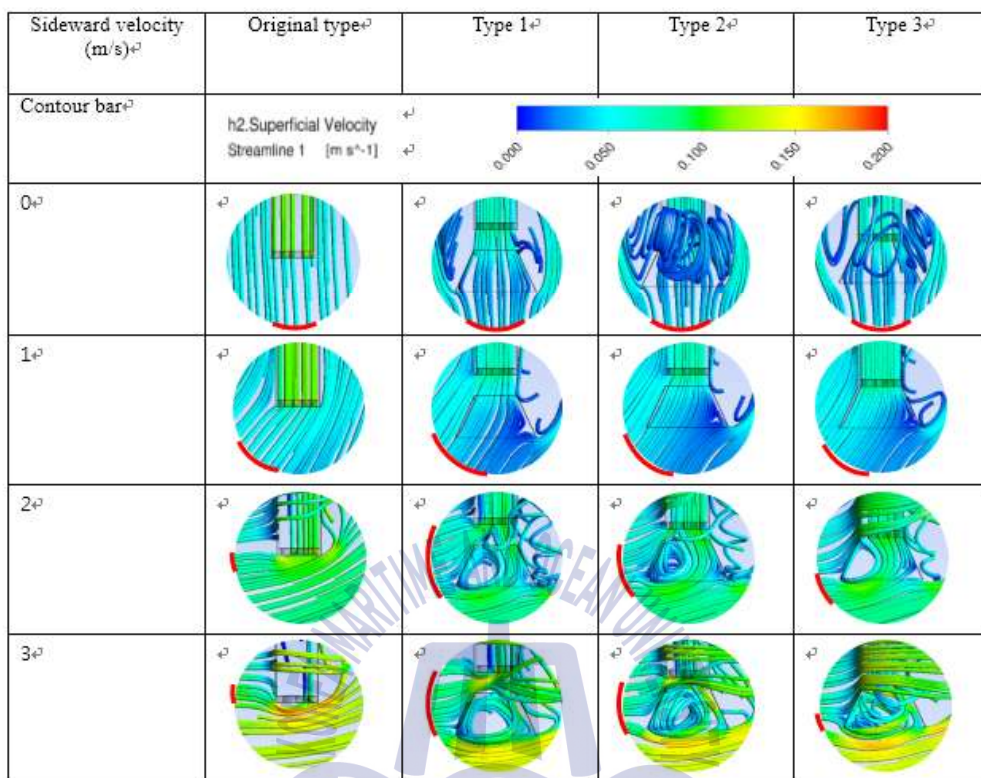
**Table 5.5** The streamline pattern of hydrogen velocity in upward-directed gas flow case



**Fig. 5.6** Hydrogen induced area of the sideward-directed gas flow case

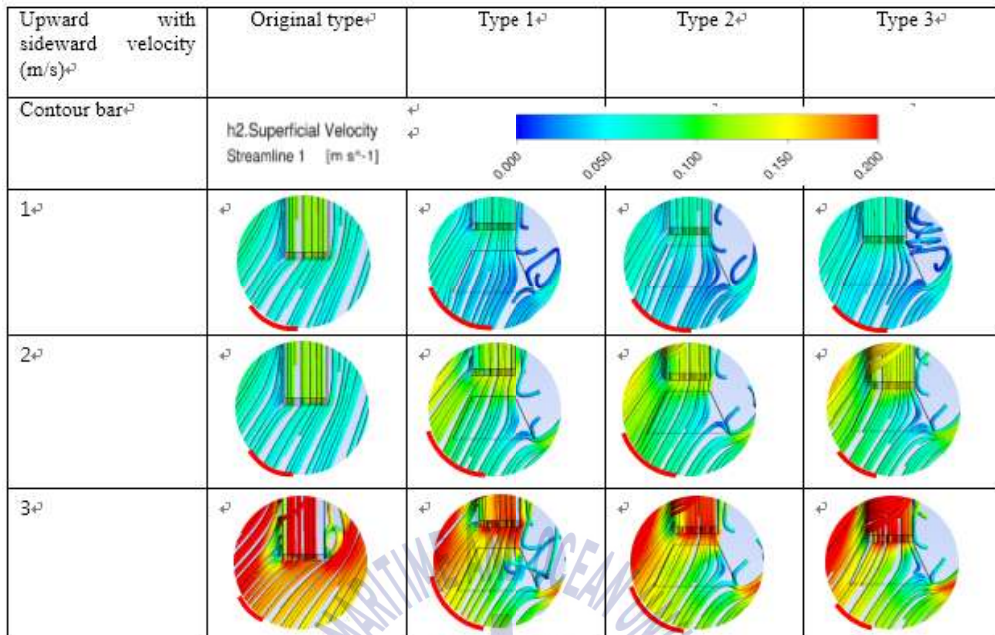
**Table 5.6** The streamline pattern of hydrogen velocity in sideward-directed gas flow case

**Fig. 5.7** Hydrogen induced area of the upward with sideward-directed



gas flow case

**Table 5.7** The streamline pattern of hydrogen velocity in upward with sideward-directed gas flow case

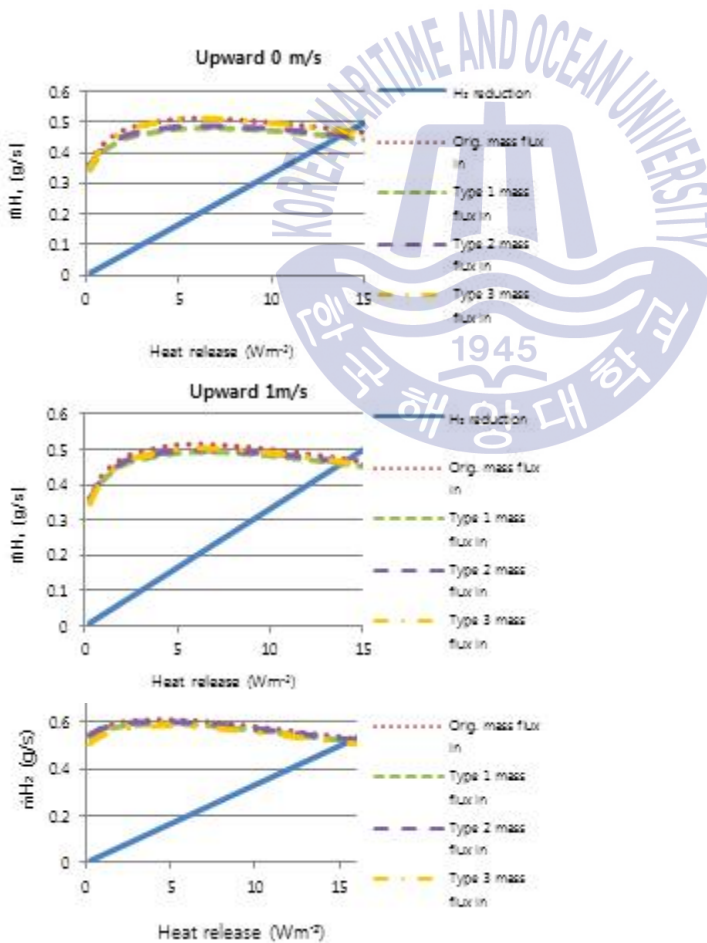


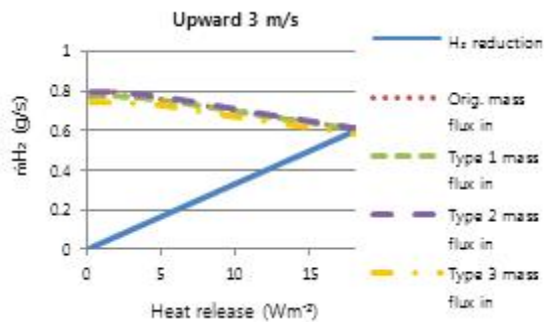
#### 5.5.4 Maximum PAR recombination performance

This section is to analyze the maximum hydrogen recombination rate with PAR modification. Hydrogen recombination rate of PAR is determined with the hydrogen concentration and limited by the hydrogen mass flux in. In the first chart of Fig. 5.8, the blue color line of  $H_2$  recombination shows the hydrogen recombination rate which theoretically calculated at the given hydrogen concentration. While the other 4 lines of PAR flux in show the mass flux into PAR at the heat release generated in the given hydrogen concentration. For example, at  $17070 \text{ W/m}^2$  mass flux in is 0.5 and hydrogen recombination rate is 0.1, so the remaining  $H_2$  is 0.4. The crossover point among the lines is where all the  $H_2$  flux in is completely reduced. So the values are the maximum recombination rate, and the maximum hydrogen concentration completely reduced..

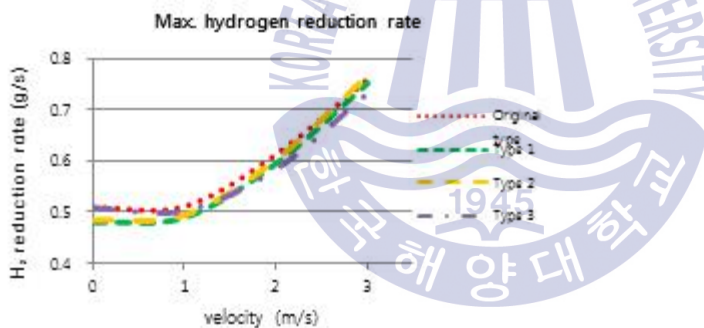
*a) Upward-directed gas flow*

In this scenario (Fig. 8), the recombination efficiency among the four types of PAR didn't seem much different but the type 2 is slightly leading the other new types of PAR. In the situation of low velocity gas cases (0 - 2 m/s), the conventional honeycomb PAR have a slight better performance than the other type of PARs but in the case of 3m/s case the type 3 PAR has the best recombination performance than the other types. (Fig. 5.9).





**Fig. 5.8** The hydrogen recombination rate mass flux in over hydrogen concentration of upward-directed flow case

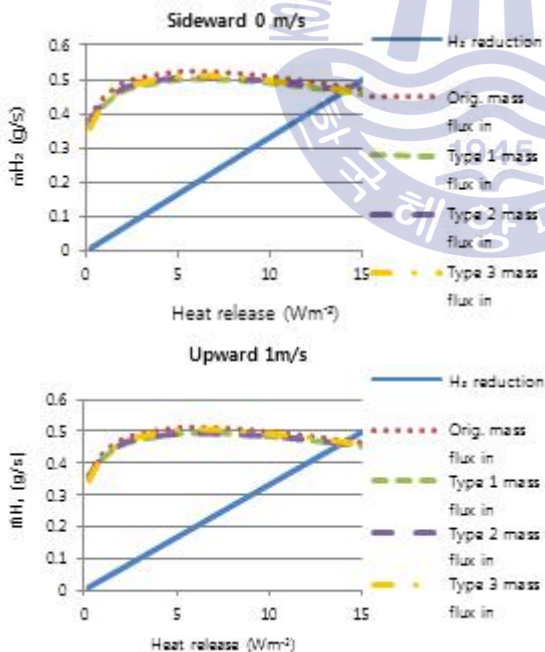


**Fig. 5.9** Maximum hydrogen recombination rate with velocity variation in upward-directed flow case

*b) Sideward-directed gas flow*

In this scenario, all the new concept-designed PARs have better

hydrogen recombination rate than the original honeycomb PAR. All the 3 types of new PARs, type 2 seemed to have the slight better recombination rate than the type 1 and type 3 (Fig. 5.10). The guidance wall worked its designation purpose to channel more gas into the catalyst for recombination process. The wall collected gas from different directions, and brought them together, channeled them into the catalyst. The original honeycomb PAR which lack of the guidance wall at the bottom, seemed to have channeled very less into its catalyst. From the streamline, we could see that most gas from sideways passed through the catalyst, without being brought into the catalyst. That resulted very low hydrogen recombination rate compared to other new concept designed PARs and it's more significant in the higher velocity case like 3m/s (Fig. 5.11).



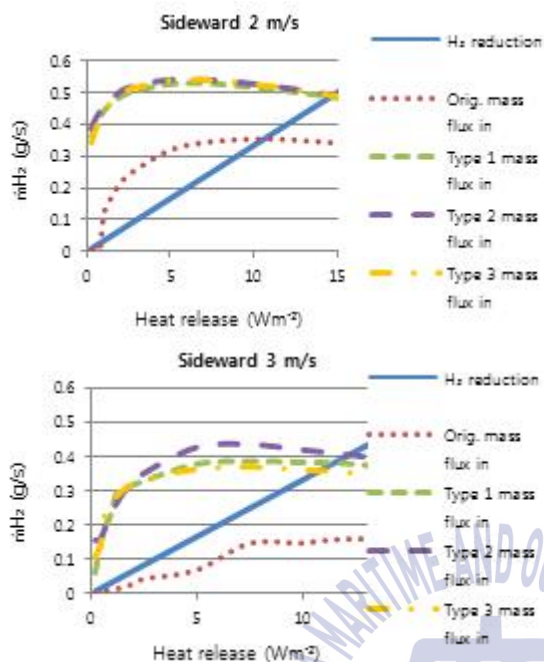


Fig. 5.10 The hydrogen recombination rate mass flux in over hydrogen concentration of sideward-directed flow case

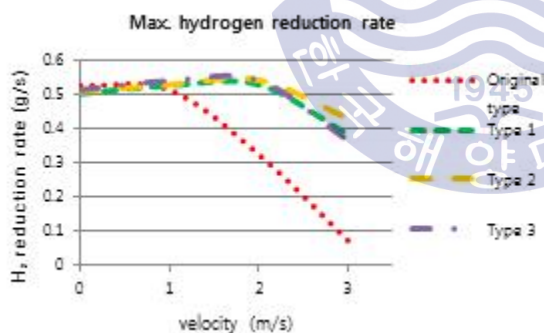
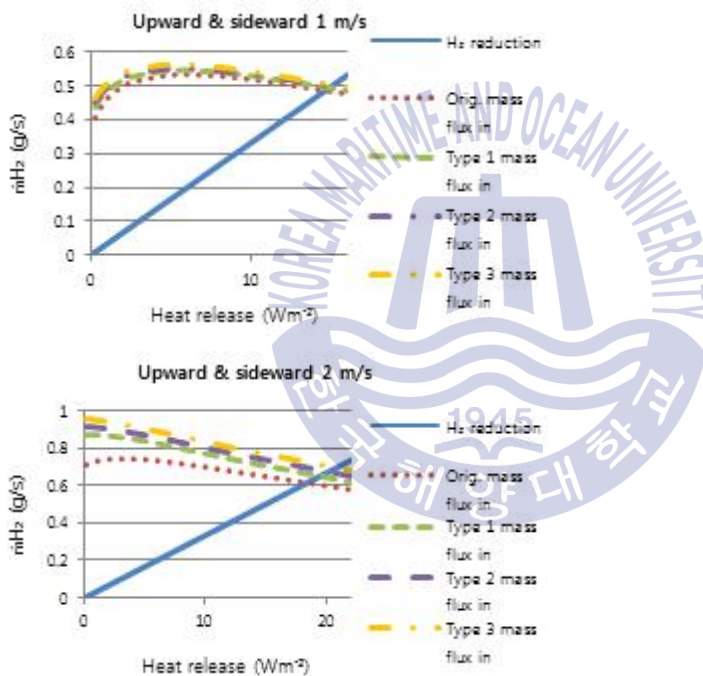


Fig. 5.11 Maximum hydrogen recombination rate with velocity variation in sideward-directed case

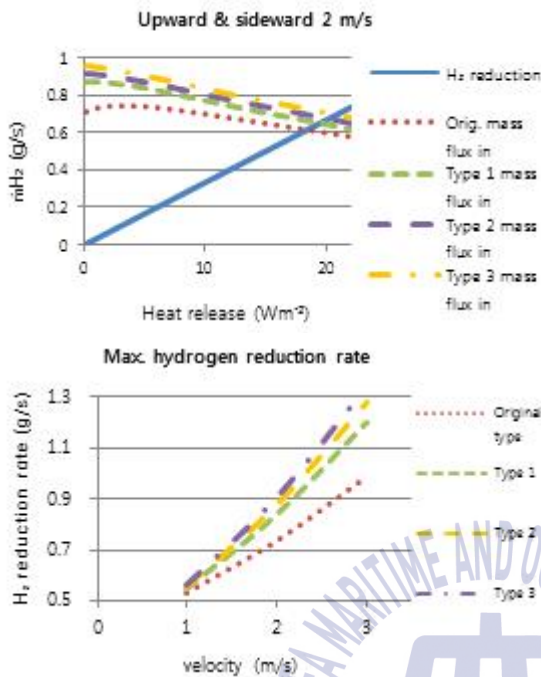
### c) Upward with sideward-directed gas flow

In this scenario, all the new concept-designed PARs also have better hydrogen recombination rate than the original honeycomb PAR. From the comparisons among these 3 new concept-designed PARs, the type 3 PAR

has the best recombination rate than the type 1 and type 2 (Fig. 9). The original honeycomb PAR has the lowest hydrogen recombination efficiency (Fig. 10). Besides, the efficiency difference was greater if the gas flow velocity increased. Although the gas velocity increased, and the gas which brought into the catalyst have increased, the efficiency was much lower compared to the new concept-designed PARs. The new concept-designed PARs received more amount of gas in any situations of this scenario



**Fig. 5.12** The hydrogen recombination rate mass flux in over hydrogen concentration of upward with sideward-directed flow case



**Fig. 5.13** Maximum hydrogen recombination rate with velocity variation in upward with sideward-directed flow case

## Chapter 6 Conclusion

This research work mainly focuses on the numerical analysis of hydrogen risk in nuclear power plant and also the numerical work to improve its counter-measurement efficiency. First, a hydrogen explosion scenario is generated in order to study the hydrogen generation mechanism, hydrogen behavior and hydrogen distribution pattern. Hence, the data is used as a reference to propose a new concept of hydrogen mitigation measure. Besides, a hydrogen mitigation measure, PAR which has been widely equipped in the power reactor containments was selected and focused on improving its performance. Those are summarized as follows:

(a) Hydrogen behavior in the containment building of the APR1400 nuclear plant from 0 until 54,000 s; a simulation lasted for 15 h to observe the process changes of hydrogen explosion in the containment when a SBLOCA occurred. The risk of hydrogen explosion largely depends on the combination of air, hydrogen and the presence of steam in the containment which acts as an insulator to prevent the contact between hydrogen and air. The first risk of hydrogen explosion throughout the time may happen at stage 3 (7000 – 14,000 s). There is a possibility of localized hydrogen explosion that could take place among the compartments in lower part of containment. An ignition could lead to a localized hydrogen explosion. This takes place where the condition of fuel is fulfilled and hydrogen gas encounter with the air. The main risk comes at the stage 5 (after 33,000 s), which take place on the top of the containment. A massive scale hydrogen explosion could bring damage to the containment structure. Better knowledge of the potential risk locations can facilitate the PAR installation and promote a more effective countermeasure against hydrogen explosion.

(b) New concept design of hydrogen mitigation system and analyzed the steam, air and hydrogen behavior during an accident takes place in the nuclear power plant, which as summarized as follows:

- during steam release, the steam gathered at the top of the containment building and pushed the air downward, which was occupying the entire containment over the failure before the hydrogen leakage happened. The air is being pushed down by the hydrogen from the upper part of containment, but the air still remains in the air reservoir until hydrogen removal, which actually provides a favorable condition for hydrogen recombination. It overcomes the problem of unsatisfactory

recombination process due to insufficient oxygen fraction.

- during hydrogen release, some part of the hydrogen gas went up to the top of the containment through the guidance wall and then to the hydrogen removal part, which hydrogen was removed. The other part of hydrogen went directly up to the top of the containment through the gap by the building wall, which hydrogen remained at the top after hydrogen release. The amount of remained hydrogen was increased with the increase of hydrogen release. The final percentages of hydrogen reduction are 55% for type I and 83% for type II respectively.

(c) PAR location analysis: hydrogen recombination rate is concluded to be proportional to the distance with the hydrogen induction location. The PAR which installed at the bottom place (nearer to the hydrogen induction source) has better hydrogen recombination rate compared to the PAR which installed at the higher place, while the PAR which installed at the center and the side of the containment does not have a significant difference to hydrogen recombination rate.

(d) PAR modification: the modified PARs have better hydrogen recombination rate compared to the original honeycomb PAR. The modification promotes and collects more gases into the catalyst, hence increases the recombination rate. The air guidance wall at the bottom of the catalyst expands the hydrogen induced area therefore allows more gases being introduced to the catalyst for recombination process. In the different scenarios, the modified PARs show better performance compared to the original honeycomb PAR



### Acknowledgement

This research work has been carried out at Engine Combustion Laboratory at Korea Maritime and Ocean University (KMOU).

First of all, I would like to express my sincere gratitude to Prof. Park Kweonha (박권하) for accepting me as a graduate student and providing me the opportunity to carry out the research works under his direct supervision. His theoretical and practical knowledge in the field of engine combustion with his relentless and patience towards me has been a huge source of motivation and inspiration during the course of study.

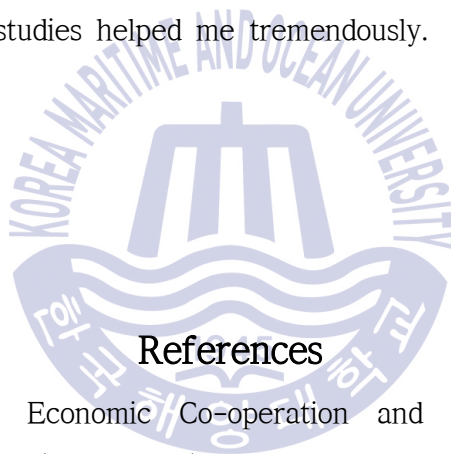
I would like to thank Prof. Lee Young-ho (이영호) and Prof. Jeong Young-ho for their valuable suggestions, endless support with valuable

comments and recommendations.

I am also highly indebted to my lab members and all fellow student of the university for great working environment and for all the memorable moments we shared. Special appreciations go to Sun Kwon and Ryu Myung-rok for guiding me with CFD skills and the collaboration in the analysis test and my study life in Busan, South Korea.

I will always miss KMOU, which nourish me the challenging spirit and the great Korean culture.

Finally, I would like to thank my parents for being my pillar of strength during my pursuit of a Master's degree. Their encouragement, and support in my studies helped me tremendously.



## References

1. Organization for Economic Co-operation and Development/Nuclear Energy Agency (OECD/NEA), Agreement on the OECD/NEA THAI-Project, Paris, France, 2007
2. Retrieved from: [www.candu.com/site/media/Parent/PARs%201124b\\_FINAL.pdf](http://www.candu.com/site/media/Parent/PARs%201124b_FINAL.pdf)
3. Nuclear Energy Agency, Implementation on severe accident management measures, In: Proc. of the Workshop on the Implementation of Severe Accident Management Measures, Villigen, Switzerland, 10-13 September 2001
4. Kim J. T., Hong S. W., Kim S. B. and Kim H. D., 2004. 3-Dimensional analysis of the steam-hydrogen behavior from a small break loss of

- coolant accident in the APR1400 containment. J. Korean Nucl. Soc. 26 (1), 2004, 24-35.
5. American Nuclear Society, Fukushima Daiichi: ANS Committee Report 2012, 2012, American Nuclear Society.
  6. Xiao J. and Travis J. R., How critical is turbulence modeling in gas distribution simulations of large-scale complex nuclear reactor containment? Ann. Nucl. Energy 56, 2013, 227-242
  7. Apanasevich P., Coste P., Niceno B., Heib C. and Lucas D., Comparison of CFD simulations on two-phase pressurized thermal shock scenarios. Nucl. Eng. Des. 266, 2014, 112-128.
  8. Chatzidakis S, and Ikononopoulos A, Phenomenological investigation of loss of coolant accident in a research reactor facility. Nucl. Eng. Des. 256, 2013, 341-349.
  9. Liu J., Peng M., Zhang Z. and Jiang L., Small-break loss of coolant accident analysis of the integrated pressurized water reactor. In: Power and Energy Engineering Conference (APPEEC), 2010 Asia Pacific, March 2010. IEEE2010, 1-4.
  10. Song J. and Kim T. W., Severe Accident Issues Raised by the Fukushima Accident and Improvements Suggested, Nulc. End. Technol. 46 (2), 2014, 207-216.
  11. Lee B. C., Cho J. S., Park C. H., Chung C. H., Development and application of two-dimensional hydrogen mixing model in containment subcompartment under severe accidents, J. Korean Nucl. Soc. 29(2), 1997, 110.
  12. Bang Y. S., Kim K., Seul K. W. and Kim H. J., Loss of coolant accident analysis during shutdown operation of YGN units 3/4. J. Korean Nucl. Soc., 31(1), 1999, 17-28.
  13. Xiong J., Yang Y. and Cheng X., CFD application to hydrogen risk

- analysis and PAR qualification. Sci. Technol. Nucl. Install. 2009, 2009, (Article ID 213981; 10 pages)
14. Sahin S. and Sarwar M. S., Hydrogen hazard and mitigation analysis in PWR containment. Ann. Nucl. Energy. 58, 2013, 132-140.
  15. Reinecke E. A., Kelm S., Jahn W., Jakel C. and Allelein H. J., Simulation of the efficiency of hydrogen recombiners as safety devices. In: Int. J. Hydrog. Energy, 38 (19), 2013, 8117-8124.
  16. Sathiah, P., Komen, E. and Roekaerts D., The role of CFD combustion modeling in hydrogen safety management - III: Validation based on homogenous hydrogen-air-diluent experiments. Nucl. Eng. Des. 289, 2015, 296-310
  17. Li H., Villanueva W. and Kudinov P., Approach and development of effective models for simulation of thermal stratification and mixing induced by steam injection into a large pool of water, Sci. Technol. Nucl. Install. 2014, 2014, (Article ID 108782; 11 pages), Hindawi Publishing Corporation.
  18. Seo Y. H. and Moon Y. T., Containment performance analysis of APR1400 in LBLOCA. In: Korean Nuclear Spring Meeting, May 2014, KNS, Jeju, Korea2014.
  19. Kim J. and Hong S. W., Analysis of hydrogen flame acceleration in APR1400 containment by coupling hydrogen distribution and combustion analysis codes. Progress in Nuclear Energy, 78, 2015, 101-109.
  20. Koh J. H., Him Y. H., Lee D. H. and Sung C. K., APR1400 steam generator tube rupture accident analysis using KNAP. In: Korean Nuclear Society Spring Meeting, May 2006, KNS, Chuncheon, Korea2006
  21. Kim. H. C, Suh N. D. and Park J. H., Hydrogen behavior in the

- IRWST of APR1400 following a station blackout, Nucl. Eng. Des, 38(2), 2006, 195-200.
22. Park and Bae, 2014 K. Park and K. H. Bae, Hydrogen concentration variation and examination of PAR installation in reactor containment building during hydrogen release from different direction failure places, Nucl. Eng. Des, 278, 2014, 229-238.
  23. The Korea Atomic Energy Research Institute (KAERI), Development of evaluation technology for hydrogen combustion in containment and accident management mode for CANDU. Report KAERI-RR-3148-2009, 2009.
  24. The Korea Atomic Energy Research Institute (KAERI), Development of evaluation technology for hydrogen combustion in containment and accident management mode for CANDU. Report KAERI-RR-3148-2009, 2009.
  25. Park and Bae, 2014 K. Park and K. H. Bae, Hydrogen concentration variation and examination of PAR installation in reactor containment building during hydrogen release from different direction failure places, Nucl. Eng. Des, 278, 2014, 229-238.
  26. S. B. Kim, D. H. Kim, and Y. M. Song. Development of Evaluation Technology for Hydrogen Combustion in containment and Accident Management Code for CANDU. Korea Atomic Energy Research Institute, Daejeon, Republic of Korea, 2011. Report KAERI-RR-3148-2009.
  27. I. K. Park, J.H. Moon, and G.C. Park, The probabilistic analysis on the containment failure by hydrogen burning at severe accident in nuclear power plants, Journal of the Korean Nuclear Society, vol. 26, pp. 411-419, 1994.
  28. International Atomic Energy Agency (IAEA), Mitigation of hydrogen hazards in water cooled power reactors. Report IAEA-TECDOC-1196, February 20,

2001.

29. E. Bachellerie, F Arnould, M. Auglaire, B. De Boeck, O. Braillard, B. Eckardt. F. Ferroni and R. Moffett. "Generic approach for designing and implementing a passive autocatalytic recombiner PAR-system in nuclear power plant containments." Nuclear Engineering and Design 221, no. 1 (2003): 151-165
30. Y. Ju, T. Niioka, Reduced kinetic mechanism of ignition of nonpremixed hydrogen/air in a supersonic mixing layer, Journal of Combustion and Flame, vol. 99, pp. 240-246, 1994.
31. D.G. Vlachos, L.D. Schmidt, and R. Aris, Ignition and extinction of flames near surfaces: Combustion of H<sub>2</sub> in air, Journal of Combustion and Flame, vol. 95, pp. 313-335, 1993.
32. R. Heck, G. Kelber, K. Schmidt, and H.J. Zimmer, Hydrogen reduction using the dual recombiner-igniter concept, Nuclear Engineering and Design, vol. 157 311-319, 1995.
33. D. G. Vlachos, Reduction of detailed kinetic mechanism for ignition and extinction of pre mixed hydrogen/air flames, Chemical Engineering Science, vol. 51(16) 3379- 3993, 1996.
34. K. R. Kim, S. W. Paek, H. J. Choi, and H. S. Chung, Catalytic recombination of hydrogen and oxygen in air stream, Journal of Industry and Engineering Chemistry, vol. 7(2), pp. 116-120, 2001.
35. E.A. Reinecke, J. Boehm, P. Drinovac, and S. Struth, "Modelling of Catalytic Recombiners: Comparison of REKO-DIREKT Calculations with REKO-3 Experiments" , Proceedings of Nuclear Energy for New Europe 2005 International Conference, Slovenia. [Online]. Available: [http:// www.nss.si/proc/bled2005/htm/pdf/00092.pdf](http://www.nss.si/proc/bled2005/htm/pdf/00092.pdf).
36. J. F Griffiths, J.A Barnard, Flame and Combustion, Blackie Academic & Professionals, 1995.

37. T. Fujii, K. Fujimoto, Yamanari S. and Yoshinari Y. A Thermal-Hydraulic Analysis Model for Catalytic Hydrogen Recombiners in the Containment Vessel of a BWR. 7th International Conference on Nuclear Engineering (ICONE-7), Tokyo, Japan, 1999.
38. T. K. Blanchat and A. Malliakos, Analysis of hydrogen depletion using a scaled passive autocatalytic recombiner, Journal of Nuclear Engineering and Design, vol. 187, pp. 229-239, 1999.
39. Park and Bae, 2014 K. Park and K. H. Bae, Hydrogen concentration variation and examination of PAR installation in reactor containment building during hydrogen release from different direction failure places, Nucl. Eng. Des, 278, 2014, 229-238.
40. J. H. SONG, and T. W. KIM, "Severe Accident Issues Raised by the Fukushima Accident and Improvements suggested." (2012)
41. R. Gido,. G. COGAP: A nuclear power plant containment hydrogen control system evaluation code. Los Alamos National Lab, NM, USA, (1983)
42. W. Breitung, and P. Royl. "Procedure and tools for deterministic analysis and control of hydrogen behavior in severe accidents.." Nuclear Engineering and Design 202.2 (2000): 249-268
43. E. Bachellerie, F Arnould, M. Auglaire, B. De Boeck, O. Braillard, B. Eckardt. F. Ferroni and R. Moffett. "Generic approach for designing and implementing a passive autocatalytic recombiner PAR-system in nuclear power plant containments." Nuclear Engineering and Design 221, no. 1 (2003): 151-165
44. S. J Han, and K. I. Ahn. "An investigation of potential risks of nuclear system from hydrogen production." Nuclear Engineering and Design 270 (2014): 119-132.
45. E. A. Reinecke, I. M. Tragsdorf and K. Gierling. "Studies on

- innovative hydrogen recombiners as safety devices in the containments of light water reactors.” Nuclear Engineering and Design 230, no. 1 (2004): 49-59
46. J. Deng, and X. W. Cao.” A study on evaluating a passive autocatalytic recombiner PAR-system in the PWR large-dry containment.” Nuclear Engineering and Design 238, no. 10(2008):2554-2560
47. C. Appel, I. Mantzaras, R. Schaeren, R. Bombach and A. Inauen. “Catalytic combustion of hydrogen-air mixtures over platinum: validation of hetero/homogenous chemical reaction schemes.” International Journal of Energy for a Clean Environment 5, no. 1(2004)
48. J. W. Park, B. R. Koh and K.Y. Suh. “Demonstrative testing of honeycomb passive autocatalytic recombiner for nuclear power plant.” Nuclear Engineering and Design 241, no. 10 (2011): 4280-4288
49. Allein H. J., Reinecke E. A., Broxtermann P., and Kelm S., Combined analytical and experimental investigations for LWR containment phenomena, Nucl. Eng. Technol. 44 (3), 2012, 249-260.
50. Babic M., Kljenak I., and Mavko B., Numerical study of interaction between NPP containment atmosphere and passive autocatalytic recombiners. In: Proc. International Conference of Nuclear Energy for New Europe 2006, Portoroz, Slovenia, September 18-21, 2006.
51. Baronov G. S., Grigoriev S. A., Kalinnikov A. A. and Fateev V. N., Development of hydrogen sensors and recombiners. In: Proc. 1st International Conference on Hydrogen Safety, Pisa, Italy, 78, 2005.
52. Heuser F. W., German risk study’ nuclear power plants, phase B. Germany. 1989

53. Breitung W. and P. Royl, Procedure and tools for deterministic analysis and control of hydrogen behavior in severe accidents. Nucl. Eng. Des. 202 (2), 2002, 249-268.
54. Boeck B. De, Prevention and mitigation measures to ensure containment integrity. Nucl. Eng. Des, 209(1), 2001, 147-154.
55. Fineschi F. and P. Vanini, Calculations concerning the capability of passive recombiners to control hydrogen concentration in the containment of an advanced PWR” . In: Proc. OECD/NEA/CSNI Workshop on the Implementation of Hydrogen Mitigation Techniques, Winnipeg, Manitoba, Canada, 1997
56. Fineschi F., Koroll G. and J. Rohde, Mitigation of hydrogen hazards in water cooled power reactors. Int. Atomic Energy Agency. IAEATECDOC-1196, ISSN, 1011-4289, 2001.
57. Bury T., Coupling of CFD and lumped parameter codes for thermal hydraulic simulations of reactor containment. Computer Assisted Methods in Eng. And Sci, 20 (3), 2015, 195-206
58. Park J. W. Park, B. R. Koh, and K. Y. Suh, Demonstrative testing of honeycomb passive recombiner for nuclear power plant. Nucl. Eng. Design, 241(10), 2011, 4280-4288.
59. Houkema M., E. Komen M. J., N. B. Siccama, and S. M. Willemsen, CFD Analyses of Steam and Hydrogen Distribution in a Nuclear Power Plant. Proc. In: 10th International Topical Meeting on Nuclear Reactor Thermal Hydraulics (NURETH-10), Seoul. South Korea, 2003.
60. Blanchat T. K., and A. Malliakos, Analysis of hydrogen depletion using a scaled passive autocatalytic recombiner. Nucl. Eng. Des, 187(2), 1999, 229-239.
61. Kelm S., Jahn W., and Reinecke E. A., Operational behavior of catalytic recombiners-experimental results and modeling approaches.

- In: Proceedings Workshop on Experiments and CFD Code Application to Nuclear Reactor Safety (XCFD4NRS), Grenoble, France, September 2008.
62. Kobayashi K., Murano K., Yamanari S. and Yamamoto Y., Application of passive auto catalytic recombiner (PAR) for BWR plants in Japan. In: Proc. 9th International Conference on Nuclear Engineering (ICONE-9), Tokyo, Japan, 2001.
  63. Martin-Valdepenas J. M., Jimenez M. A., Martin-Fuertes F., and Fernandez J. A., Improvements in a CFD code for analysis of hydrogen behavior within containments. Nucl. Eng. Des, 237 (6), 2007, 627-647.
  64. Reinecke E. A., Bentaib A., Kelm S., Jahn W., Meynet and Caroli C., Open issues in the applicability of recombiner experiments and modeling to reactor simulations. In: Progress in Nucl. Energy, 52 (1), 2001, 136-147.
  65. Rohde J., Schwinges B., and Sonnenkalb M., Implementation of PAR systems in German LWRs” . In: Proc. OECD Workshop on the Implementation of Severe Accident Management Measures (SAMI-2001), PSI-Villigen, Switzerland, 10-13 September 2001.
  66. Wilkening H., Kljenak I., Ambrosini W., Bentaib A., Blumenfeld L. and Dabbane F., ... and Travis J. R., European research on issues concerning hydrogen behaviors in containment within the SARNET network of excellence. In: Proc. 9th International Congress on Advances in Nuclear Power Plants (ICAPP’ 08), Anaheim. CA, USA, June, 2008.
  67. Wurster W., Ana G., Eichelhardt F., Pfeifer P. and Cristescu I., Combustion of hydrogen from the ITER water detritiation system” . In Fusion Engineering, 2009. SOFE 2009. 23<sup>rd</sup> IEEE/NPSS Symposium on

(pp. 1-4). IEEE, June, 2009.

68. Reinecke E. A., Kelm S., Jahn W., Jakel C. and Allelein H. J., Simulation of the efficiency of hydrogen recombiners as safety devices. In: Int. J. Hydrog. Energy, 38 (19), 2013, 8117-8124.

